LBL-28266

Lawrence Berkeley Laboratory
UNIVERSITY OF CALIFORNIA

APPLIED SCIENCE DIVISION

Reactive Absorption of Hydrogen Sulfide by a Polyglycol Ether Solution of Sulfur Dioxide

R.M. Hix* and S. Lynn

*(Ph.D. Thesis)

December 1989

APPLIED SCIENCE DIVISION

LOAN COPY
Circulates
for 2 weeks
Bldg. 50 Library.
LBL-28266
Copy 2

Prepared for the U.S. Department of Energy under Contract Number DE-AC03-76SF00098.

DISCLAIMER

This document was prepared as an account of work sponsored by the United States Government. While this document is believed to contain correct information, neither the United States Government nor any agency thereof, nor the Regents of the University of California, nor any of their employees, makes any warranty, express or implied, or assumes any legal responsibility for the accuracy, completeness, or usefulness of any information, apparatus, product, or process disclosed, or represents that its use would not infringe privately owned rights. Reference herein to any specific commercial product, process, or service by its trade name, trademark, manufacturer, or otherwise, does not necessarily constitute or imply its endorsement, recommendation, or favoring by the United States Government or any agency thereof, or the Regents of the University of California. The views and opinions of authors expressed herein do not necessarily state or reflect those of the United States Government or any agency thereof or the Regents of the University of California.

LBL-28266

REACTIVE ABSORPTION OF HYDROGEN SULFIDE BY A POLYGLYCOL ETHER SOLUTION OF SULFUR DIOXIDE

by

Richard M. Hix and Scott Lynn

Applied Science Division
Lawrence Berkeley Laboratory
1 Cyclotron Road
Berkeley, California 94720

December 1989

This work was supported by the Morgantown Energy Technology Center, Assistant Secretary for Fossil Energy, Office of Coal Utilization, Advanced Research and Technology Development, Division of Surface Coal Gasification through the U.S. Department of Energy under Contract No. DE-AC03-76SF00098.

Reactive Absorption of Hydrogen Sulfide by a Polyglycol Ether Solution of Sulfur Dioxide

by
Richard Marshall Hix

Abstract

The absorption of hydrogen sulfide (H_2S) by a polyglycol ether solution of sulfur dioxide (SO_2) is but one step in a process under development to recover sulfur from sour-gas streams. The process makes use of the catalyzed, irreversible, second-order liquid-phase reaction between H_2S and SO_2, forming sulfur and water as products, to improve absorption rates in the primary absorber and to make it unnecessary to strip H_2S from ninety percent of the total solvent flow. As part of this development, tray efficiencies for both physical absorption of H_2S and SO_2 and efficiencies for absorption with chemical reaction of H_2S are needed to design the absorbers in the process.

Tray efficiencies were determined for physical absorption of H_2S and SO_2 on a single sieve tray at atmospheric pressure. These efficiencies were well-predicted by correlations available in the literature. The efficiency correlations were used to predict the high-pressure tray efficiencies needed to design the primary absorber. Absorption rates were measured for absorption of H_2S followed by chemical reaction. The H_2S absorption rate, relative to strictly physical absorption, is increased by three-fold or higher, and depends on SO_2 concentration, plate inventory, and reaction-rate constant. This system is a case of absorption with irreversible, second-order chemical reaction by a solution containing a volatile dissolved reactant. A penetration-model analysis indicated that the reaction is too slow to cause an enhancement of the liquid-phase mass-transfer coefficient. From this finding it was concluded that the tray efficiency for reactive absorption would be equal to that for physical absorption. The increased absorption rate is due to the reaction's occurring in the bulk solvent and causing a reduction in the

bulk concentration of H_2S. The lower concentration of H_2S in the bulk solvent gives rise to a greater driving force for mass transfer. Second-order reaction-rate constants were determined from the reactive-absorption measurements. These rate constants compared favorably to those measured by others. The reaction-rate constants and tray efficiencies determined here were used to design the high-pressure primary absorber in the sulfur-recovery process.

Acknowledgments

My past few years at U. C. Berkeley have been sometimes very difficult, but mostly, the "graduate-student experience" has been professionally and culturally rewarding as the result of the many wonderful people I have encountered here. I would like to express my appreciation to my research advisor, Professor Scott Lynn. His kind patience and encouraging guidance kept me on course. I've learned a great deal from Dr. Lynn by observing his amazing insight into process design. Special thanks go to my labmates, past and present. Dan Neumann, Steve Sciamanna, Dan Crean, David Weingartner, Chuck Higdon, Tom Colson, Jim Russell, Craig Stevens, and Dannes Hutapea have all, in their own special ways, enriched my stay. I especially enjoyed our weekly basketball games. Getting through all the U. C. red tape would have been nearly impossible without the help of Kay Ekman and Ferne Karsada. Their office, always a haven for the research-weary, was a clearing house for outrageous stories, personal reviews for restaurants both at home and abroad, and the occasional goody (fill out a form - have a cookie).

My wife, Laurie Sasaki, deserves recognition for her sacrifices as a graduate student's wife. She had to endure long periods of near desertion, complaints of set-backs and broken equipment, and the jitters of a caffeine-wired husband. In spite of all these hardships she was able to support me with tremendous amounts of love.

This work was supported by the Morgantown Energy Technology Center, Assistant Secretary for Fossil Energy, Office of Coal Utilization, Advanced Research and Technology Development, Division of Surface Coal Gasification, through the United States Department of Energy under contract DE-AC03-76SF00098.

TABLE OF CONTENTS

Nomenclature v

Chapter 1: Introduction

1.1 Background 1
1.2 Conventional Sulfur-Recovery Technology 1
1.3 The U.C. Berkeley Sulfur-Recovery Process 3
1.4 Previous Work 6
1.5 Scope of This Work 7

Chapter 2: Reactive-Absorption Theory

2.1 Background 12
2.2 Mass-Transfer Models 13
2.3 Enhancement with a Nonvolatile Reactant 14
2.4 Past Work on Reactive-Absorption with a Volatile Reactant 17
2.5 Numerical Solution to Penetration Theory 18
A. Method 18
B. Results 22
C. Enhancement of H_2S absorption by solutions of SO_2 27

Chapter 3: Tray-Efficiency Theory

3.1 Introduction 41
3.2 Tray-Efficiency Models 42
3.3 Tray Efficiency for Absorption with Chemical Reaction 47
3.4 Reaction in the Bulk Liquid on the Tray 49

Chapter 4: Apparatus

4.1 Introduction 53
4.2 Apparatus Description and Operation 53
4.3 Chemical Analysis 55
A. Gas-Phase Analysis 55
B. Liquid-Phase Analysis 56
4.4 Liquid Hold-up 58

Chapter 5: Gas Solubilities

5.1 Past Studies 64
5.2 Present Study 66

Chapter 6: Gas Absorption

6.1 Physical Absorption 72
A. Tray Efficiencies for Sulfur Dioxide 72
B. Tray efficiencies for Hydrogen Sulfide 73
6.2 Tray-Efficiency-Model Predictions 74
6.3 Absorption with Chemical Reaction 76
A. Calculations 76
B. Reactive-Absorption Results 81
1. Verification of Reaction-Rate Constant 81
2. Effect of 3-PC Concentration on Reaction-Rate Constant 82
3. Effect of Reaction on H_2S Absorption 83
6.4 Summary 85

Chapter 7: Absorber Design

7.1 Introduction 94
7.2 Design Method 95
7.3 Results 97

References 107

Appendices

A Penetration-Model Solution and Code 109

B Absorber-Design Method and Code 136

C Tables of Absorption Data 188

NOMENCLATURE

a_i - interfacial area per unit volume of liquid, cm^2/cm^3

A - concentration ratio C_A/C_{Ae}, dimensionless

A_a - active area of tray, m^2

$(A/R)_i$ - fitted parameters from eqn 5-3

B - concentration ratio C_B/C_{Bo}, dimensionless

C - coefficient in eqn 3-13 and defined in eqn 3-15, dimensionless

C_A - liquid-phase concentration of A, $mole/cm^3$

C_B - liquid-phase concentration of B, $mole/cm^3$

D_e - eddy diffusivity, m^2/s

D_L - molecular diffusivity in liquid, cm^2/s

D_v - molecular diffusivity in vapor, cm^2/s

E_a - Activation energy, kcal/mole

E_{mv} - Murphree vapor tray efficiency, dimensionless

E_{oc} - overall column efficiency, dimensionless

E_{ov} - point efficiency, dimensionless

f - fractional approach to flooding, U_a/U_{af}

f_2 - fugacity of solute (component 2), kPa

F_{va} - F-factor (eqn 3-18) through active area of tray, $m/s(kg/m^3)^{1/2}$

h_L - height of clear liquid holdup on tray, cm

h_w - weir height, cm

H_A - Henry's law coefficient for component A, kPa cm^3/mole

H_L - hold-up of clear liquid on tray, cm^3

$H_{2,1}$ - Henry's law coefficient for solute (2) in solvent (1), kPa/m.f.

$H^o_{2,1}$ - Henry's law coefficient at 298 ^oK, kPa/m.f.

ΔH^{soln} - Heat of solution, J/mole

k_1 - first-order rate constant, s^{-1}

k_2 - second-order reaction-rate constant, cm^3/(mole-s), or liter/mole-s

k_2Ph^o - fitted parameter of eqn 6-14, liter/mol-s

k_3 - third-order reaction-rate constant, $liter^2/mole^2$-s

k_g - gas-phase mass-transfer coefficient, mole/kPa-cm^2-s ($=k_v/(RT)$)

k_L - liquid-phase mass-transfer coefficient, cm/s

k_L^* - liquid-phase mass-transfer coefficient for reactive absorption, cm/s

k_v - gas-phase mass-transfer coefficient, cm/s

K_c - equilibrium constant for catalyst/H_2S complex (eqn6-9), liter/mole

K_L - overall liquid-phase mass-transfer coefficient, cm/s

K_s - capacity parameter (eqn 3-16), m/s

L - molar flow rate of Liquid, mole/s

m - slope of the equilibrium line ($m=H_{2,1}/P$), dimensionless

M - parameter, $(k_1 D_{LA})/k_L^2$ or $(k_2 C_{Bo} D_{LA})/k_L^2$ for film theory;

- or, $(\pi/4)\theta$ for penetration theory, dimensionless

N_L - number of liquid mass-transfer units

N_{ov} - number of mass-transfer units based on overall gas-phase driving force

N_v - number of gas-phase mass-transfer units

p_A - partial pressure of component A in the bulk gas, kPa

P - total pressure, kPa

Pe - Peclet number, dimensionless

q_L - liquid flow rate per unit length of overflow weir, m^3/m-s

q - concentration ratio C_{Bo}/C_{Ae}, dimensionless

Q_{phys} - amount of gas physically absorbed per unit interfacial area, mole/cm^2

Q_{rxn} - amount of gas reactively absorbed per unit interfacial area, mole/cm^2

Q_L - volumetric liquid flow rate, cm^3/s

r - diffusivity ratio, D_{LB}/D_{LA}, dimensionless

r_A - reaction rate of component A per unit volume, mole/cm^3-s

r_w - ratio of weir width to average width of liquid flow path, dimensionless

R - gas constant, 8.314 J/(mole ^oK)

$\bar{R}$ - rate of absorption per unit interfacial area, mole/cm^2-s

t - contact time (penetration model), s

t_L - average liquid residence time, s

t_v - average vapor residence time, s

T - temperature, ^oK, T^o=298.15 ^oK

U_a - gas velocity through active area of tray, m/s

U_{af} - gas velocity through active area at flooding, m/s

V - molar gas flow rate, mole/s

x - distance into liquid from interface, cm

x_i - liquid mole fraction (1=solvent, 2=solute), m.f.

y_i - vapor mole fraction, m.f.

y^* - vapor composition in equilibrium with liquid exiting tray, m.f.

Z - $\sqrt{[k_2 C_{Bo}/D_{LA}]}\, x$, dimensionless

Z_L - length of liquid flow path, m

Greek Symbols

γ_A - $k_{gA} H_A/\{D_{LA} \sqrt{[k_2 C_{Bo}/D_{LA}]}\}$, dimensionless

γ_B - $k_{gB} H_B/\{D_{LB} \sqrt{[k_2 C_{Bo}/D_{LA}]}\}$, dimensionless

δ - film thickness, cm

η - parameter defined by eqn 3-9, dimensionless

θ - $k_2 C_{Bo} t$, dimensionless

λ - ratio of slopes of equilibrium line to operating line, mV/L, dimensionless

ν - stoichiometric coefficient, moles B per moles A, dimensionless

ρ_L - liquid density, kg/m^3

ρ_v - vapor density, kg/m^3

τ - CSTR-Tray Liquid residence time (H_L/Q_L), s

ϕ - enhancement factor for reactive absorption mass transfer

ϕ_a - enhancement factor for absorption with instantaneous reaction

ϕ_e - relative effective froth density, dimensionless

Concentration Subscripts

A - component A

B - component B

e - in equilibrium with bulk gas-phase composition

i - at gas-liquid interface

o - in bulk liquid solution as C_{Ao}, or total concen. as $[H_2S]_o$

in - at tray inlet

out - at tray outlet

loc - at local position on tray

1. INTRODUCTION

1.1 Background

Hydrogen sulfide, as a highly undesirable contaminant, is present in a variety of gas streams such as natural gas, coal gas, and refinery gases. It occurs in natural gas in concentrations that range from several parts per million (ppm) to many percent. When coal is gasified, most of the total sulfur content is converted to hydrogen sulfide (H_2S) or, to a lesser extent, carbonyl sulfide (COS). The H_2S concentration in the coal gas depends on the amount of sulfur initially present in the coal and on the nature of the coal-gasification process used. Gas-phase concentrations are typically several thousand ppm H_2S. At the refinery, hydrodesulfurization of petroleum feedstocks produces gas streams of several percent H_2S. Because of both environmental restrictions and process requirements, hydrogen sulfide must be removed from these gas streams. Hydrogen sulfide is a poison for many catalysts which may be present in downstream process equipment; it is toxic, corrosive in wet or hot environments, and quite unpleasant smelling.

The required degree of H_2S removal depends on use of the gas. Natural gas of "pipeline quality" generally must contain no more than 4 ppm H_2S, whereas hydrotreater recycle gases may contain several thousand ppm H_2S. In some cases, selective absorption of H_2S is desirable. In other cases, co-absorption of CO_2 and light hydrocarbons allows these components to be recovered as separate products. To meet this wide range of processing requirements, the U. C. Berkeley Sulfur Recovery Process (UCBSRP) is being developed as a less-costly alternative to conventional sulfur-recovery technology.

1.2 Conventional Sulfur-Recovery Technology

An example of conventional sulfur-recovery technology, shown by block-flow diagram in Figure 1.1, consists of an amine absorber and stripper, a Claus

sulfur-recovery unit, and a suitable tail-gas process. First, H_2S is absorbed from the H_2S-containing gas stream by an amine solvent. The resulting H_2S-rich solvent is then stripped of most of its H_2S, cooled and recycled back to the absorber. The H_2S-rich gas stream from the amine stripper is sent to a Claus plant which relies on the high-temperature, gas-phase Claus reaction, equation 1-1, to convert the H_2S to gaseous sulfur.

$$2\ H_2S + SO_2 \longleftrightarrow 3/x\ S_x + 2\ H_2O \qquad (1\text{-}1)$$

The SO_2 required for the reaction is obtained by burning a portion of the H_2S in a lean amount of air such that only one third of the H_2S is oxidized to SO_2. Because the gas-phase Claus reaction is equilibrium-limited, the conversion of H_2S to sulfur must be performed in stages to achieve high conversions. Sulfur condensation and gas reheat are necessary between the stages. Typically, one thermal converter and three catalytic converters are required to achieve a 96% conversion of the H_2S to liquid sulfur. The remaining 4% leaves the Claus process in the gas stream as a combination of H_2S, SO_2, and sulfur vapor.

The unrecovered sulfur compounds must be removed in a tail-gas unit before the gas stream is released to the air. There are three basic types of tail-gas processes available: those that reduce all the sulfur compounds to H_2S for subsequent recovery and recycle back to the Claus unit, those that oxidize all the sulfur compounds to SO_2 which is a recovered and recycled back to the Claus plant, and those that reduce the total sulfur content to H_2S for subsequent oxidation to sulfur in a non-Claus reaction. The SCOT process is an example of the first type: all sulfur compounds in the tail-gas stream from the Claus plant are reduced catalytically to H_2S. The H_2S is absorbed by an amine solvent, and the H_2S-rich gas stream which results from stripping the solvent is sent back to the front end of the Claus unit. The Wellman-Lord process, an example of the second type, oxidizes

the H_2S and sulfur in the tail gas to SO_2 which is absorbed by an alkali metal sulfite-bisulfite solution. The solution is stripped to concentrate SO_2 into a gas stream that is recycled back to the Claus plant. An example of the third type of tail-gas process is the Beavon-Stretford process. In this process the total sulfur content is reduced catalytically to H_2S by the Beavon process, and the H_2S is then absorbed by a aqueous solution of sodium carbonate and vanadate in the Stretford process. The sulfide in solution is oxidized to elemental sulfur by the vanadate ion. In the same vessel, air is used to regenerate the vanadate ion. A fairly low quality sulfur precipitate is recovered from the aqueous solution. More detailed descriptions of these processes and others can be found in Kohl and Riesenfeld (1985).

The disadvantages of the conventional technology are several. If the process gas must meet a very strict H_2S specification, the amine stripper becomes very energy-intensive. Amines are chemical solvents for H_2S, and it generally requires more energy to strip out a chemically-bound gas than stripping from a physical solvent requires. The gas-phase Claus reaction is equilibrium-limited; therefore staging is required in the Claus process to achieve large conversions of H_2S. Tail-gas processes are often very complicated and are capital and energy-intensive.

1.3 The U.C. Berkeley Sulfur-Recovery Process

The goal in developing the U.C. Berkeley Sulfur Recovery Process is to design a single integrated process which has the flexibility to process a variety of gas streams, and either to co-absorb certain other gases, or to remove H_2S selectively. The UCBSRP consists of five basic steps. First, H_2S is absorbed by a polar organic solvent. Diethylene glycol methyl ether was used in this study. Second, by mixing the H_2S-rich solvent with a slight excess of SO_2 dissolved in the same solvent, all the H_2S can be reacted away to form sulfur by the following irreversible liquid-phase reaction:

$$2\ H_2S + SO_2 \text{ ---> } 3/8\ S_8 + 2\ H_2O \qquad (1\text{-}2)$$

Third, the dissolved sulfur formed by the reaction is crystallized and separated from the solvent. Fourth, the water of reaction and any residual dissolved gases must be stripped from the solvent. And finally, a portion of the recovered, marketable sulfur product is burned in air to produce SO_2, which is reabsorbed by the cool, lean solvent from the solvent stripper to provide the SO_2-rich solvent stream used in step two. The heat of combustion is recovered in a waste-heat boiler and provides an energy credit for the process.

The key to this process is the irreversible liquid-phase Claus reaction, equation 1-2. This reaction, even when carried out at temperatures below 100°C, proceeds rapidly to completion in the presence of an appropriate homogeneous liquid-phase catalyst (3-pyridyl carbinol was used in this study). By this reaction the large H_2S stripping costs associated with most conventional technologies are avoided, and the cooled H_2S-free solvent from the crystallizer can be recycled back to the top of the primary absorber without further processing. Because the solvent that is fed to the primary absorber is free of H_2S, the treated gas can easily meet a 1-ppm-or-less outlet specification.

Figure 1.2 shows the UCBSRP configuration for high H_2S selectivity. Sour gas enters the primary absorber where cool, H_2S-free solvent absorbs H_2S from the gas stream. The H_2S-rich solvent leaving the primary absorber is split into two streams. Approximately 90% of the solvent flow is sent to the SO_2-rich reactor/crystallizer while the remaining portion of solvent flows to the H_2S-rich settler/surge tank. An excess amount of the process solvent rich in SO_2 is mixed with the H_2S-rich feed prior to the reactor/crystallizer so that this unit operates SO_2 rich. The feed pipe to the reactor /crystallizer, therefore, acts as a plug-flow reactor. Reaction continues in the reactor/crystallizer which is operated at very

near the pressure of the primary absorber and at temperature low enough to cause precipitation of solid sulfur. The reactor/crystallizer operates as a continuously-stirred-tank reactor (CSTR) in which crystallization is occurring. Since the excess amount of SO_2 completely depletes any H_2S present in the solvent, the clarified H_2S-free solvent from the reactor/crystallizer requires no further processing and can be pumped back to the primary absorber. The maximum amount of SO_2 that can be fed to the primary absorber in this solvent stream is set by the solubility limit of sulfur in the absorber (see reaction 1-2).

High H_2S selectivity is achieved because other absorbed gases such CO_2, H_2 and light hydrocarbons are not removed from this chemically-regenerated solvent stream which accounts for about 90% of the solvent flow in the primary absorber. The concentrations of these gases in the solvent recycle stream reach equilibrium with their gas-phase concentrations in the sour-gas feed, so very little net absorption occurs. Only the small amounts of these gases that are dissolved in the solvent passing to the H_2S-rich settler/surge tank are actually removed from the gas stream.

A sulfur slurry leaves the bottom of the SO_2-rich reactor/crystallizer and mixes with the remainder of the H_2S-rich solvent from the primary absorber in ratios that maintain an H_2S-rich solution in the settler/solvent surge tank. The solid sulfur from the settler is separated from the solvent and washed with water in a pusher-type centrifuge. Water and solid sulfur are separated by heating to above the melting point of sulfur and decanting the molten sulfur phase from the water phase. Clarified solvent from the H_2S-rich settler/surge tank is easily stripped of H_2S and the water of reaction in the solvent stripper, which is operated at near atmospheric pressure. The water from the top of the solvent stripper is cleaned of its H_2S content in the sour-water stripper and is used as wash water in the primary and SO_2 absorbers and in the centrifuge. The lean solvent from the

bottom of the solvent stripper is cooled by exchange with the stripper feed and then used to reabsorb SO_2 in the SO_2 scrubber. The lean solvent is also used in the middle section of the primary absorber to capture any SO_2 which might desorb from the solvent on the top trays of the main (lower) section of the primary absorber. The SO_2 for the SO_2 scrubber is produced by burning one-third of the product sulfur in the furnace. Residual CO_2 and H_2S from the solvent stripper and all flash gas also are sent to the furnace. The heat of combustion is recovered in a waste-heat boiler which produces high-pressure steam.

1.4 Previous Work

Adequate process design and evaluation of the UCBSRP require studies of gas solubilities in a variety of promising solvents, reaction kinetics in different catalysts, absorber tray efficiencies, crystallization kinetics, and corrosion rates. Sciamanna (1986) performed a solvent survey and measured gas and sulfur solubilities in several polyglycol ether solvents. Neumann (1986) carried out a catalyst survey, determined the order of the catalyzed reaction, measured reaction-rate constants in several catalyst/solvent combinations, and developed a process simulation for evaluating the many process configurations that were considered. Crean (1987) studied the reaction kinetics further and investigated corrosion rates of mild and stainless steel in hot, wet, H_2S-rich and SO_2-rich solvents saturated with sulfur at elevated temperatures. Lynn, *et al.*, (1987) compared the UCBSRP with a conventional sulfur-recovery process for treating a recycle gas from a crude oil residuum hydrotreater. The conventional technology used a SCOT tail-gas unit. They found that the direct fixed capital for the UCBSRP would be approximately 61% of that for the conventional technology and that the utility costs of the UCBSRP would be less than the credit for the high-pressure steam that would be produced in the SO_2 furnace. For the conventional technology the utility costs would be

much more than the credit for steam produced. Colson (1989) synthesized and evaluated a process for producing hydrogen from coal. The UCBSRP was used in this process to remove both H_2S and CO_2 from the syngas stream. Stevens (1989) measured low-temperature sulfur solubilities in two different solvents and developed a model which accurately predicts the crystal-size distribution and crystallization kinetics of sulfur formed in a bench-scale reactor/crystallizer. His crystallizer produced 99.8% pure sulfur crystals with a mass-average particle size of over 200 microns.

1.5 Scope of this Work

It is the mass-transfer characteristics in the two absorbers that are the subject of this work. Design of both the primary absorber and the SO_2 absorber requires knowing the tray efficiencies and gas solubilities in the solvent. Absorption in the SO_2 absorber is by physical solubility only; however, the main solvent feed to the primary absorber contains a small amount of SO_2 that reacts with the H_2S being absorbed on the upper trays until all the SO_2 is depleted. Chemical reaction in the liquid phase can enhance the rate of mass transfer of a gas that is being absorbed. The effect that the simultaneous chemical reaction has on H_2S absorption rates, and thereby tray efficiencies, is studied both by modelling and by experimentation in this work: On the lower trays, all the dissolved SO_2 has been depleted and H_2S absorption is strictly by physical means; therefore, physical-absorption tray efficiencies are required for this section.

Sieve-tray efficiencies for physical absorption of H_2S and SO_2 were determined with the aid of the gas-solubility data of Sciamanna (1986). Absorption rates with chemical reaction were measured and compared to those for physical absorption. Tray-efficiency correlations from the literature were used to correlate the experimental data and to predict the high-pressure tray efficiencies that are necessary for designing the high-pressure primary absorber. The primary-absorber

design routine incorporates tray efficiencies, reaction on the trays, and heat and mass balances to design a multiple-section column.

List of Figures for Chapter 1

1-1 Conventional Sulfur-Recovery Technology

1-2 UCBSRP Configuration for High H_2S Selectivity

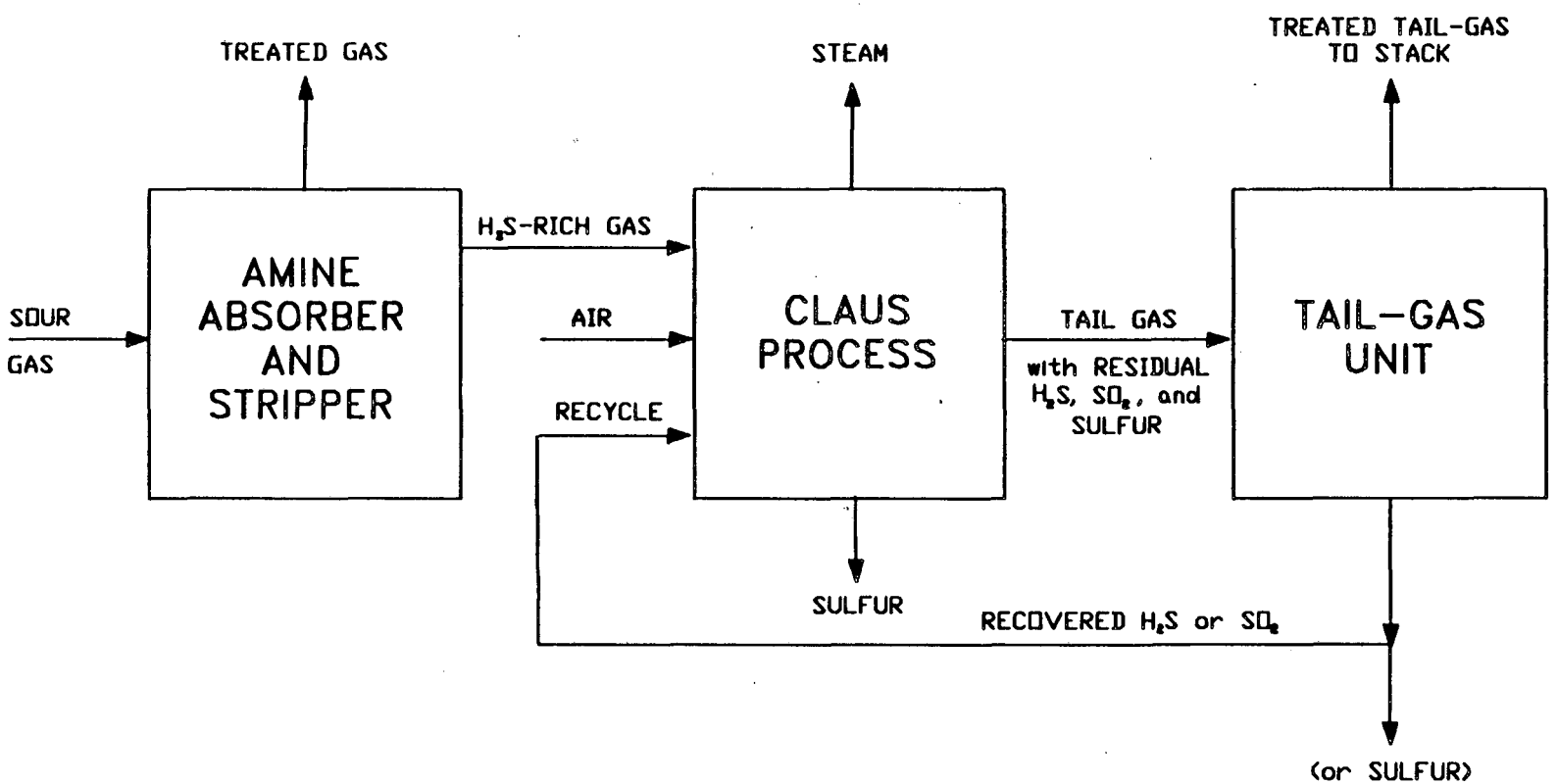

Figure 1-1: Conventional Sulfur-Recovery Technology

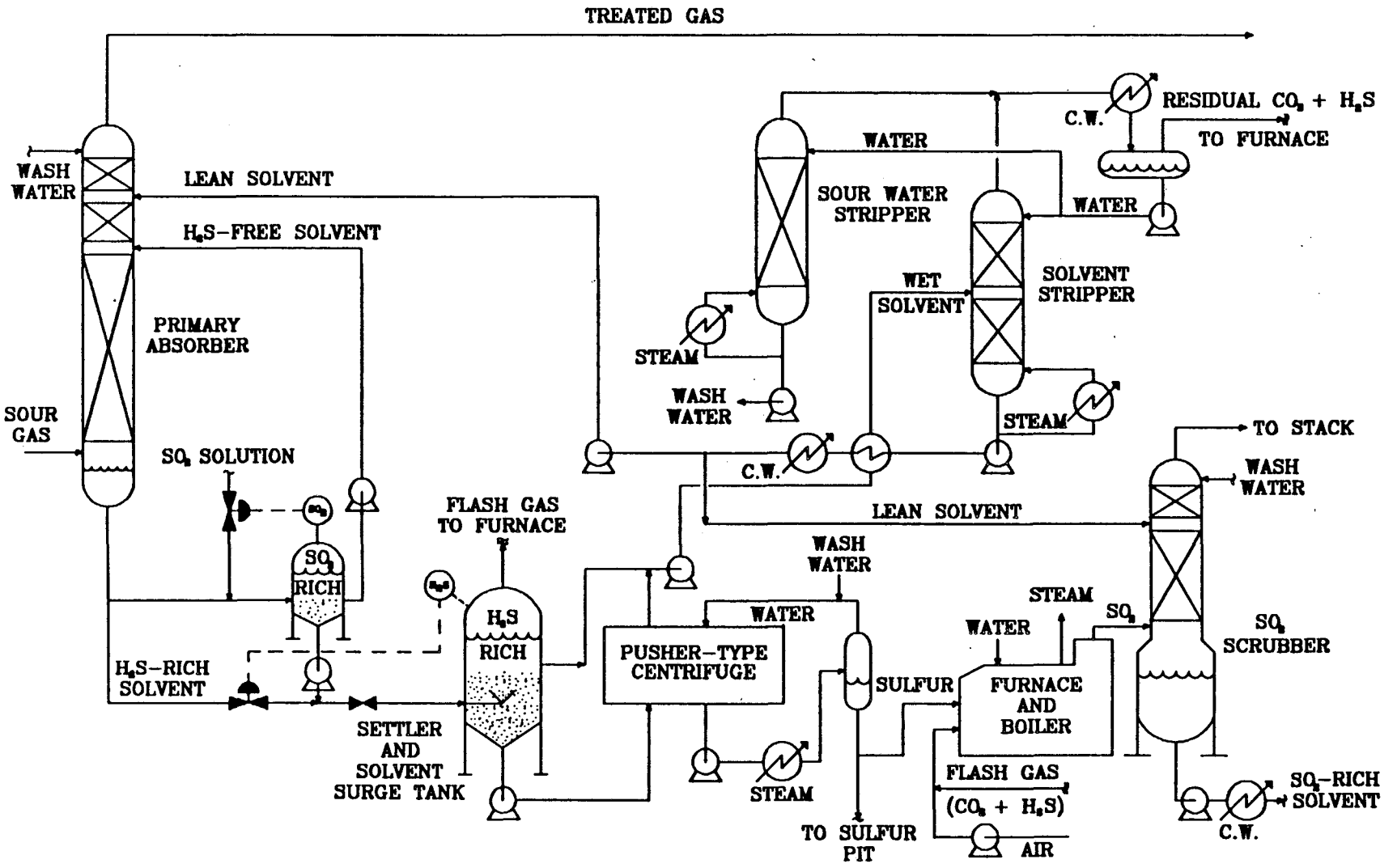

Figure 1-2: UCBSRP Configuration for High H_2S Selectivity

2. REACTIVE-ABSORPTION THEORY

2.1 Introduction

The U. C. Berkeley Sulfur Recovery Process uses a solution of sulfur dioxide in a polyglycol ether solvent to absorb hydrogen sulfide from a sour-gas stream. The absorbed H_2S can then react with the sulfur dioxide. The reaction

$$2\ H_2S + SO_2 \dashrightarrow 3/8\ S_8 + 2\ H_2O \tag{2-1}$$

is irreversible and second-order overall (first-order in each of the reactants).

$$\text{Rate} = k_2\ [H_2S]\ [SO_2] \tag{2-2}$$

If the reaction is fast enough, an enhancement to the liquid-phase mass-transfer coefficient can result because the reaction depletes the concentration of the dissolving gas (H_2S) in the liquid diffusion film at the gas-liquid interface. This depletion leads to a greater mass-transfer driving force at the interface than would occur for absorption without reaction. The increased driving force provides an increased mass-transfer coefficient. The improvement in absorption is generally characterized by an enhancement factor, ϕ, which is equal to the ratio of the liquid-phase mass-transfer coefficient for reactive absorption to that for physical absorption.

$$\phi = k_L^* / k_L \tag{2-3}$$

The rate of absorption per unit interfacial area is found by

$$\overline{R} = \phi\ k_L\ (C_{Ai} - C_{Ao}) \tag{2-4}$$

where k_L is the liquid-phase mass-transfer coefficient for physical absorption and

C_{Ai} and C_{Ao} are the liquid-phase concentrations of A at the gas-liquid interface and in the bulk liquid respectively.

Much work has been done in the area of predicting enhancement factors for gas absorption under various reaction regimes and reaction orders by using different mass-transfer models for gas-liquid contacting. The texts on mass transfer with chemical reaction by Dankwerts (1970), Astarita (1967), and Astarita, *et al.* (1983) are excellent, in-depth sources to consult on the subject of gas absorption with liquid-phase chemical reaction. Most of the cases that have been treated in the literature assume negligible gas-phase mass-transfer resistance (to the gas being absorbed) and a nonvolatile dissolved reactant (in the case of a second-order reaction). However, very little work has been devoted to studying absorption accompanied by reaction with a volatile dissolved reactant. For the case of reactive absorption of H_2S by solutions of SO_2, the sulfur dioxide is volatile and its desorption from the solvent may have an effect on the degree of mass-transfer enhancement. The magnitude of this effect and the conditions under which it will be important are of interest.

2.2 Mass-Transfer Models

Several mass-transfer models have been proposed to describe the mechanism of gas absorption and transport into an agitated liquid. Only two of the models, the film and the penetration models, will be discussed here. A comparison of these two models and several others is given elsewhere (Dankwerts, 1970; Glasscock and Rochelle, 1989). The earliest of these models is the film model (Whitman, 1923) which proposes that the gas diffuses through a stagnant liquid film of thickness δ before the gas passes into a well-mixed bulk liquid of uniform concentration. This steady-state model is very simplistic, but easily solved, and it often gives good results. For physical absorption the liquid-phase mass-transfer coefficient is given by the ratio of the liquid-phase molecular diffusivity to the film thickness

$$k_L = D_L/\delta \tag{2-5}$$

The penetration model (Higbie, 1935) is an unsteady-state model in which mass transfer occurs by the gas diffusing into small packets of stagnant liquid which are brought to the surface from the bulk solution by turbulence. All the packets are assumed to have the same residence time, t, at the surface. During this time the gas is transported into the liquid by molecular diffusion before turbulence mixes the packet back into the bulk liquid. The concentration of the dissolved gas at the gas-liquid interface is assumed to be in equilibrium with the gas composition at the interface. The initial concentrations of all species in the packet of liquid are at their bulk concentrations, and the contact time before remixing into the bulk is short enough that the concentrations deep in the packet remain at their bulk values. Therefore, the depth of the packet of liquid is considered to be semi-infinite. The analytical solution of the penetration model for physical absorption (Dankwerts, 1970) gives the average liquid-phase mass-transfer coefficient as

$$k_L = 2\,[\,D_L/\pi\,t\,]^{1/2} \tag{2-2}$$

The penetration model, although still very simple, is more realistic than the film model. Glasscock and Rochelle (1989) point out that the experimentally determined dependency of the mass-transfer coefficient on molecular diffusivity (diffusivity to the 0.5 to 0.75 power) is more closely predicted by the penetration model (diffusivity to the one-half power) than by the film model (diffusivity to the first power).

2.3 Enhancement with a Nonvolatile Reactant

Before analyzing the effects on mass transfer of having a volatile dissolved reactant and a significant gas-phase mass-transfer resistance, a few general results

for first-order, pseudo-first-order, and second-order reactions with a nonvolatile reactant will be presented (Dankwerts, 1970). In this discussion the gas-phase mass-transfer resistance to absorption of the gas is assumed to be negligible. These results will aid in analyzing the results of the volatile-reactant case. For a gas (component A) which is absorbed and undergoes an irreversible, first-order (or pseudo-first-order) reaction the rate is

$$r_A = k_1 C_A \tag{2-7}$$

where k_1 is the first-order rate constant (or pseudo-first-order rate constant) and C_A is the local concentration of component A. If the bulk concentration of dissolved A is zero, the film-model prediction for mass-transfer enhancement is

$$\phi = \sqrt{M}/[\tanh\sqrt{M}] \tag{2-8}$$

where $M=k_1 D_{LA}/k_{LA}^2$. The parameter M is a measure of the amount of gas which reacts in the diffusion film relative to the amount of unreacted gas which diffuses into the bulk liquid. When $\sqrt{M} >> 1$ (*i.e.*, for fast reactions occurring predominately in the film) the enhancement is equal to $\sqrt{M}$. This result is the same as that obtained from the penetration model for fast, irreversible, first-order and pseudo-first-order reactions, with M defined for the penetration model as $M=(\pi/4)k_1 t$.

For an irreversible, second-order reaction between an absorbed gas (component A) and a nonvolatile dissolved reactant (component B)

$$A + \nu B \text{ ---> } P \tag{2-9}$$

the local rate of reaction is

$$r_A = k_2 C_A C_B \tag{2-10}$$

For the case of an instantaneous reaction and equal diffusivities, both the film and the

penetration models predict that the enhancement factor will be given by

$$\phi_a = 1 + r\,q\,/\,\nu \qquad (r=1) \qquad (2\text{-}11)$$

where $r=D_{LB}/D_{LA}$ and $q=C_{Bo}/C_{Ae}$. The concentration of B in the bulk liquid is C_{Bo}, and the concentration of A at the interface is C_{Ae} and is in equilibrium with the bulk-gas partial pressure of A. For an instantaneous reaction, components A and B cannot coexist, and the instantaneous-reaction enhancement ϕ_a is established by the rate of molecular diffusion of A into the liquid toward the reaction zone with B. Component B is fed to the reaction zone from the opposite direction by molecular diffusion of B from deep in the liquid.

Although equation 2-11 holds for the film model when the diffusivities are not equal, for the penetration model the relationship when the diffusivities are unequal can be approximated (Dankwerts, 1970) by

$$\phi_a \simeq (1 + r\,q\,/\nu)/\sqrt{r} \qquad (r\neq 1) \qquad (2\text{-}12)$$

For the case when the reaction is not instantaneous, there is no analytical solution, and approximations or numerical solutions must be used. For the film model the well-known approximation by van Krevelen and Hoftijzer (1948) should be consulted, but since the present study is concerned with the penetration theory, only the approximation by Brian, *et al.* (1961) for the penetration-model solution will be given

$$\phi = \frac{\sqrt{M}\,\sqrt{[(\phi_a - \phi)/(\phi_a - 1)]}}{\tanh(\sqrt{M}\,\sqrt{[(\phi_a - \phi)/(\phi_a - 1)]})} \qquad (2\text{-}13)$$

When ϕ_a is large and ϕ is much less than ϕ_a, equation 2-13 reduces to the solution for a first-order reaction, equation 2-8. Under these conditions, very little of the dissolved reactant is depleted and the reaction can be considered as pseudo-first-order

where $k_1=k_2C_{Bo}$. However, as $\sqrt{M}$ becomes very large, the enhancement approaches asymptotically the enhancement for an instantaneous, irreversible, second-order reaction, ϕ_a.

Equation 2-13 is accurate to within about 8% when r is equal to one. The accuracy improves as r increases above one and suffers as r decreases below one. However, better accuracy is desired for comparing enhancement factors for the case of a volatile dissolved reactant to the case for a nonvolatile reactant. To achieve greater accuracy, the partial differential equations which describe the penetration model for gas absorption with irreversible, second-order reaction will be solved numerically.

2.4 Past Work on Reactive-Absorption with Volatile Reactants

Pangarkar (1974) and later Shaikh and Varma (1984) used similar film-model analyses to study the effect of a volatile dissolved reactant on mass-transfer enhancement factors for absorption with irreversible, second-order chemical reaction. In both studies, a linear concentration profile for the dissolved reactant (B) in the film was assumed. The resulting differential equation, for the absorbed gas (A), which describes steady-state absorption and chemical reaction was converted to a Bessel's equation and solved. The enhancement factor was then calculated in a straightforward manner. Shaikh and Varma concluded from their analysis that the volatility can be very detrimental to mass-transfer enhancement, but its effect becomes less significant in both the slow- and the instantaneous-reaction regimes.

Hikita, *et al.* (1979) used a different approach to solve the nonlinear differential equations derived from the film model. Their method was to assume a linear concentration profile of the dissolved gas (A) in the film and then to linearize the resulting differential equation. This equation was then easily solved analytically to provide the information necessary for determining the enhancement

factor by a set of easy-to-use algebraic equations. This approximate solution was checked by solving the nonlinear differential equations by a numerical technique. A comparison of the results showed a maximum deviation from the numerical solution of only 7%. The approximate solution overpredicted enhancement factors at low M and under predicted enhancements at high M. The results, which follow, of this study's numerical solution to the penetration-model analysis of gas absorption and chemical reaction with a volatile reactant will be compared to the approximate solution of Hikita, *et al.*

2.5 Numerical Solution to Penetration Theory

A. Method

For an irreversible, second-order reaction between an absorbed gas (A) and a dissolved reactant (B) as in equations 2-9 and 2-10, the differential equations based on the penetration model for diffusion and reaction in a semi-infinite stagnant liquid are written in dimensionless form for each component.

$$\frac{\partial^2 A}{\partial Z^2} - \frac{\partial A}{\partial \theta} = A\,B \tag{2-14}$$

$$r\,q\,\frac{\partial^2 B}{\partial Z^2} - q\,\frac{\partial B}{\partial \theta} = \nu\,A\,B \tag{2-15}$$

where

$A = C_A/C_{Ae}$

$B = C_B/C_{Bo}$

$r = D_{LB}/D_{LA}$

$q = C_{Bo}/C_{Ae}$

$Z = \sqrt{[\,k_2\,C_{Bo}/D_{LA}\,]}\;x$

$\theta = k_2\,C_{Bo}\,t$

$$M = (\pi/4)\,\theta \quad \text{(penetration theory)}$$

The initial conditions are

$$\text{at } \theta = 0, \qquad A = 0 \text{ for } 0 \le Z \le \infty \qquad B = 1 \text{ for } 0 \le Z \le \infty \tag{2-16}$$

For the case of a nonvolatile dissolved reactant and the absence of gas-phase mass-transfer resistance to the gas being absorbed, the boundary conditions are

for $\theta > 0$,

$$A = 1 \text{ and } \partial B/\partial Z = 0 \quad \text{at } Z = 0, \qquad A = 0 \text{ and } B = 1 \quad \text{at } Z = \infty \tag{2-17}$$

The interfacial liquid-phase concentration of A is assumed to be in equilibrium with its bulk gas-phase concentration (C_{Ai}=C_{Ae}) at all times greater than zero. When component B is nonvolatile, the concentration gradient ($\partial C_B/\partial x$) at the interface is zero.

If component B is volatile and the gas-phase mass-transfer resistances for both components are not negligible, the boundary conditions must be modified so that the mass flux of each component in the gas phase is equal to its liquid-phase flux measured right at the gas-liquid interface. The gas-phase mass flux was determined by diffusion through a gas-phase film at the interface (Flux = $k_g(p_o-p_i)$). The liquid-phase mass flux at the interface was determined by Fick's law (Flux = $-D_L(\partial c/\partial x)_{x=o}$). The interfacial liquid-phase concentration of both components A and B are assumed to be in equilibrium with their interfacial gas-phase concentrations for all times greater than zero. The dimensionless equations which describe these conditions are

for $\theta > 0$,

$$[\partial A/\partial Z]_{Z=o} = \gamma_A\,(A_i - 1) \tag{2-18}$$

$$[\partial B/\partial Z]_{z=o} = \gamma_B (B_i - B_e) \tag{2-19}$$

where

$$A_i = C_{Ai}/C_{Ae}$$

$$B_i = C_{Bi}/C_{Bo}$$

$$B_e = C_{Be}/C_{Bo}$$

$$\gamma_A = k_{gA} H_A/\{ D_{LA} \sqrt{[k_2 C_{Bo}/D_{LA}]} \}$$

$$\gamma_B = k_{gB} H_B/\{ D_{LB} \sqrt{[k_2 C_{Bo}/D_{LA}]} \}$$

The subscript 'i' indicates the concentration at the interface, 'o' indicates bulk concentrations, and 'e' indicates the liquid concentration that would be in equilibrium with the bulk gas composition according to Henry's Law ($p_{Ao} = H_A C_{Ae}$).

The solution of equations 2-14 and 2-15 followed the procedure used by Brian *et al.* (1961) in which they converted these equations into implicit finite-difference equations of the Crank-Nicholson form, linearized them, and then solved the equations numerically. A few modifications were needed to handle the different boundary conditions that were used in this study. These modifications required that the solution at each time step be found by adjusting the interfacial concentrations A_i and B_i until equations 2-18 and 2-19 were satisfied. The finite-difference equations and a detailed description of their solution on a personal computer are given in Appendix A.

The goal in solving for A and B as functions of θ and Z is to determine the enhancement factor at various values for r, q, γ_A, γ_B, B_e, and θ. Generally the enhancement factor is defined, as in equation 2-3, as the ratio of the liquid-phase mass-transfer coefficient for reactive absorption to the liquid-phase mass-transfer coefficient for physical absorption. The mass-transfer coefficients are based on the average rate of absorption for a given contact time. A numerically equivalent procedure would be to calculate ϕ by the ratio of the total amount of component A that has been reactively absorbed since time zero (Q_{rxn}) to the amount that would

be physically absorbed during that same contact time (Q_{phys})

$$\phi = Q_{rxn}/Q_{phys} \tag{2-20}$$

There is an analytical solution to Q_{phys} for the case of negligible gas-phase mass-transfer resistance; however, if the gas-phase resistance is not negligible, Q_{phys} must be solved for numerically. The partial differential equations which describe physical absorption of component A for the penetration model were made dimensionless by using the same dimensionless variables as were used for reactive absorption (equation 2-3).

$$\frac{\partial^2 A}{\partial Z^2} - \frac{\partial A}{\partial \theta} = 0 \tag{2-21}$$

The same initial conditions and boundary conditions (equations 2-16 and 2-17) that were used in the reactive-absorption case for component A apply here. Equation 2-21 was written as an implicit finite-difference equation and solved numerically by the procedure which is discussed in detail in Appendix A.

Once the concentration profiles for component A are solved as functions of contact time for the reactive absorption and physical absorption cases, Q_{rxn} and Q_{phys} can be calculated by integrating their respective instantaneous absorption rates over the contact time. The instantaneous absorption rate is determined by Fick's Law for diffusion at the interface. For both cases the amount of gas absorbed was calculated by using the dimensionless mass-transfer driving force at the liquid interface, $(\partial A/\partial Z)_{z=o}$.

$$Q = \frac{C_{Ae}}{\sqrt{[\, k_2\, C_{Bo}/D_{LA}\,]}} \int_0^{\theta} \left. \frac{\partial A}{\partial Z} \right|_{z=o} d\theta \tag{2-22}$$

The integrations were performed numerically by using Simpson's Rule.

B. Results

The results of the penetration-model solution for gas absorption accompanied by an irreversible, second-order reaction with a *nonvolatile* dissolved reactant are shown in Figure 2-1, which depicts the relationship between enhancement and $\sqrt{M}$ for different cases of ϕ_a. Also shown as a dashed line is the solution for the case of a pseudo-first-order reaction. When the reaction is slow or the contact time is very short, *i.e.* $\sqrt{M}<<1$, very little reaction occurs in the diffusion layer and the mass-transfer enhancement is negligible. If the reaction is faster and/or the contact time is longer ($\sqrt{M}>1$), the portion of reaction which occurs in the diffusion layer before the liquid mixes back into the bulk liquid becomes significant, and the mass-transfer is enhanced. As long as $\sqrt{M}$ remains below approximately $\phi_a/3$, the enhancement factor falls along the solution for a pseudo-first-order reaction. Above this point, the reaction begins to deplete the concentration of dissolved reactant in the diffusion layer (at very large values of $\sqrt{M}$); the mass-transfer enhancement then levels off and approaches the asymptotic limit for an instantaneous, irreversible, second-order reaction, ϕ_a. In this plateau region the rate of absorption is controlled by diffusion of A into a stagnant liquid, since B is absent from the liquid near the interface.

When dissolved reactant B is both volatile and absent from the gas phase (B_e=0), the mass-transfer enhancement is adversely affected. As is shown in Figure 2-2, the enhancement falls off from that for the nonvolatile case as the volatility parameter, γ_B, increases. Increases in γ_B can result from reduced gas-phase mass-transfer resistance (larger k_{gB}), reduced solubility of the dissolved reactant (larger H_B), or lower liquid-phase molecular diffusivity of B (lower D_{LB}). Less gas-phase mass-transfer resistance and reduced reactant solubility both facilitate the desorption of the dissolved reactant from the liquid. As B is lost from the liquid near

the interface, the local reaction rate is reduced, less A is consumed by reaction, and a corresponding drop in the enhancement results. A lower diffusivity of B will further reduce the enhancement by hindering the resupply of dissolved reactant from the bulk liquid towards the interfacial region. The units of both the numerator and the denominator of γ_B are cm/s. The numerator might thus be considered as a velocity of reactant desorption and the denominator as a velocity of reactant resupply.

Figure 2-3 shows the relationship between volatility and enhancement at various values of ϕ_a and M. For equal diffusivities (r=1), ϕ_a is dependent on only q, the ratio of the concentration of dissolved B in the bulk to the concentration of A that would be in equilibrium with the bulk-gas composition. For larger ϕ_a, there is proportionally more B near the interface to desorb, and therefore the volatility is more detrimental to enhancement. As Shaikh and Varma (1984) found, the enhancement is less sensitive to reactant volatility at both very low and very high values of $\sqrt{M}$. By the penetration model, M is a function of reaction-rate constant and contact time. At low $\sqrt{M}$, either the reaction is too slow to cause any appreciable reduction in A no matter what the concentration of B, or the contact time is too short to allow much B to desorb. At very high $\sqrt{M}$, the reaction may be so fast that very little B can diffuse to the interface to desorb before being consumed by reaction, or the contact time is very long and gives ample opportunity for B to diffuse from the bulk liquid toward the interface to resupply any loss due to desorption.

Figure 2-4 shows the effect on enhancement of the presence of B in the bulk gas. The dimensionless parameter B_e in the figure is the ratio of the concentration of B that would be in equilibrium with the bulk-gas composition to the concentration of B dissolved in the bulk liquid. When no B is present in the bulk gas (B_e=0), the enhancement is adversely affected for the reasons discussed above.

As the amount of B in the bulk gas increases, the enhancement, although reduced in comparison to the nonvolatile case at lower $\sqrt{M}$, eventually exceeds the enhancement for nonvolatile B at higher $\sqrt{M}$. The reason for the improved enhancement can be understood by comparing the concentration profiles (Figures 2-5a and 2-5b) at various values of θ, the dimensionless contact time ($\theta=\pi M/4$). At early contact times ($\theta=3$, $\sqrt{M}=1.5$), the concentration profile of B at the interface is such that B can desorb. Less B in the liquid near the interface prevents the full mass-transfer-enhancing effect caused by reaction, and the enhancement is reduced. At the longer contact times ($\theta=50$, 150, and 750, or $\sqrt{M}=6.3$, 10.9, 24.3), the slope in the concentration profile of B at the interface has changed signs, and the driving force for mass-transfer is such that B (as well as A) is absorbed by the liquid. This replenishment of B from the bulk gas keeps the local concentration of B higher at the interface than would be the case if B were nonvolatile and were only resupplied by diffusion from the bulk liquid. A higher local concentration of B in the liquid at the interface maintains higher local reaction rates and improves the enhancement. As B_e approaches 1.0, the enhancement approaches that obtained for a pseudo-first-order reaction ($\phi=\sqrt{M}$ for $\sqrt{M}>5$). For B_e greater than one, the enhancement would exceed that for a pseudo-first-order reaction.

The effect of gas-side mass-transfer resistance to absorption of A on enhancement is shown in Figure 2-6. The cases shown are for a nonvolatile dissolved reactant ($\gamma_B=0$). The dashed enhancement curves (see eqn. 2-20) are based on physical absorption of A with the same gas-side mass-transfer resistance to absorption of A as for reactive absorption. The dotted-dashed curves are based on physical absorption without gas-side resistance to absorption of A. As expected, the enhancement is hindered as the gas-phase mass-transfer resistance increases (smaller γ_A) from the case of no resistance ($\gamma_A=\infty$). At low values of M the enhancement curves for the same values of γ_A are quite different, but as the contact time

increases (larger M) the curves approach each other. At very long contact times, full enhancement, compared to reactive absorption with no resistance (solid curve), may be achieved.

The minimum enhancement factor for the dashed curves is unity because the rates of reactive absorption and physical absorption are calculated using the same gas-side resistance, and therefore the amount of A reactively absorbed can never be less than the amount that would be physically absorbed. For the dotted-dashed curves the amount of A that is reactively absorbed in the presence of significant gas-side resistance is compared to the amount of A that would be physically absorbed if there were no gas-side resistance. In this case, at early contact times, the gas-side resistance prevents the rate of reactive absorption from being as great as that for physical absorption, and the enhancement factors which result will be less than one.

If the gas-side mass-transfer resistance to absorption of A is appreciable, the resistance will prevent the concentration of A at the interface from achieving equilibrium with the gas (A=1) as would be achieved instantly for the case of no gas-side resistance. Because the interfacial concentration is initially much lower than the equilibrium concentration (A<<1), the rate of absorption is much less than that for the case of no gas-side resistance at the same contact time. The mass-transfer enhancement is, therefore, much lower compared to the enhancement for no gas-side resistance. The low enhancement which results from this situation, however, is eventually recovered at long contact times.

In nonsteady-state absorption the rate of absorption always decreases with time as the concentration of the absorbing gas in the liquid near the interface increases since the concentration gradient of A in the liquid is reduced. The lower concentration gradient provides an increase in the liquid-side resistance to diffusion of A into the liquid. With a decreasing rate of absorption of A caused by an

increasing liquid-side resistance, the gas-side resistance to absorption of A becomes less significant and the interfacial concentration of A slowly increases towards equilibrium with the bulk gas. As the contact time increases, the rate of absorption for the case with an initially significant gas-side resistance approaches the rate of absorption without any gas-side resistance. Eventually, most of the dissolved B near the interface has been depleted by reaction with A. The rate of absorption of A then becomes controlled by the rates of molecular diffusion of A and B toward the reaction zone, with A diffusing from the surface and B diffusing from deep in the liquid. When this situation occurs, the enhancement has reached its maximum value, ϕ_a. Because the initial rate of absorption of A is higher when there is no gas-side resistance to absorption of A, ϕ_a is reached sooner.

In Figure 2-7 the solution of Hikita, *et al.*, (1979) is compared to the results of the present study for a case in which the ratio of the diffusivities, r, is equal to one. The agreement is quite good (within 6%) over the range shown. The curve generated for the nonvolatile-reactant case by the present study lies above the Hikita curve over most of its range. In Figure 2-1 the curves of the present study lie slightly above the curve, obtained from equation 2-8, for a pseudo-first-order reaction. It is concluded that the present study is slightly over-predicting enhancement factors at lower values of M. The good agreement between the present study and that of Hikita, *et al.*, and the ease of computation of their solution indicate that the Hikita solution should be used when the ratio of the diffusivities (r) is very near one.

If the ratio of the diffusivities is not near one, the two solutions would diverge since the mass-transfer rates of the two models are based on different dependencies on diffusivity. Figure 2-8 shows the divergence between the two models when r is equal to 0.5 and q is equal to 10. The solid lines represent the penetration-model solution by this study. By equation 2-12, the limiting enhance-

ment, ϕ_a, is approximately 8.5. The dashed line represents the solution of Hikita for the film model, and for the same r and q the limiting enhancement is 6.0 by equation 2-11. It can be seen that the film model solution greatly underestimates the enhancements that are predicted by the penetration model for the same values of r and q. If, however, the film-model is solved for the case where ϕ_a is the same as that for the penetration model, much better agreement between the two models at the higher values of $\sqrt{M}$ is achieved (dotted-dashed line). If gas-side mass-transfer resistance to the absorbed gas is important, or if concentration profiles of A and B are desired at any contact time, the penetration model solution by the present study should be used.

C. Enhancement of H_2S absorption by solutions of SO_2

To determine the mass-transfer enhancement for H_2S absorption by solutions of SO_2 in the primary absorber of the UCBSRP, it is necessary to estimate the values of r, q, M, γ_A, γ_B, and B_e. The pressure of the primary absorber will be about 2500 kPa, and the temperature will average about 40°C. The value of r can be estimated by using the Wilke-Chang correlation for molecular diffusivity in liquids, (Sherwood, *et al.*, 1975). To estimate q, concentrations on the trays must be estimated. It is on the upper trays of the lower section of the primary absorber where most of the reactive absorption of H_2S occurs. On these trays the concentration of dissolved SO_2 in the solvent is at its highest, approximately 0.00035 m.f.; and the concentration of H_2S in the gas is at its lowest, approximately 10 ppm. The value of q is, therefore, maximized here. On these upper trays the concentration of SO_2 in the gas will also be at its highest and will be nearly in equilibrium with its liquid-phase concentration. The contact time of the gas with the liquid on a sieve tray of the primary absorber will be used as the exposure time of the liquid to the gas for the penetration model, although this exposure time is probably greatly overestimated. Gas solubilities were calculated by the correlations of Sciamanna

(1986). The gas-phase mass-transfer coefficients and gas contact time were estimated by the correlations of Chan and Fair (1984), and an assumed value of the interfacial area per unit volume of 3 cm^2/cm^3 was used. The second-order reaction-rate constant was estimated to be 100 liters/mole-s. Table 2.1 lists the estimated values of the parameters which affect enhancement.

The results of the penetration-model solution for the conditions of Table 2.1 is shown in Figure 2-9. At the estimated value of M equal to 0.3, the predicted enhancement is less than three percent and will be neglected. Because the value of q is very high compared to the small value of M, the reaction occurs in the pseudo-first-order regime. The effect of gas-side mass-transfer resistance and the volatility of SO_2 does not have any effect on mass-transfer enhancement of H_2S absorption at such small values of M.

List of Tables for Chapter 2

2.1 Parameters Affecting Enhancement of H_2S Absorption

List of Figures for Chapter 2

2-1 Effect of M and ϕ_a on Enhancement Factor for a Nonvolatile Reactant

2-2 Effect of Reactant Volatility on Enhancement

2-3 Effect of Volatility on Enhancement at Various ϕ_a

2-4 Effect of B_e and M on Enhancement Factor

2-5a Effect of Contact Time, θ, on Concentration Profiles of Component B

2-5b Concentration Profiles of Component B Near Gas-Liquid Interface

2-6 Effect of Gas-Side Resistance to Absorption on Enhancement

2-7 Comparison of Hikita's Model to Present Study

2-8 Comparison of Hikita's Model to Present Study at r = 0.5

2-9 Predicted Enhancement for H_2S Absorption in Primary Absorber

Table 2.1: Parameters Affecting Enhancement of H_2S Absorption

Temp.	= 313°K	Press.	= 2500 kPa
A	= H_2S	B	= SO_2
D_{LA}	= 1.43E-5 cm^2/s	D_{LB}	= 1.18E-5 cm^2/s
H_A	= 1.35E+3 kPa cm^3/mol	H_B	= 1.10E+2 kPa cm^3/mol
k_{gA}	= 9.3E-7 mol/kPa-cm^2-s	k_{gB}	= 8.3E-7 mol/kPa-cm^2-s
p_A	= 2.5E-2 kPa	B_o	= 2.9E-6 mol/cm^3
t_v	= 0.44 s		

Dimensionless Parameters

r	= 0.83	q	= 18
ν	= 0.5	φ_a	$\simeq$ 34
γ_A	= 62	γ_B	= 5.4
M	= 0.3	B_e	= 0.99

Figure 2–1: Effect of M and φ_a on Enhancement Factor for a Nonvolatile Reactant

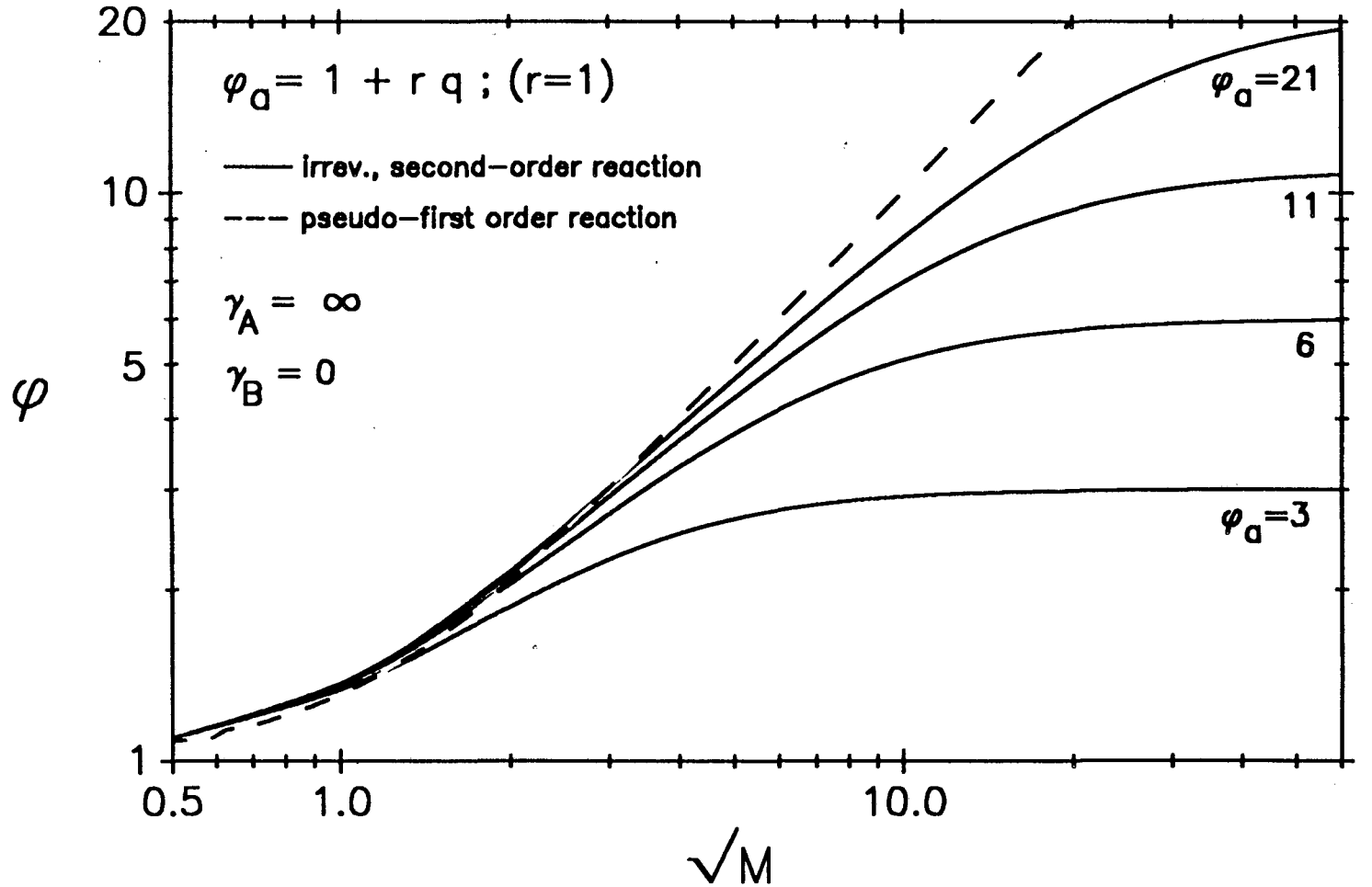

Figure 2–2: Effect of Reactant Volatility on Enhancement

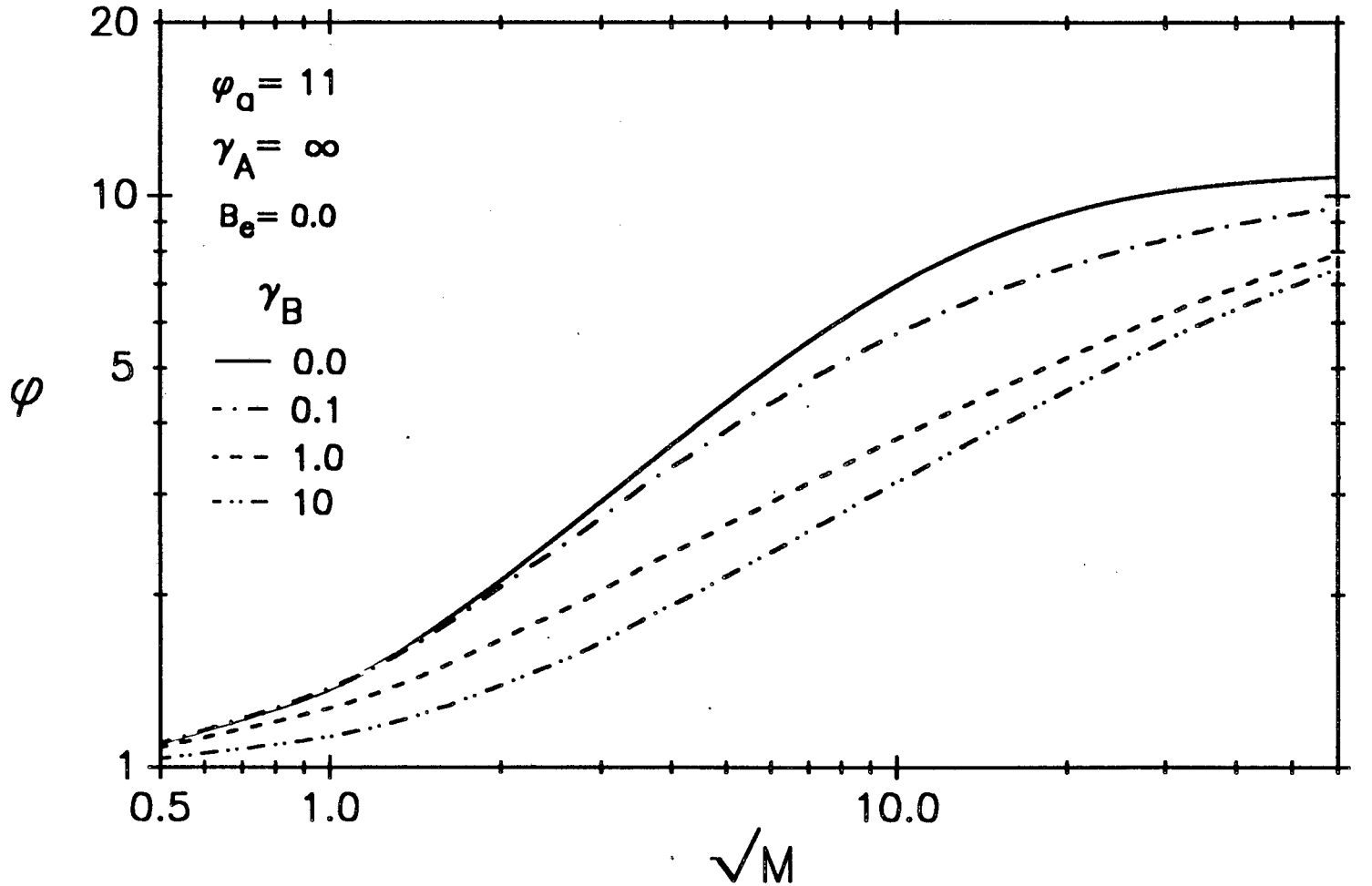

Figure 2–3: Effect of Volatility on Enhancement at Various φ_a

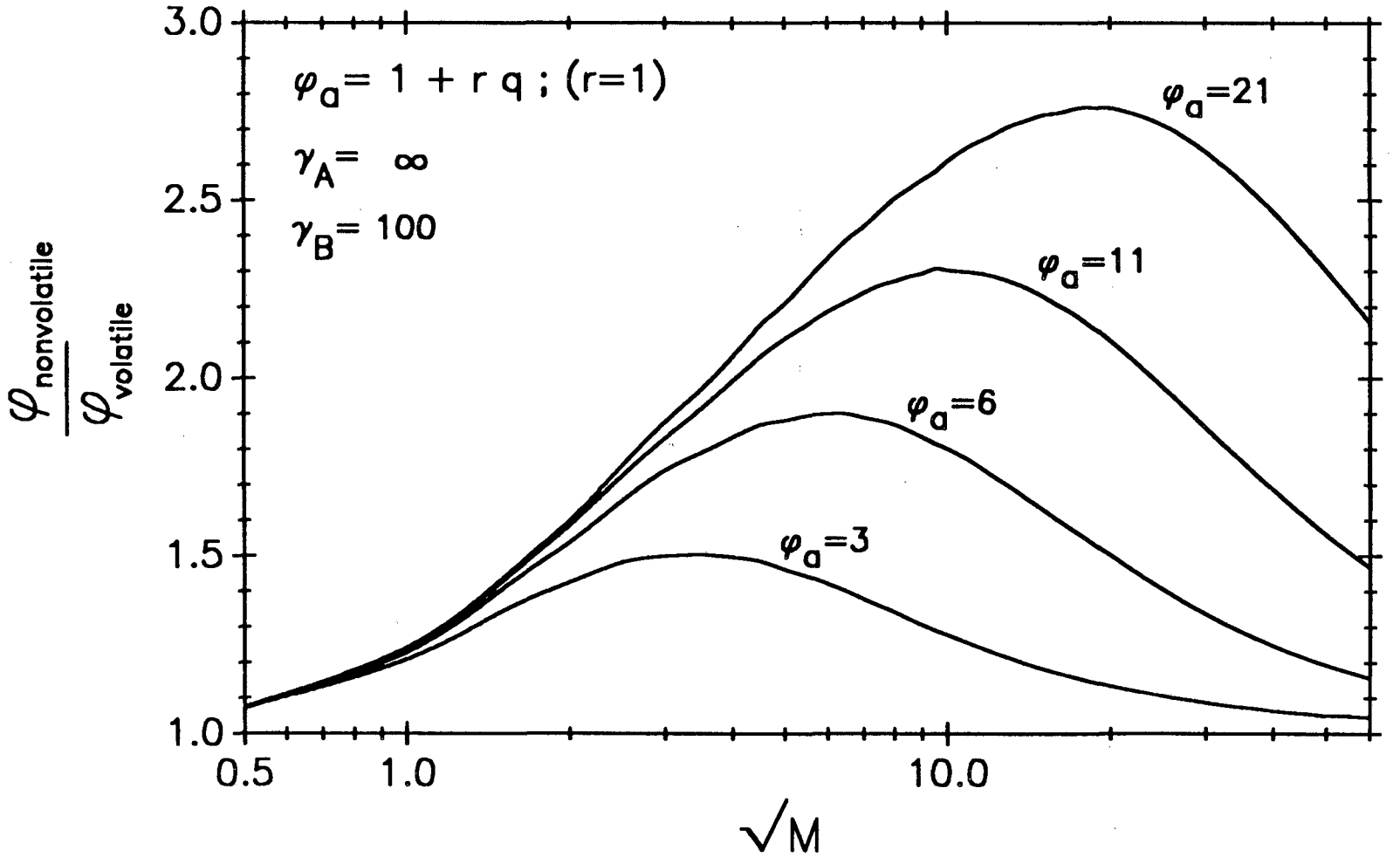

Figure 2–4: Effect of B_e and M on Enhancement Factor

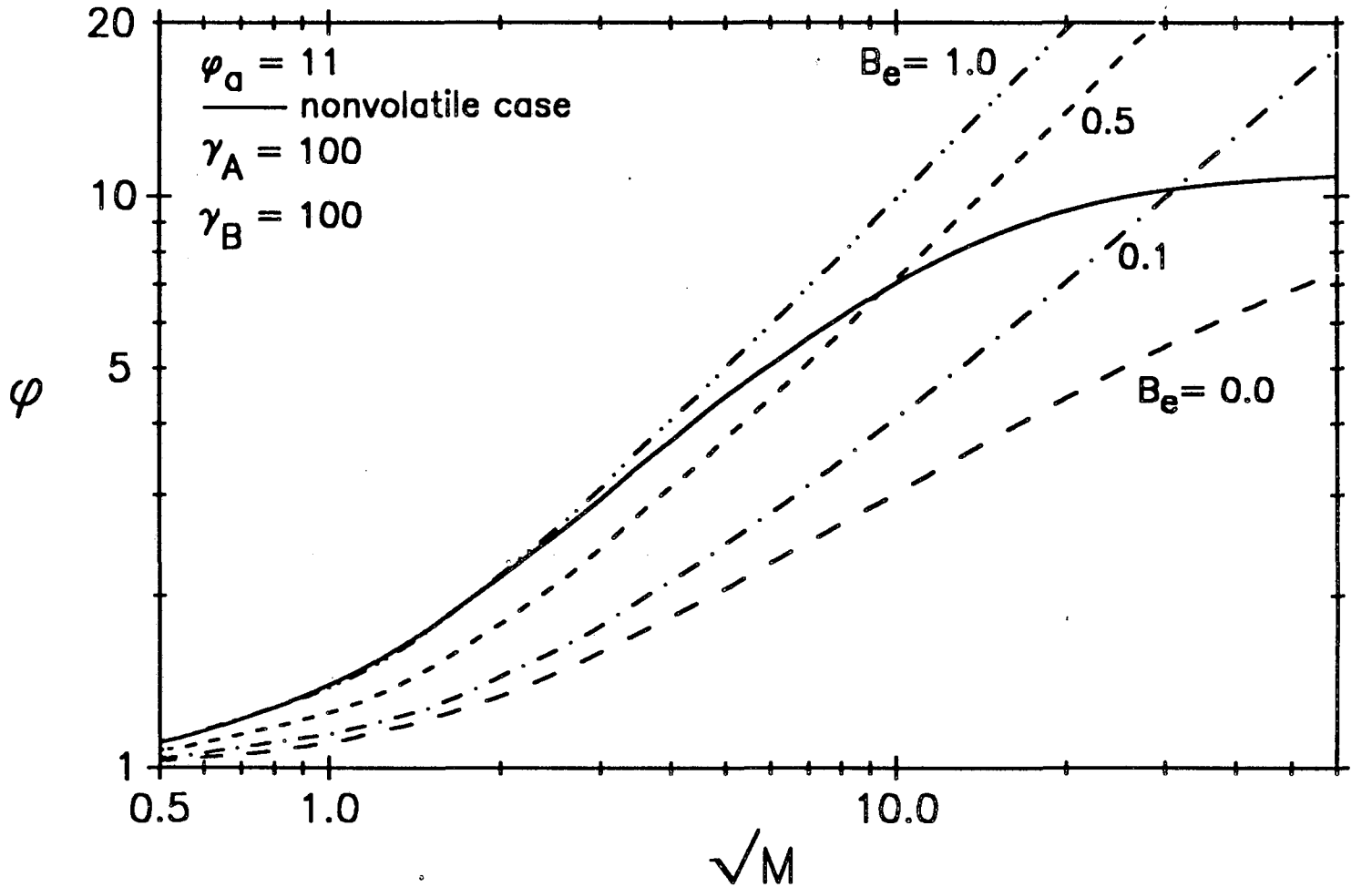

Figure 2–5a: Effect of Contact Time, θ, on Concentration Profiles of Component B

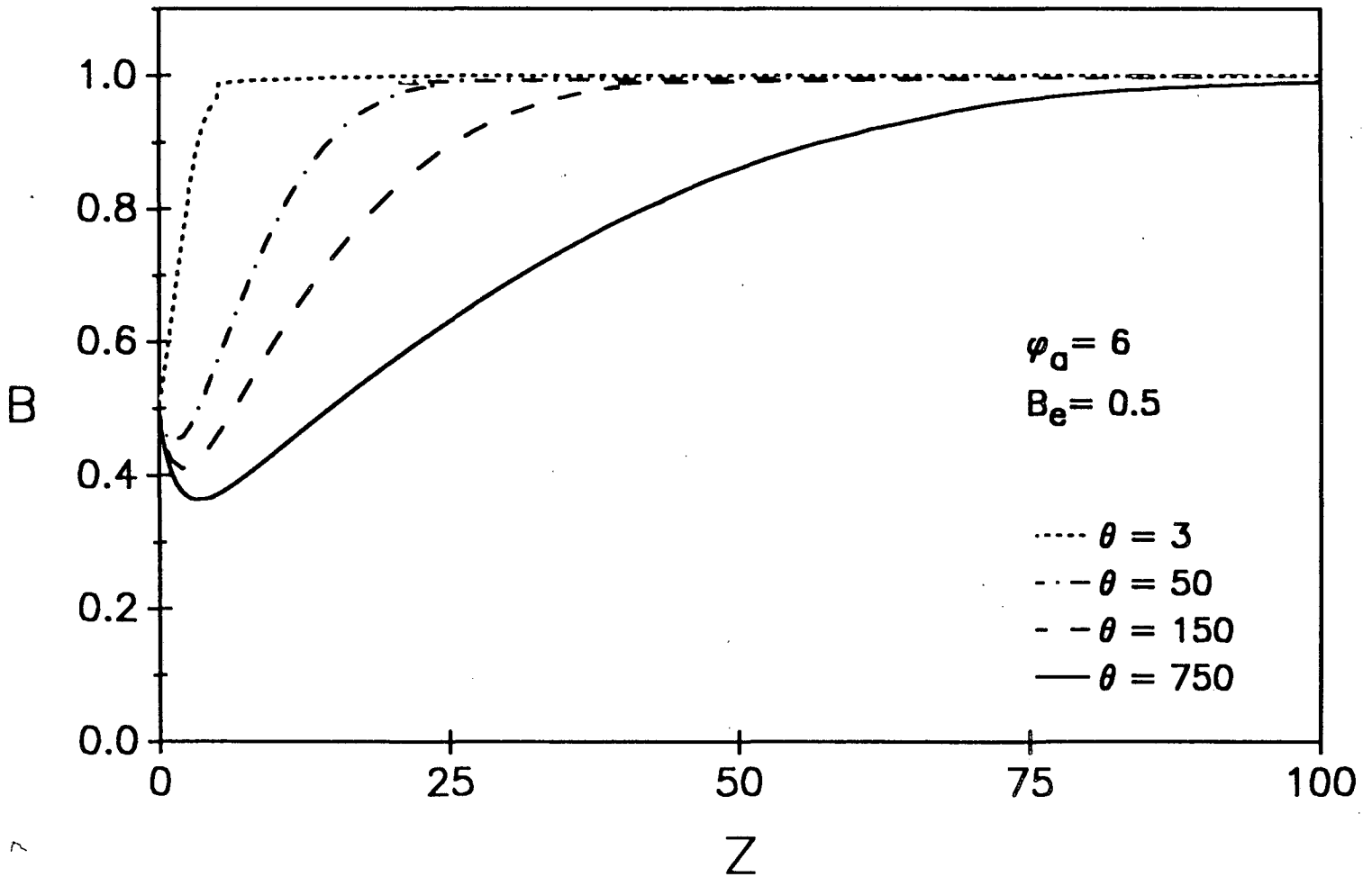

Figure 2–5b: Concentration Profiles of Component B Near Gas–Liquid Interface

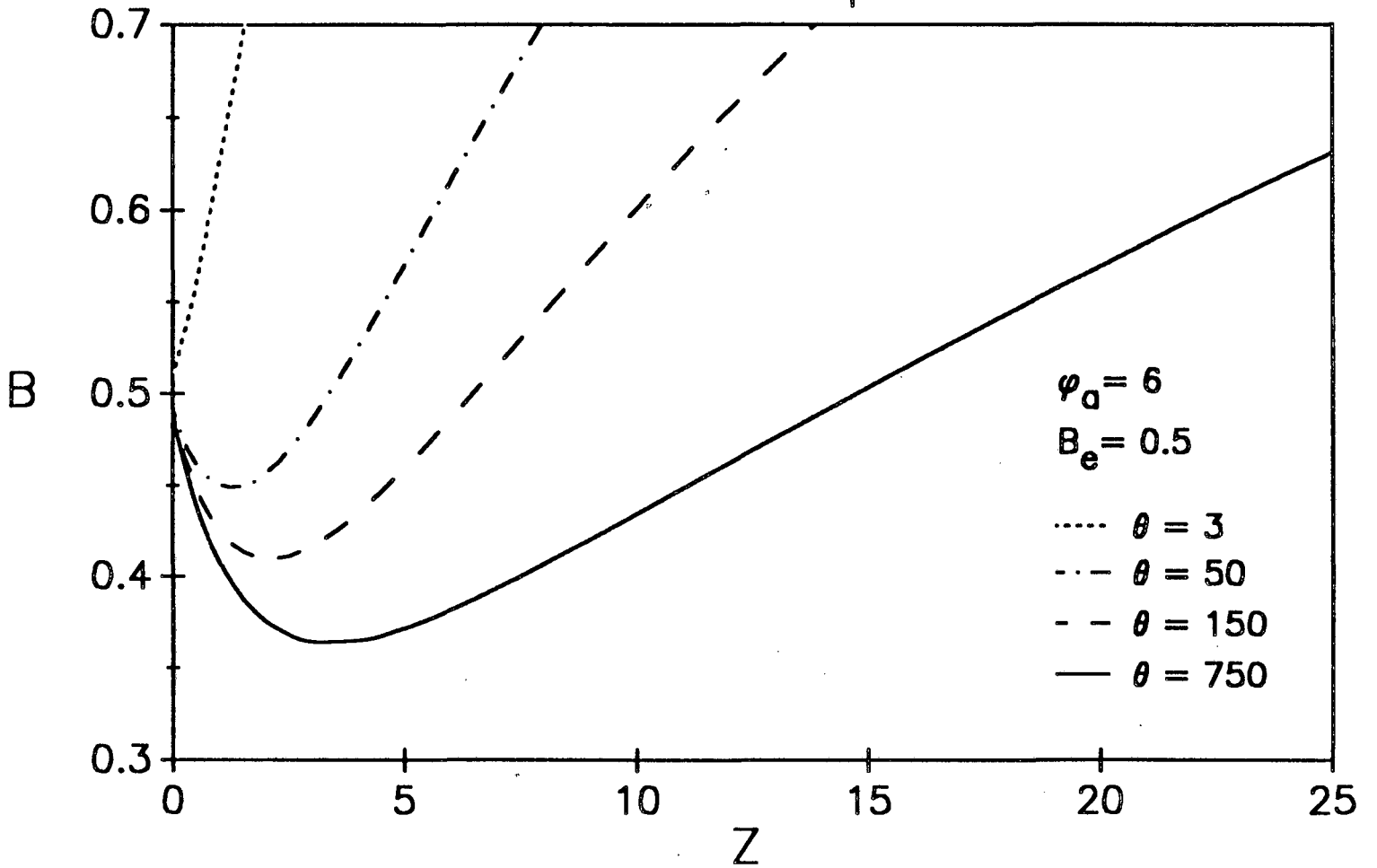

Figure 2–6: Effect of Gas–side Resistance to Absorption on Enhancement

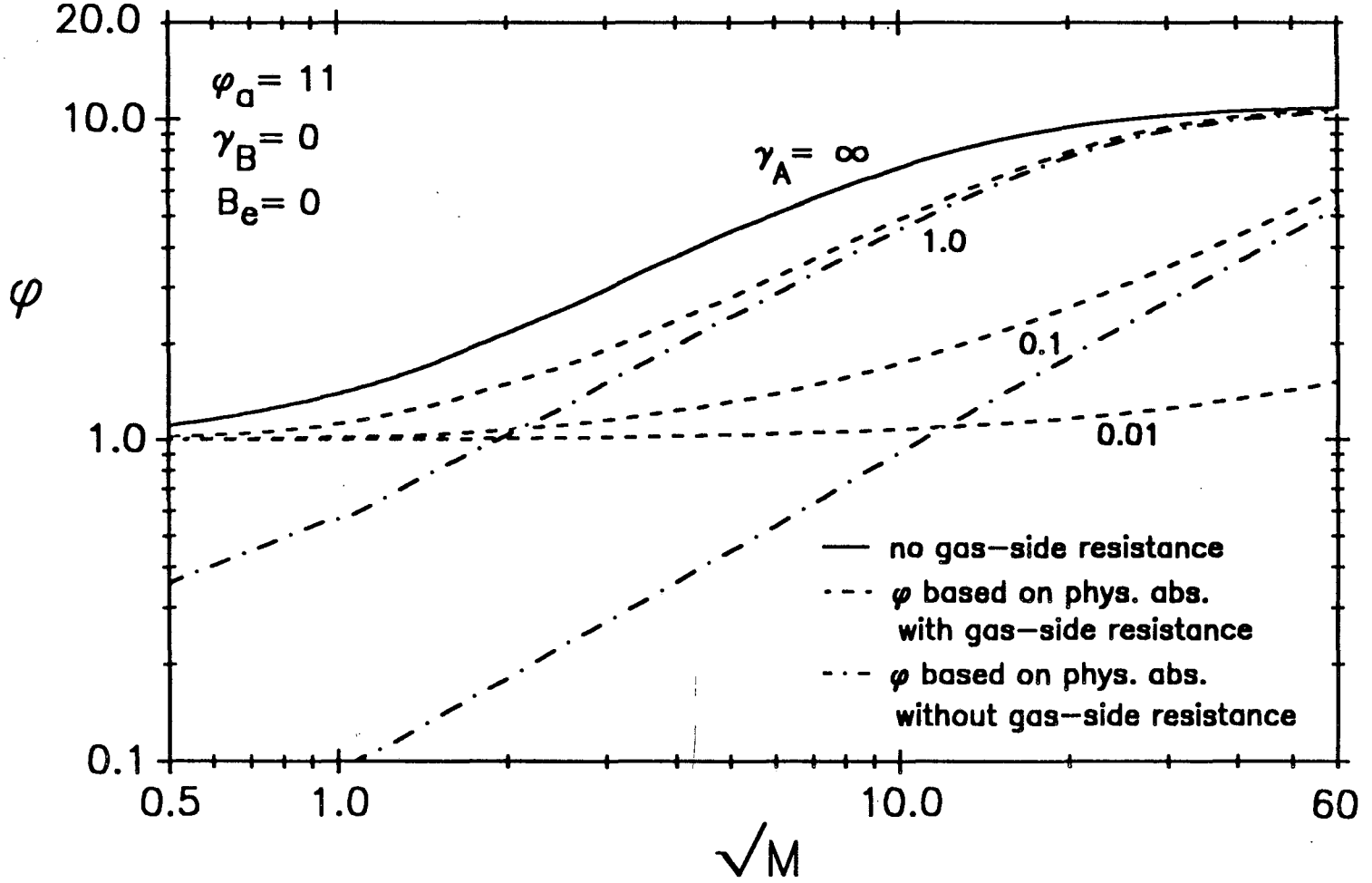

Figure 2–7: Comparison of Hikita's Model to Present Study

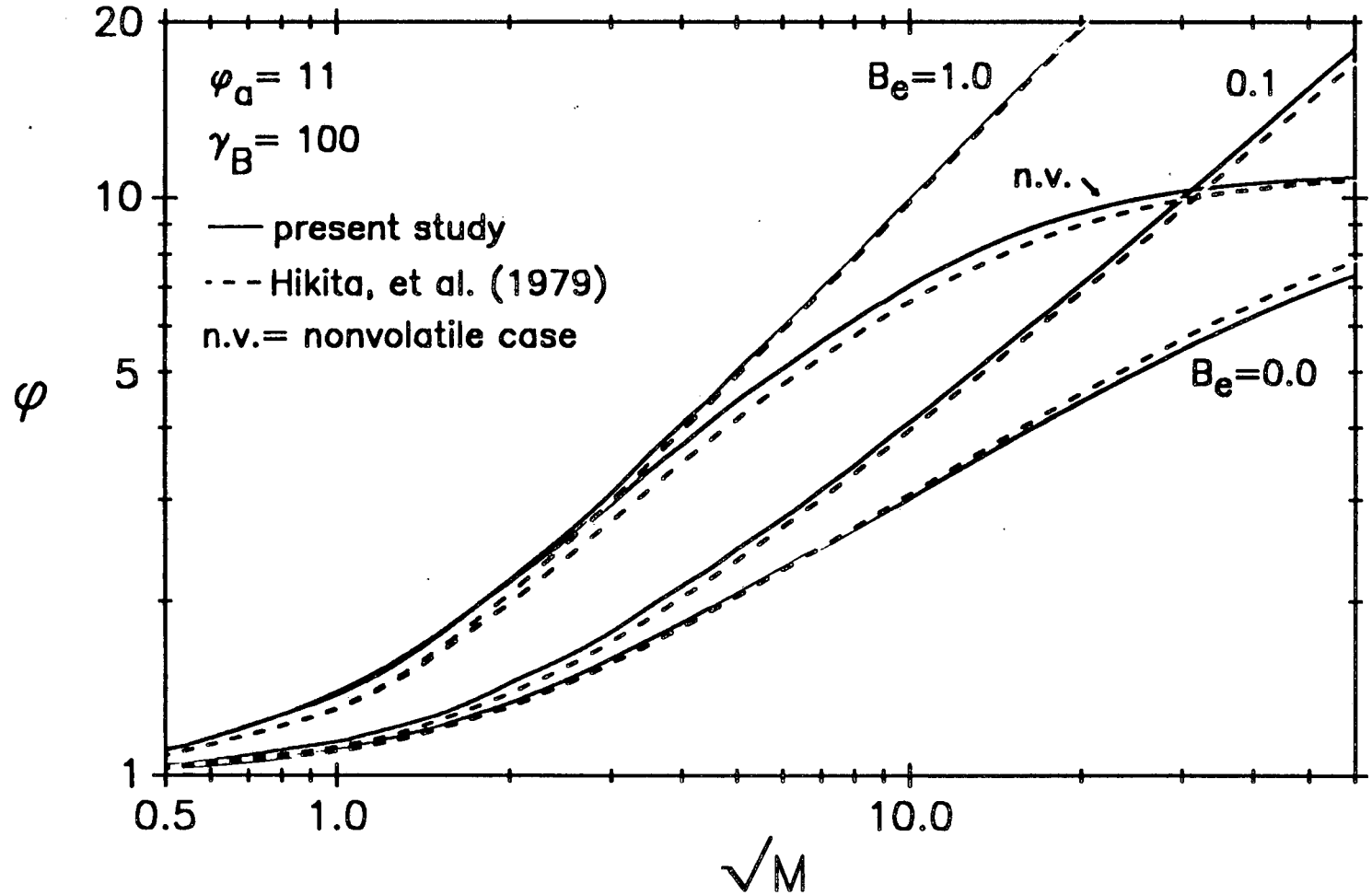

Figure 2–8: Comparison of Hikita's Model to Present Study at r = 0.5

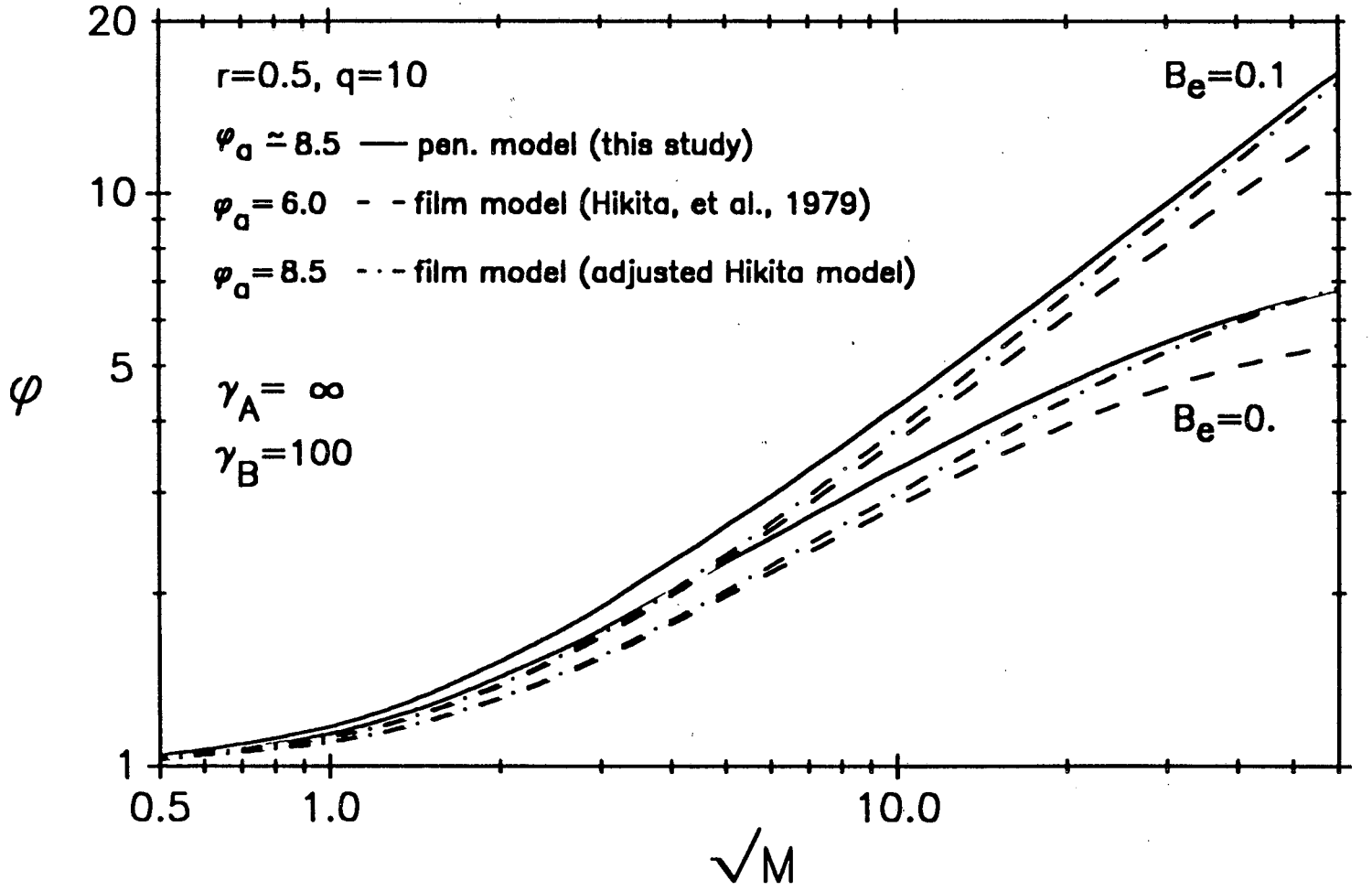

Figure 2–9: Predicted Enhancement for H_2S Absorption in Primary Absorber

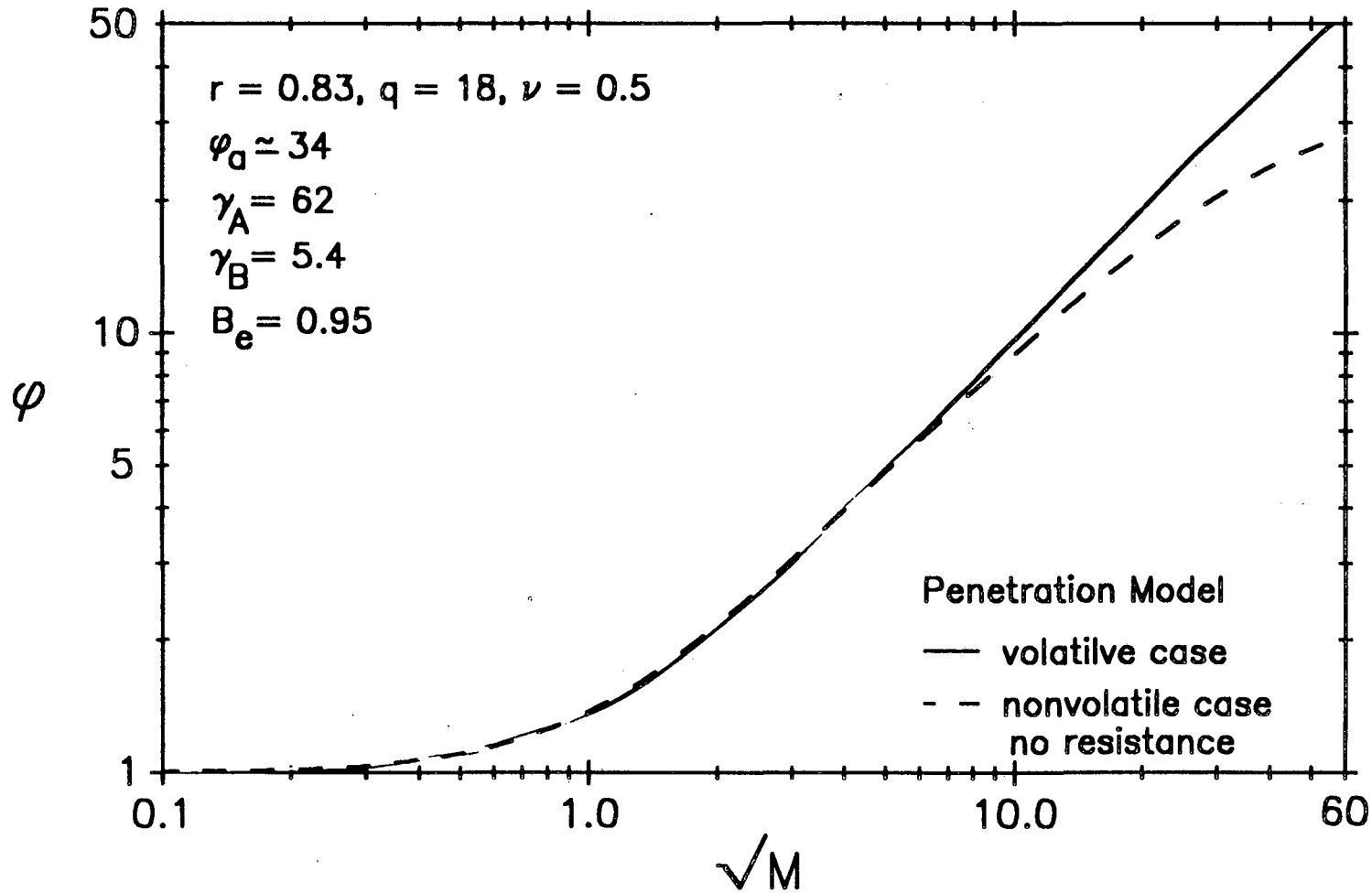

3. TRAY-EFFICIENCY THEORY

3.1 Introduction

When designing an absorber, one needs to know the average tray efficiency to calculate the number of trays required to achieve a desired separation. Chemical engineers work with several types of efficiencies: overall column efficiency, the Murphree liquid and vapor tray efficiencies, and the point efficiency. Point efficiency is the efficiency of mass transfer at a location on the tray with an area small enough that the liquid contacting the gas at that location can be assumed to have uniform composition. Point efficiencies are extremely difficult to measure, but there are procedures, as will be discussed in section 3.2, for estimating their values. Point efficiencies are very useful because they can be used to calculate efficiencies for the entire tray. The Murphree tray efficiencies are efficiencies for the whole tray and are based on either the liquid-phase or gas-phase compositions. In general, tray efficiency is a complex function of gas and liquid flow, tray geometry, gas solubility, and fluid properties such as viscosity and density; however, the Murphree tray efficiency is fairly easy to measure as it requires only measuring the bulk compositions of the gas and liquid. By knowing the tray efficiency, the overall column efficiency can be calculated. Dividing the number of equilibrium stages required to meet an exit-gas specification by the overall column efficiency gives the number of actual trays that is necessary to achieve this separation.

If equipment, manpower, money, and time are available, one may choose to measure the tray and column efficiencies and then use the results to design a column. Often, it is more cost- and time-effective to estimate the efficiencies by procedures that have been shown to be reliable for the system and conditions of interest. In this study, Murphree vapor sieve-tray efficiencies will be measured for physical absorption of H_2S and SO_2 by diethylene glycol methyl ether (DGM) at

near-atmospheric pressure and moderate temperatures. Because the absorption apparatus cannot withstand very high pressures, a tray-efficiency model which accurately predicts the measured low-pressure efficiencies will be used to estimate tray efficiencies necessary for designing the high-pressure primary absorber of the UCBSRP.

3.2 Tray-Efficiency Models

One of the most readily available and widely used procedures for estimating tray efficiencies is the procedure developed in the late 1950's by the American Institute of Chemical Engineers (AIChE). A concise summary of the AIChE tray design method is given in King (1980). This procedure uses mass-transfer correlations first to predict the point efficiency and then to convert the point efficiency to a Murphree tray efficiency. The basic procedure, without presenting the AIChE correlations, is given below.

Point efficiency, E_{ov}, is defined as

$$E_{ov} = (y_{in} - y) / (y_{in} - y^*) \tag{3-1a}$$

where

$$y^* = m\, x_{loc} \tag{3-1b}$$

The inlet and outlet gas compositions to and from the element of solvent are y_{in} and y respectively; y^* is the gas composition that would be in equilibrium with x_{loc}, the uniform composition of the solvent at the location of interest. The slope of the equilibrium line is m. A more useful equation for estimating the point efficiency has been derived by analyzing the mass-transfer process by using the addition-of-resistances theory along with the assumption that the gas moves upward, in plug flow, through a well-mixed liquid. The results of the derivation are

$$E_{ov} = 1 - \exp\{ -N_{ov} \} \tag{3-2}$$

where N_{ov} is the number of mass-transfer units based on the overall gas-phase mass-transfer driving force. The overall number of transfer units is related to number of transfer units based on the mass-transfer driving forces of the individual phases by

$$N_{ov} = [1 / N_v + \lambda / N_L]^{-1} \tag{3-3}$$

where

$$N_v = k_v a_i t_v \tag{3-4}$$

$$N_L = k_L a_i t_L \tag{3-5}$$

$$\lambda = (m V)/L \tag{3-6}$$

If the individual gas- and liquid-phase mass-transfer coefficients, $k_v a_i$ and $k_L a_i$, and their respective contact times, t_v and t_L, are known or can be estimated reasonably by correlations, the number of gas- and liquid-phase mass-transfer units, N_v and N_L, can be determined. The interfacial area per unit volume, a_i, is assumed to be the same for each phase. To calculate N_{ov} by equation 3-3, one needs to know λ, the ratio of the slope of the equilibrium line, m, to the slope of the operating line, L/V. The point efficiency is then calculated by equation 3-2. It still remains to convert the point efficiency to a Murphree tray efficiency.

Murphree vapor tray efficiency, E_{mv}, as defined by equations 3-7a and b below, is a measure of how close the change in gas composition across a tray approaches the composition change that would occur if the gas were to leave the tray in equilibrium with the liquid exiting the tray. The gas streams above and below the tray are assumed to be perfectly mixed.

$$E_{mv} = (y_{in} - y_{out}) / (y_{in} - y^*) \tag{3-7a}$$

where

$$y^* = m\, x_{out} \tag{3-7b}$$

The equilibrium backpressure of the absorbed gas, y^*, for the Murphree vapor tray efficiency is based on the concentration of dissolved gas in the solvent at the tray outlet, x_{out}, whereas the point efficiency is based on local solvent concentration, x_{loc}, which may be changing as the solvent flows across the tray. By using an eddy-diffusion model for crosscurrent flow to describe liquid mixing on the tray, and by assuming that the inlet gas is perfectly mixed, the two efficiencies can be related to each other through λ and the dimensionless Peclet number, *Pe*, (King, 1980).

$$\frac{E_{mv}}{E_{ov}} = \frac{1 - e^{-(\eta+Pe)}}{(\eta+Pe)[1 + (\eta+Pe)/\eta]} + \frac{e^{\eta} - 1}{\eta\,[1 + \eta/(\eta+Pe)]} \qquad (3\text{-}8)$$

where

$$\eta = \frac{Pe}{2}\left([\,1 + 4\,\lambda\,E_{ov}/Pe]^{1/2} - 1\right) \qquad (3\text{-}9)$$

and

$$Pe = Z_L^2 / (\,D_e\,t_L\,) \qquad (3\text{-}10)$$

The length of the liquid flow path, Z_L, is the distance between the inlet and outlet weirs on the tray. The eddy diffusivity, D_e, must be measured experimentally or be calculated from correlations.

Two limiting regimes are encountered. For complete mixing of the solvent on the tray, corresponding to *Pe* equal to zero, E_{mv} is equal to E_{ov}. When the solvent flows across the tray in plug flow, corresponding to *Pe* equal to infinity, the maximum improvement of E_{mv} over E_{ov} is obtained, and equation 3-8 reduces to

$$E_{mv} = (\,e^{\lambda\,Eov} - 1\,)\,/\,\lambda \qquad (3\text{-}11)$$

The accuracy of this efficiency-prediction procedure depends on how good

the mass-transfer correlations are for the system of interest. Chan and Fair (1984) have outlined much of the recent work done to improve the original correlations that were presented in the AIChE report. By using the best correlations from the literature in addition to developing their own mass-transfer correlation for $k_v a_i$, they were able to improve greatly the accuracy of their efficiency predictions over the predictions by the AIChE model. Their model was tested on a data sample of 143 binary-system distillation tray efficiencies collected on a variety of commercial-scale sieve trays at pressures that ranged from about 13 kPa to 2800 kPa. The average absolute deviation for the Chan and Fair model was 6.3% as compared to 22.9% for the AIChE model. The correlations that are recommended by Chan and Fair are present tions are given in the nomenclature at the end of this chapter.

The average liquid residence time

$$t_L = (h_L A_a) / (100 Q_L) \tag{3-12}$$

requires a value for the height of clear liquid hold-up on the tray, h_L,

$$h_L = \phi_e h_w + 1533 \phi_e C (q_L/\phi_e)^{2/3} \tag{3-13}$$

where

$$\phi_e = \exp\{ -12.55 K_s^{0.91} \} \tag{3-14}$$

$$C = 0.0327 + 0.0286 \exp\{ -1.378 h_w \} \tag{3-15}$$

$$K_s = U_a [\rho_v / (\rho_L - \rho_v)]^{1/2} \tag{3-16}$$

The liquid-phase mass-transfer coefficient (s^{-1}) is obtained by

$$k_L a_i = (0.40 F_{va} + 0.17) (197 D_L^{1/2}) \tag{3-17}$$

where

$$F_{va} = U_a \rho_v^{1/2} \tag{3-18}$$

F_{va} is the active area F-factor, and D_L is the liquid-phase molecular diffusivity. The gas velocity, U_a, is based on the active area of the tray, and ϕ_e is the effective

relative froth density, which is equal to the liquid hold-up height divided by the average froth height.

The average gas-phase contact time, t_v, is based on the gas rising in plug flow through a froth

$$t_v = (1 - \phi_e) h_L / (100 \phi_e U_a) \tag{3-19}$$

To develop their correlation for $k_v a_i$ (s^{-1}), Chan and Fair backed out values for $k_v a_i$ from their data bank of tray efficiencies, and then used computer routines to fit various combinations of variables to the data. The expected theoretical dependence of $k_v a_i$ on these variables was used in deciding which combinations to try. The best fit gave the following relationship in terms of the gas-phase molecular diffusivity, D_v, the fractional approach of the gas velocity to flooding, f, and the height of clear liquid on the tray.

$$k_v a_i = D_v^{1/2} (1030 f - 867 f^2) / (h_L)^{1/2} \tag{3-20}$$

where

$$f = U_a / U_{af} \tag{3-21}$$

Because the Chan and Fair $k_v a_i$ correlation was fit to the mass-transfer coefficients that were calculated from the same data bank that was used to compare their model to the AIChE model, it is no surprise that their model would perform better than the AIChE model. However, because the data bank contained efficiencies for such a wide variety of systems, operating conditions, and tray designs, it is felt that the Chan and Fair model is superior.

For the present study the gas and liquid molecular diffusivities will be estimated by the Wilke-Chang equation for D_L and the equation of Fuller, Schettler and Giddings for D_v, (Sherwood, *et al.*, 1975). The point efficiency can now be calculated by equation 3-2 after obtaining N_{ov} from equation 3-3. To convert

E_{ov} to E_{mv} by equation 3-8, Chan and Fair recommend the following correlation for D_e, which is needed to calculate the Peclet number.

$$D_e = 6.675(10^{-3})\, U_a^{1.44} + 0.922(10^{-3})\, h_L - 5.62(10^{-3}) \qquad (3\text{-}22)$$

In interpreting the work presented below, the accuracy of the Chan and Fair model for prc will be checked by determining the Murphree vapor tray efficiencies for these systems. To calculate E_{mv} by equation 3-7a, one needs to know the inlet and outlet gas compositions, y_{in} and y_{out} respectively, the concentration of gas dissolved in the solvent leaving the tray, x_{out}, and the equilibrium relationship, m, for the gas solubility in the solvent. The gas and liquid compositions were determined during operation of the absorber apparatus described in Chapter 4. The equilibrium relationships have been expressed as Henry's Law correlations for H_2S and SO_2 in DGM by Sciamanna (1986). These correlations will be discussed in Chapter 5.

3.3 Tray Efficiency for Absorption with Chemical Reaction

If absorption with chemical reaction is occurring, the liquid-phase mass-transfer coefficient may increase relative to the coefficient for strictly physical absorption due to the reaction depleting the concentration of the absorbed gas near the gas-liquid interface. To obtain this enhancement, a significant portion of the reaction must occur in the liquid diffusion film near the gas-liquid interface rather than in the bulk solvent. This case corresponds to the square root of the Hatta number, $M = k_2\, C_{Bo}\, D_L/k_L^2$, being of the order one or larger (Dankwerts, 1970). When this is the case, $k_L a_i$ should be multiplied by an enhancement factor, $\phi \geq 1$, to obtain the liquid-phase mass-transfer coefficient for reactive absorption, $k_L^* a_i$, which is then used in equation 3-5 to obtain N_L.

$$k_L^* a_i = \phi\, k_L a_i \qquad (3\text{-}23)$$

To find ϕ, an appropriate mass-transfer model, such as the film model, Higbie penetration model or the Dankwerts surface-renewal model, must be chosen. The reaction regime (slow, fast, or instantaneous), the order of the reaction, and the reaction equilibrium (reversible or irreversible) must be determined. Then, as discussed in Chapter 2, a value for the enhancement factor may be obtained from one of the well-known solutions to the differential equations that describe absorption with chemical reaction under these models.

If the tray is well-mixed ($Pe = 0$) the calculation of E_{mv} is straightforward. However, a more rigorous treatment (Pohorecki, 1983 a, b, c) is required when the enhancement factor is a function of one or more of the reactant concentrations and these concentrations vary along the liquid-flow path on the tray. In this case the point efficiency will vary with concentration across the tray and will complicate the calculation of E_{mv}. Pohorecki used the film model to analyze the effect of slow and fast irreversible first-order and pseudo-first-order reactions on the Murphree vapor tray efficiency. A numerical solution of the differential equation that describes diffusion and reaction in crosscurrent flow provided the concentration profile of the bulk concentration of the dissolved reactant with position across the tray. This solution provided a profile of point efficiency with position on the tray which was integrated across the tray to give E_{mv}.

One of the assumptions Pohorecki made which greatly simplified the point efficiency equation was that the equilibrium backpressure of the absorbed gas (y^*) was zero. This is a good assumption for very fast reactions in which most of the absorbed gas reacts in the film and never makes it to the bulk solvent. For slow reactions very little reaction occurs in the diffusion film. Most of the absorbed gas passes into the bulk liquid where it reacts, and y^* should properly reflect the actual concentration of absorbed gas in the bulk liquid. This presents a problem if one desires to determine E_{mv} since it would require an *in situ* method of measuring

the concentration of dissolved gas right at the tray outlet in order to calculate y^*. However, in the case of slow reactions, because very little reaction is occurring in the liquid film near the interface, no mass-transfer enhancement is expected, and the tray efficiency for absorption with slow reaction should be equal to the tray efficiency for physical absorption. If the presence of a catalyst or of the dissolved reactant or product affects the solubility of the absorbed gas, the new gas solubility must be used in calculating the tray efficiency.

3.4 Reaction in the Bulk Liquid on the Tray

In well-mixed flow absorber operating at steady-state, as for example a sieve-tray absorber, the concentrations of dissolved gas and reactants are uniform throughout the bulk liquid on the tray and remain constant over time. The absorber can then be modeled as a continuously-stirred-tank reactor (CSTR). The design equation for a sieve tray acting as a CSTR/absorber requires the flow of dissolved component A in the liquid being fed to the tray plus the rate of absorption of A from the gas to be equal to the flow of dissolved, unreacted A that leaves the tray plus the rate at which A is consumed by reaction while the liquid is on the tray. For reaction 2-9 with rate expression 2-10, the design equation is

$$Q_L C_{Ain} + \phi\, k_L a_i\, (C_{Ai} - C_{Ao}) = Q_L C_{Ao} + H_L k_2\, C_{Ao} C_{Bo} \qquad (3\text{-}24)$$

where Q_L is the volumetric flow of liquid to and from the tray and H_L is the hold-up (volume) of liquid on the tray. By rearranging and introducing τ as the residence time (Q_L/H_L) of the liquid in the tray, the equation becomes

$$\bar{R} a_i = \phi\, k_L a_i\, (C_{Ai} - C_{Ao}) = (C_{Ao} - C_{Ain})/\tau + k_2\, C_{Ao}\, C_{Bo} \qquad (3\text{-}25)$$

For a *very* slow reaction, of course, the enhancement factor is equal to one, and the reaction term on the right-hand side of the design equation is negligible.

For this case the reaction has no effect on the rate of absorption ($\overline{R}a_i$), and both the rate of absorption and the tray efficiency will be the same as for strictly physical absorption of the gas.

A slow reaction is one for which the reaction term is not negligible although the enhancement factor is still equal to one. For the enhancement factor to be one while substantial reaction is occurring in the bulk solution, the condition that the rate of reaction in the film is much less than the rate of absorption must be satisfied (Dankwerts, 1970). On a per unit interfacial area basis this requires that

$$\delta \; r_A << k_L \, (C_{Ai} - C_{Ao}) \tag{3-36}$$

Within the film, the reaction rate varies with depth, but the maximum concentrations of A and B (C_{Ai} and C_{Bo} respectively) set the maximum reaction rate in the film ($r_A = k_2 C_{Ai} C_{Bo}$) for comparison purposes. The film thickness, δ, is D_{LA}/k_L, so the condition becomes

$$D_{LA}/k_L \; k_2 \, C_{Ai} \, C_{Bo} << k_L (C_{Ai} - C_{Ao}) \tag{3-27}$$

Because the reaction in the bulk liquid is substantial, C_{Ao} is small compared to C_{Ai}, and the condition for negligible reaction in the film becomes

$$M = D_{LA} \, k_2 \, C_{Bo}/k_L^2 << 1 \tag{3-28}$$

When the condition of equation 3-28 is met, the tray efficiency will remain unchanged from the efficiency for physical absorption even though the rate of reaction in the bulk liquid on the tray is appreciable. The rate of absorption, however, will be greatly improved because the reaction reduces the concentration of component A in the bulk solution (C_{Ao}) thus improving the driving force for mass transfer. When operating within this regime, the reaction rate constant, k_2,

can be calculated from equation 3-25 if the rate of absorption and the concentrations of A and B are known.

In analyzing the case of H_2S absorption by solutions of SO_2 on the sieve tray of the apparatus, for the reaction to be too slow to cause an enhancement of the liquid-phase mass-transfer coefficient, the parameter M, equal to $(k_1 D_L)/k_L^2$ by the film model, should be much less than one. For a second-order rate constant of 100 liter/(mole-s) and an SO_2 concentration of 0.001 m.f., the pseudo-first-order rate constant, $k_1=k_2[SO_2]_{out}$, would be about 1 s^{-1}. The diffusivity of H_2S in the solvent is of the order of 10^{-5} cm^2/s. The liquid-phase mass-transfer coefficient, $k_L a_i$, was found in section 6.2 to be about 0.3 s^{-1}. Interfacial areas per unit volume, a_i, on sieve trays generally range from 2 to 5 cm^{-1} (Sharma and Gupta, 1967). Using a value of 3 cm^{-1} for a_i gives k_L equal to 0.1 cm/s. Therefore, the estimated value of M is 0.001. This value is small enough that the reaction should occur predominately in the bulk solution and the enhancement factor, ϕ, should be equal to one as was thought. The reaction, then, occurs predominately in the bulk liquid.

For a fast reaction (for which eqn. 3-38 is not satisfied) a substantial amount of the absorbed gas reacts in the diffusion film, thus the enhancement factor is greater than one. When this is the case, the concentration of A in the bulk liquid, C_{Ao}, approaches zero, and the rate of absorption should be related to the more easily measured change in concentration of B across the tray.

$$\phi\, k_L C_{Ai} = (C_{Bin} - C_{Bo})/(\nu\, \tau) \qquad (3\text{-}29)$$

If there is substantial gas-phase mass-transfer resistance, the absorption term must be modified to include the overall mass-transfer coefficient, K_L, and equation 3-25 becomes

$$\bar{R} a_i = K_L a_i (C_{Ae} - C_{Ao}) = (C_{Ao} - C_{Ain}) / \tau + k_2 C_{Ao} C_{Bo} \qquad (3\text{-}30)$$

where

$$K_L = [1/(\phi\, k_L) + 1/(H\, k_g)]^{-1} \tag{3-31}$$

and by Henry's law

$$C_{Ae} = p_A/H_A \tag{3-32}$$

4. APPARATUS

4.1 Introduction

Murphree vapor tray efficiencies for physical absorption of H_2S and SO_2 were determined using the gas-absorption apparatus shown schematically in Figure 4-1. The experiments for reactive absorption of H_2S into SO_2-rich solutions of DGM used the same apparatus. The apparatus consists of a single 0.10-meter (4-inch) sieve tray with 4% free area placed in a circulating gas stream. Solvent is fed to the tray continuously, on a once-through basis. With this apparatus H_2S and SO_2 gas feed rates, gas- and liquid-phase compositions and temperatures, and total gas and liquid flows can be measured to determine absorption rates and tray efficiencies. The description which follows is for operation when H_2S is reactively absorbed. For physical absorption the solvent feed would be free of dissolved gas.

4.2 Apparatus Description and Operation

Gas flow through the apparatus is driven by a 4-stage centrifugal blower enclosed in a water-cooled box pressurized with nitrogen (N_2) to slightly above system pressure. A small amount of N_2 flows from the box, through the blower-shaft seal, and into the blower and gas loop to provide positive shaft sealing against H_2S leakage from the blower. The N_2 also acts to pressurize the apparatus system to 122 kPa (3.0 psig), which is set by a small bleed stream of gas from the gas loop to a water column of the desired head. The gas stream flows from the blower to the sieve tray where the gas bubbles up through the solvent which flows across the tray. From the tray the gas stream passes through a heat exchanger which, if necessary, is used to remove the heat added to the gas stream by the blower. The temperature increases resulting from both the heat of solution and the exothermic reaction are negligible. After leaving the cooler, the gas flows through a globe valve for manually controlling the gas flow. Next in line is a 12.7-mm (0.5-

inch) orifice meter for measuring the gas flow before the gas returns to the blower to complete the gas loop. Gas sampling ports are placed above and below the tray. The rate of absorption is set by the feed rate of 99.9% pure H_2S that is metered into the gas stream at a point downstream from the heat exchanger. The balance of the gas stream is predominately nitrogen.

Sulfur dioxide-rich solvent is fed to the tray continuously, on a once-through basis. The solvent flows from a constant-head feed tank, through a calibrated rotameter for measuring solvent flow, through a heat exchanger for heating the solvent to the desired tray temperature, and onto the tray where H_2S is absorbed and reacted with the SO_2 dissolved in the solvent. After flowing over the weir and into the tray downcomer, the solvent flows over a gooseneck which controls the solvent level in the downcomer. From the gooseneck the solvent flows into a spent solvent holding tank. At any time during a run, liquid samples can be withdrawn through septums in the tray inlet or outlet for analysis. To prepare the solvent for reuse in a subsequent run, the water of reaction and any dissolved gases are removed by stripping the solvent at 110°C with nitrogen in a 15-tray glass Oldershaw column. The sulfur produced by the reaction can be removed by crystallization and settling. Complete tray specifications are given in Table 4.1.

The stainless-steel tray was connected to 2-foot lengths of 4-inch-diameter glass pipe above and below the tray. Stainless-steel reducing flanges connected the glass sections to 2-inch schedule 80 polypropylene pipe. The polyproplyene pipe interconnected the heat exchanger, globe valve, and orifice meter, all of which were made of stainless steel. Flexible Neoprene hose joined the polypropylene pipe to the blower box and connected the blower box to the blower inside. The solvent tanks were made of polypropylene. All the solvent piping was stainless-steel tubing.

At start-up the gas was circulated to bring the equipment up to temperature.

As the equipment was warming, the desired concentration of SO_2 in the solvent feed was prepared by dissolving the required weight of SO_2 in 500 ml of solvent and then adding this concentrated solution to the much larger volume of solvent in the feed tank. The final concentration was determined by titrating the feed solvent for SO_2. Once the apparatus was warmed up and the total pressure inside reached the desired level, solvent was allowed to flow to the tray. The temperature of the solvent on the tray reached its setpoint after about ten minutes. After starting the solvent flow to the tray, H_2S gas was metered into the gas loop. The H_2S feed rate was either set to a fixed flow to set the rate of absorption or adjusted to achieve a desired steady-state H_2S concentration in the gas below the tray. The flow of H_2S was determined by bubbling the H_2S gas through a soapy solution and then timing the rate of bubble rise in a volume-calibrated glass tube. This method was necessary because the feed-gas rotameter calibration was not sufficiently accurate at low H_2S flows. A small, continuous gas-sample stream, selected from above or below the tray, was sent to the gas analyzer. After about 45 minutes, steady-state was achieved as indicated by steady gas-phase concentrations and temperatures. Another twenty minutes was allowed before a solvent sample was withdrawn from the tray-outlet septum and analyzed and the final gas-phase concentrations and tray temperature were recorded. The apparatus was then shut down.

4.3 Chemical Analysis

A. Gas-Phase Analysis

The gas-phase concentration of SO_2 in the sample stream was analyzed by a pulsed fluorescent SO_2 analyzer. For the H_2S analysis, a catalytic H_2S converter, which was placed upstream of the SO_2 analyzer, first oxidized the H_2S to SO_2. Then total SO_2 was measured, and H_2S concentration was obtained by subtracting the SO_2 concentration measured when H_2S was not converted. A switch on the

H_2S converter directed the gas-sample stream to the catalytic converter or bypassed the converter as required. The specifications of these instruments are given in Table 4.2. Because the H_2S converter requires an oxygen source, the sample stream, which has a nitrogen background, was mixed with air ahead of the converter. Oxygen, however, quenches SO_2 fluorescence and reduces the analyzer output signal, so the gas mixture to be analyzed should have nearly the same concentration of oxygen as was in the gases that were used to calibrate the analyzer. The SO_2 analyzer was calibrated with analyzed gases of 400 ppm and 3500 ppm SO_2 in air. By mixing the gas-sample stream from the apparatus with air in a ratio of at least three parts air to one part sample gas, a mixture was achieved which gave an analyzer response equal to a gas that had a true air background. For physical absorption of SO_2 the SO_2 analyzer was calibrated with analyzed standards of SO_2 in a nitrogen background. This allowed the gas samples to be analyzed directly by the SO_2 analyzer without the need to premix the sample stream with air.

B. Liquid-Phase Analysis

The accuracy of the Murphree vapor tray-efficiency calculations is strongly dependent on the accuracy of the measurement of the concentration of gas dissolved in the solvent leaving the sieve tray. Various methods for determining tray-outlet concentrations of SO_2 in DGM were investigated. These included analysis by UV-spectrophotometry, gas chromatography, acid-base titration, and iodometric titration. UV-spectrophotometry was ruled out because impurities in the solvent absorb light of the same wavelength as SO_2 and H_2S. Gas chromatography was eliminated because of the very small SO_2 and H_2S peaks relative to the solvent peak; they were generally less than 1% by area of the solvent peak. Acid-base titrations gave indistinct endpoints at very low concentrations of dissolved gas in the solvent samples.

Iodometric titrations were the most accurate of all the methods tested. In

these titrations a 10-ml solvent sample was withdrawn from the sampling septum with a syringe and then injected into an acidic aqueous solution containing a known amount of potassium dichromate in excess of the SO_2. The dichromate oxidized all the SO_2 to sulfate. Then excess potassium iodide was added to the solution to react with the remaining dichromate to give triiodide ion. The triiodide was titrated back to iodide with a standardized thiosulfate solution. Starch solution was added as an indicator, and a very sharp endpoint was signaled by the disappearance of the dark blue iodine-starch color. The amount of thiosulfate solution that was required to titrate to the endpoint was equivalent to the amount of dichromate that remained unreacted by the SO_2. Since the initial amount of dichromate was known, the amount of dichromate that was consumed by the SO_2 could be calculated. The advantage of this method was the very vivid endpoint color change. One disadvantage was the slow oxidation of DGM, but this could be corrected for by running a titration on the SO_2-free solvent feed to the apparatus. The results of this "blank" titration would then be subtracted from the results of outlet solvent titration.

The H_2S physical-absorption experiments required analyzing for dissolved H_2S. The analysis by using dichromate as the oxidizing agent gave inconsistent results. However, iodimetric titrations gave very good results when the H_2S solution was injected into an aqueous solution of excess iodine, which converts the sulfide to sulfur, followed by back titration with thiosulfate.

The concentration of the catalyst, 3-pyridyl carbinol (3-PC), in the solvent was analyzed by gas chromatography. Because of the very small 3-PC peak relative to DGM, 3-PC was calibrated against an internal standard of normal heptane. Heptane was added to the solvent sample to make a solution with 0.5 weight percent heptane. The gas chromatograph was calibrated with 0.5 wt % heptane solutions of DGM with various known concentrations of 3-PC. This provided a re-

sponse curve which related the concentration of 3-PC to the area ratios of the 3-PC peaks to the heptane peaks. A solution of unknown 3-PC concentration could then be analyzed after adding 0.5 wt % heptane to it.

4.4 Liquid Hold-up

Liquid hold-up on the sieve tray is defined as the volume of clear liquid above the tray during operation. It is a necessary parameter for calculating overall mass-transfer coefficients and reaction rates on the tray. To measure the hold-up, two valves were placed on the tray. One valve was placed at the solvent inlet to stop solvent flow to the tray. The other was placed at the bottom of the tray downcomer to drain any solvent in the downcomer and level-control gooseneck to a flask. With a steady flow of solvent and gas to the tray, the two valves were simultaneously turned to close the inlet valve and to open the drain valve. This allowed all solvent in the downcomer and gooseneck to flow into the collection flask. The solvent on the tray at the time the valves were turned eventually passed over the weir, down the downcomer, and out the drain valve. The total amount of solvent collected was weighed. From this weight of solvent was subtracted the weight of the solvent that was in the downcomer and gooseneck up to the gooseneck overflow before draining. The weight of the small amount of solvent that remained on the tray after draining was added to the result. The adjusted weight of solvent was converted to a volume which should be a good estimate of the hold-up of clear liquid on the tray during operation. The weight of the solvent that remained on the tray after draining was measured by soaking up this solvent with a paper towel and noting the increased weight of the wet towel. The weight of solvent in the downcomer and gooseneck before draining was estimated by filling the downcomer with solvent until its level reached the level set by the gooseneck overflow. The solvent was then drained and its weight measured.

Liquid hold-up was measured over the projected tray operating conditions of the tray-efficiency experiments. The hold-up on the apparatus sieve tray was measured at various liquid and gas flows, weir heights, and temperatures. Liquid flow, Q_L, was varied from 2.25 cm^3/s to 6.97 cm^3/s, a 210% increase. Gas flow was varied from 3.33 x 10^{-3} m^3/sec (STP) (0.464 m^3/m^2-s) to 3.83 x 10^{-3} m^3/sec (0.534 m^3/m^2-s), a 15% increase. Two flow regimes were encountered. The spray regime, in which the liquid is sprayed off the tray by the gas, occurred at only the lowest solvent flow tested. The froth regime, in which the gas bubbles up through the liquid on the tray without causing violent spraying, occurred at the higher liquid flows. This is the regime of main interest.

Within the froth regime at a given gas flow, increasing the liquid flow from 2.77 cm^3/s to 3.75 cm^3/s had very little effect on the liquid hold-up, but further increases in liquid flow resulted in measurable increases in hold-up. At a fixed liquid flow, increasing the gas flow had such slight effect in decreasing hold-up (about 2%) that this effect was neglected. Liquid hold-up was found to be fairly insensitive to temperature over a 10^oC change. Weir height, h_w, had the greatest effect on liquid hold-up, H_L. The hold-up results for 40^oC, 122 kPa, 3.33 x 10^{-3} m^3/sec nitrogen (STP) (0.464 m^3/m^2-s) are given in Table 4.4. These were the operating conditions for the majority of the absorption experiments.

List of Tables for Chapter 4

4.1 Tray Specifications

4.2 Equipment Specifications

4.3 Physical Properties

4.4 Variation of Liquid Hold-up with Weir Height and Liquid Flow

List of Figures for Chapter 4

4-1 Gas-Absorption Apparatus

TABLE 4.1: Tray Specifications

Sieve Tray

Diameter	1.02×10^{-1}	m
Active Area	7.17×10^{-3}	m^2
Hole Area	2.85×10^{-4}	m^2
Percent Free Area	4.0 %	
Number of Holes	36	
Hole Diameter	3.18×10^{-3}	m
Pitch (triangular)	1.45×10^{-2}	m
Weir Length	7.62×10^{-2}	m
Liquid Flow Path	6.67×10^{-2}	m
Weir Height (adjustable)	1.91	cm
	2.54	cm

TABLE 4.2: Equipment Specifications

Analyzers

Pulsed Fluorescent SO_2 Analyzer - Model 40
Thermo Electron Corp.
Hopkinton, MA

Ranges	0 - 50 ppm, 0 - 100 ppm
	0 - 500 ppm, 0 - 1000 ppm
	0 - 5000 ppm
Accuracy	derived from the calibration gas
Span Precision	± 0.5 %

Hydrogen Sulfide Converter - Model 340
Thermo Electron Corp.

Calibration Gases

Matheson Gas Products

Certified Standards	400 ppm
	3500 ppm
Accuracy	± 2 % of analyzed concentration

Gas Chromatograph

Hewlet-Packard - Model 5890 with Model 3392A Integrator

Thermal Conductivity Detector
HP-17 Capillary Column (intermediate polarity)

Blower

4-stage Centrifugal - Model Z4
B.V.C. Ltd.
Leatherhead, Surrey, England

TABLE 4.3: Physical Properties

Solvent

Dowanol DM (diethylene glycol methyl ether)
Dow Chemical U.S.A.

Structural Formula	$CH_3O(C_2H_4O)_2H$
Molecular Weight	120.1
Boiling Point	194°C
Specific Gravity	1.021 @ 25/25°C
Viscosity	3.5 centipoise @ 25°C
Specific Heat	0.54 cal/gm°C @ 25°C
Surface Tension	34.8 dyne/cm @ 25°C

Catalyst

3-Pyridyl Carbinol
Aldrich Chemical Co., Inc.

Structural Formula	$C_5H_4NCH_2OH$
Molecular Weight	109.13
Boiling Point	154°C/28 mm Hg
Specific Gravity	1.124 @ 20/4°C

Table 4.4: Variation of Liquid Hold-up with Weir Height and Liquid Flow

Q_L	h_w	H_L	STD. DEV.
cm^3/s	cm	cm^3	cm^3
3.25	1.91	61.7	1.5
3.25	2.54	78.6	1.4
4.55	2.54	83.6	1.9
6.97	2.54	92.6	2.1

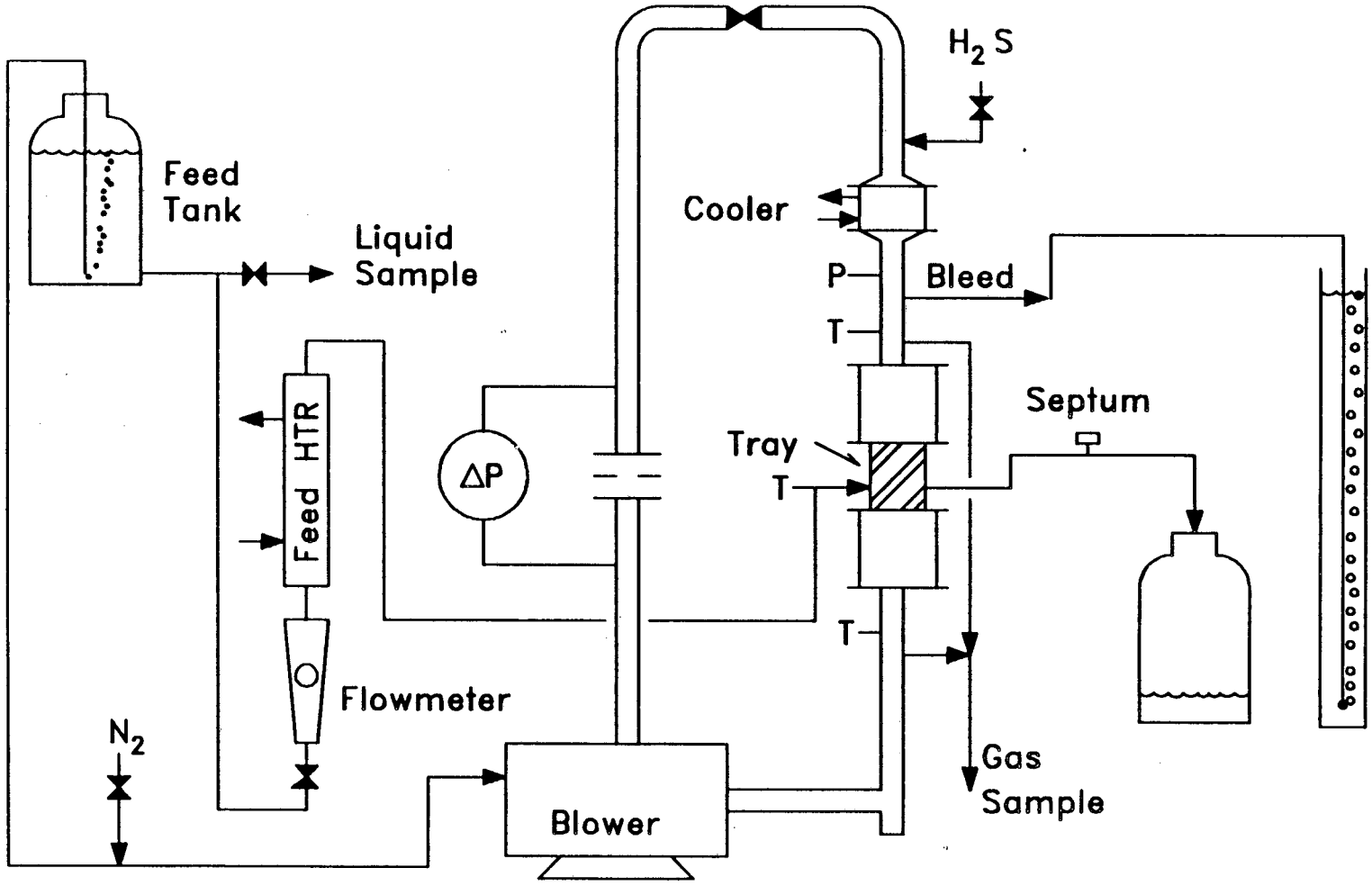

Figure 4-1: Gas-Absorption Apparatus

5. GAS SOLUBILITY

5.1 Past Studies

To calculate a Murphree vapor tray efficiency, the solubility of the absorbed gas in the solvent must be known. Sciamanna (1986) measured gas solubilities for H_2S, CO_2, propane, and n-butane in five different polyglycol ether solvents. He found that the solubility of these gases in the solvents obeyed Henry's Law, which requires a linear dependence of liquid-phase composition on gas-phase composition. Henry's Law is generally applicable to dilute solutions of gases in liquids. Sciamanna fit his data to the Henry's Law correlation of equation 5-1. The fit provided values for the Henry's Law constant of the solute (1) in the solvent (2) at 298°K, $H^{o}_{2,1}$, and the heat of solution, ΔH^{soln}. The values of these constants for the four solute gases in DGM are given in Table 5.1.

$$H_{2,1} = H^{o}_{2,1} \exp\{ (\Delta H^{soln} / R)(1/T - 1/T^{o}) \} \qquad (5\text{-}1)$$

where T^{o} = 298.15°K, and the gas constant R = 8.314 J/(mole K).

Sciamanna noted several solubility trends. He found that H_2S solubility is a strong function of the number of ether linkages in the solvent molecule, that the physical solubility of the gases increases as the number of solvent molecules per unit mass increases, that hydrogen bonding between solvent molecules decreases physical solubility of the gas (H_2S was the least sensitive to this effect), and that the solubility of hydrocarbon gases is improved by increasing the size of alkyl functional groups on the solvent molecule. To achieve high H_2S selectivity, Sciamanna recommended choosing a solvent with large molecules that have many ether linkages and terminal hydroxyl groups.

For sulfur dioxide solubilities Sciamanna correlated the data of Demyanovich (1984). Sciamanna had technical difficulties with using SO_2 in his equilibrium apparatus and hence used the extensive solubility data already collected by

Demyanovich in the solvents of interest. The Demyanovich data covered a concentration range from 0.05 m.f. to 0.27 m.f. SO_2 and a temperature range from about 45°C to 100°C. Sciamanna found a concentration dependence on SO_2 solubilty and derived a modified form of the Krichevsky-Ilinskaya equation to account for this dependence.

$$\ln (f_2 / x_2) = \ln H_{2,1} + (A/RT) (x_1^2 - 1) \tag{5-2}$$

with

$$(A/R) = (A/R)_0 + (T - T^0) (A/R)_1 \tag{5-3}$$

where

f_2	- fugacity of solute (SO_2), kPa.
$H_{2,1}$	- Henry's Law coefficient at infinite dilution, kPa/m.f.
x_1	- solvent (DGM) concentration in liquid, m.f.
x_2	- solute concentration in liquid, m.f.
$(A/R)_i$	- fitted parameters.

By holding temperature constant and varying composition, a plot of $\ln(f_2/x_2)$ vs. $(x_1^2 - 1)/T$ yielded values for $\ln(H_{2,1})$ and (A/R) at the chosen temperature from the plot slope and the intercept respectively. At a particular temperature, $H_{2,1}$ is the Henry's Law coefficient that is found by extrapolating the gas solubility to infinite dilution. To find the temperature dependence of $H_{2,1}$ and (A/R), this plotting procedure was repeated at even temperature increments. The two-parameter Antoine equations were used to calculate the gas solubility at even temperature increments from 25°C to 100°C. The parameters for these equations were provided by Demyanovich for SO_2 vapor pressure above the solvent at each SO_2 concentration that he tested Then, in a similar fashion, a plot of (A/R) vs. $(T - T^0)$ provided values for $(A/R)_1$ and $(A/R)_0$, and a plot of $\ln(H_{2,1})$ vs. $(1/T - 1/T^0)/R$ gave values for ΔH^{soln} and $H^0_{2,1}$. These values are given in Table 5.2 as the data of Demyanovich.

5.2 Present Study

Accurate gas-solubility data are critical for determining tray efficiencies; however, certain experiments of this study cast doubt on the validity of the SO_2/DGM Henry's Law coefficients that were derived from the correlation of the Demyanovich data. It appeared that the Henry's Law coefficients were too low, representing a much higher SO_2 solubility than was being seen in the absorber. To verify the SO_2 solubility relationship of equation 5-2, the Sciamanna correlation was confirmed to be an accurate representation of the Demyanovich data. Next, to verify the accuracy of the Henry's Law coefficients, equilibrium data were measured for the SO_2/DGM/Air system at 122 kPa over a temperature range of 23°C to 50°C and a concentration range of 0.001 m.f. to 0.005 m.f. SO_2 dissolved in DGM.

Two methods were used to measure the equilibrium data. In the first method, the absorber apparatus was used to collect these data. The absorber pressure was set to 122 kPa. A solution of SO_2 dissolved in DGM was heated to the desired temperature and fed to the absorber sieve tray. A gas stream of air was continuously circulated through the tray. Once steady state was reached, the concentration of SO_2 in the circulating gas stream was assumed to be in equilibrium with the SO_2 dissolved in the solvent on the tray. Solvent samples were withdrawn from the tray and the concentration of SO_2 in DGM was measured. A continuous gas-sample stream was sent to the SO_2 analyzer to measure the equilibrium concentration of SO_2 in parts-per-million (ppm) in the gas stream.

The second equilibrium apparatus consisted of a temperature-controlled 500-ml round-bottom flask which contained a 400-ml sample of SO_2-rich DGM. The liquid sample was continuously stirred and maintained at a set temperature. A gas sample containing SO_2 in air was pumped from the gas space above the liquid, through the SO_2 analyzer, and back to the flask where the gas was made to bubble up through the liquid sample. The system pressure, which remained near atmos-

pheric pressure, was measured by a manometer. After a steady liquid temperature and gas-phase SO_2 concentration were reached, a 10-ml sample of solvent was withdrawn with a syringe and analyzed for SO_2.

Over the very low range of SO_2 concentrations used in the present study, no concentration dependence on SO_2 solubility in DGM was determined so that $H_{2,1}$ could be calculated directly from equation 5-4. This finding is supported by equation 5-2 in which the concentration term at very low solute concentrations is negligible compared to the solubility term. The data collected by both procedures agreed with each other but differed from the data of Demyanovich.

$$H_{2,1} = (y_2 P) / (x_2) \tag{5-4}$$

The Henry's Law coefficients determined in this study were correlated by equation 5-1 to find the Henry's Law constant at 298°K, $H^{o}_{2,1}$, and the heat of solution, ΔH^{soln}. In Figure 5-1 the natural log of the Henry's Law coefficient ($H_{2,1}$) is plotted against $-(1/T - 1/T^{o})/R$. The negative slope of the plot gives ΔH^{soln} and the intercept is $H^{o}_{2,1}$. The data collected in this study by both methods is plotted as the data of Hix and is compared to the Sciamanna correlation of Demyanovich's data. The Henry's Law coefficient at 298°K and the heat of solution for this study were determined to be 44.88 kPa/m.f. and -38.05 kJ/mole respectively, and for the Sciamanna correlation of the Demyanovich data they were reported as 31.15 kPa/m.f. and -37.13 kJ/mole respectively. Although the heats of solution agree within three percent, the Henry's Law coefficients of this study are about 50% higher than those determined from the Demyanovich data. A higher Henry's Law constant represents lower gas solubility.

The reason for this discrepancy in equilibrium data is not clear. No fault could be found in Demyanovich's method of collecting his data, and several possible causes of errors to the data of this study were investigated and ruled out.

Fortunately, a search through the raw data of Sciamanna uncovered three sets of data for the SO_2/DGM system with which he had used to test his equilibrium apparatus. Because of difficulties in using SO_2 in his apparatus and because of the extensive SO_2-solvent data previously collected by Demyanovich, Sciamanna chose not to investigate further the SO_2-solvent systems. He never reduced his raw SO_2 data for the Henry's Law correlations, but instead correlated Demyanovich's data. Each set of Sciamanna's SO_2-solubility data was collected at equal temperature increments over a temperature range of 15°C to 95°C and a concentration range of 0.01 to 0.10 m.f. SO_2 in DGM. Only Sciamanna's first set of data was correlated well by equation 5-3, however all three sets fit equation 5-2 and gave consistent values of $H_{2,1}$. The problems that Sciamanna had with SO_2 swelling the seals and valve seats in his apparatus may have begun to affect the results for the latter two data sets. A fit of the first data set yielded a Henry's Law coefficient at 298°K of 49.70 kPa/m.f. and a heat of solution of -33.24 kJ/mole. This correlation is also plotted in Figure 5-1 as the data of Sciamanna, although only data up to 50°C are shown.

The Henry's Law coefficient at 298°K from this study is 10% lower than that from the Sciamanna data, and the heats of solution differ by 14%. However in Figure 5-1, one can see very good agreement between the Hix and Sciamanna data in the range of 30° to 50°C. The different heats of solution may be due to this study's narrow temperature range of data collection (23°C to 50°C), which is smaller than the range Sciamanna used. The smaller range would likely result in a less accurate slope of the straight line fitted through this study's data in Figure 5-1. The negative slope of the line is the heat of solution. Although more work should be done to confirm the SO_2/DGM gas-solubility relationship, the Henry's Law constant at 298°K and the heat of solution which were established by this study will be used to calculate the Murphree vapor tray efficiencies.

List of Tables for Chapter 5

5.1 Constants for Henry's Law Equation

5.2 Sulfur Dioxide Solubility in DGM

List of Figures for Chapter 5

5-1 Effect of Temperature on Henry's Coefficient

Table 5.1: Constants for Henry's Law Equation*
(Solubilities in Diethylene Glycol Methyl Ether, DGM)

$$H_{2,1} = H^{o}_{2,1} \exp\{ (\Delta H^{soln} / R)(1/T - 1/T^{o}) \}$$

$H_{2,1}$ - Henry's Law constant, kPa/m.f.
- DGM = 1, solute gas = 2.
- m.f. = mole fraction

$H^{o}_{2,1}$ - Henry's Law constant at 298°K.

T^{o} - 298.15 °K

Solute	$H^{o}_{2,1}$ (kPa/m.f.)	ΔH^{soln} (kJ/mole)
Hydrogen Sulfide	843.4	-16.16 ± 1.0%
Carbon Dioxide	6476.	-10.40 ± 2.5%
Propane	5755.	- 9.44 ± .02%
n-Butane	2120.	-13.92 ± .08%

* Data of Sciamanna, 1986

Table 5.2: Sulfur Dioxide Solubility in DGM

$$\ln (f_2 / x_2) = \ln H_{2,1} + (A/RT) (x_1^2 - 1)$$

$$(A/R) = (A/R)_0 + (T - T^{o}) (A/R)_1$$

(T^{o} = 298.15 °K)

Data Source	$H^{o}_{2,1}$ (kPa/m.f.)	ΔH^{soln} (kJ/mole)	$(A/R)_0$ °K	$(A/R)_1$
Demyanovich (correlation)	31.15	-37.13	-590.5	2.564
Hix	44.88	-38.05	-----	-----
Sciamanna	49.70	-33.24	-419.2	2.990

Figure 5–1: Effect of Temperature on Henry's Coefficient

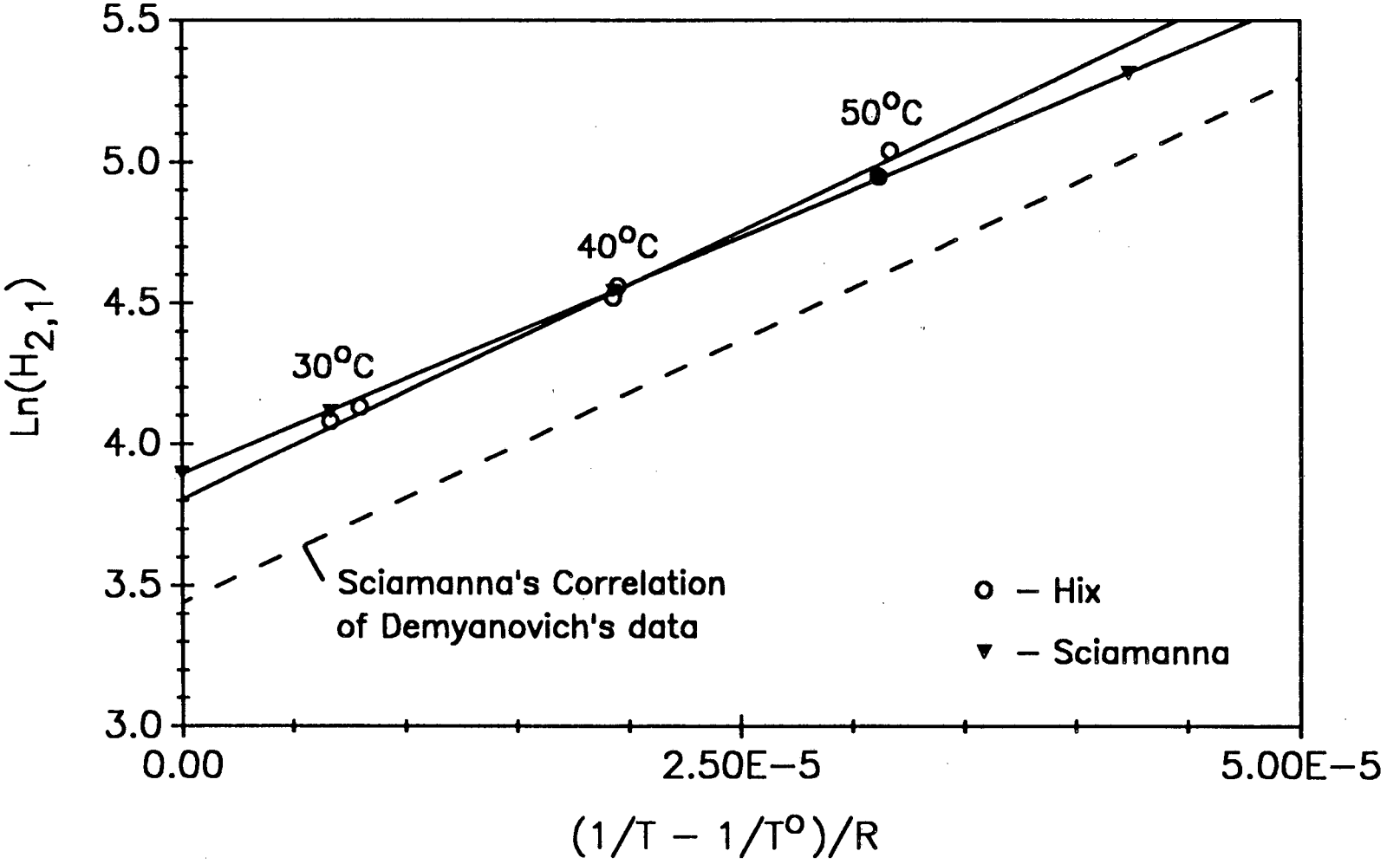

6. GAS ABSORPTION

6.1 Physical Absorption

A. Tray Efficiencies for Sulfur Dioxide

Murphree vapor tray efficiencies, E_{mv}, for physical absorption of SO_2 by DGM were determined at 40°C and 122 kPa. With the gas and liquid flows held constant at 8.57 mole/min and 1.62 mole/min respectively, the inlet gas-phase concentration of SO_2 was varied from about 300 ppm to about 5000 ppm. Tray efficiencies at these conditions were determined for two different weir heights, 1.91 cm and 2.54 cm. The average tray efficiency for the 7 runs at each weir height was 0.50 ± 0.14 in both cases; however, the expected trend is that E_{mv} increases with weir height.

That E_{mv} should increase with weir height is arrived at by analyzing the effect of changing weir height on point efficiency, E_{ov}. As the weir height increases, so does the liquid holdup on the tray. The average gas and liquid contact times (equations 3-12 and 3-19) are proportional to the liquid holdup, and penetration theory predicts that the mass-transfer coefficients are inversely proportional to the square root of the contact times.

$$k_v = 2\sqrt{[D_v / (\pi t_v)]} \tag{6-1}$$

$$k_L = 2\sqrt{[D_L / (\pi t_L)]} \tag{6-2}$$

By equations 3-3 through 3-5, the number of transfer units in each phase, N_v and N_L, and the overall number of transfer units, N_{ov}, should be proportional to the square root of the liquid holdup. Data from Table 4.3 show that the holdup increases by 27% when the weir height is increased from 1.91 cm to 2.54 cm for a liquid flow of 1.62 mole/min (3.25 cm^3/s). A 27% increase in holdup will result in a 13% increase in N_{ov}, and at point efficiency, E_{ov}, near 0.50, a 13% increase in

N_{ov} provides a 9% increase in E_{ov}. Although this increase in tray efficiency was not seen, one cannot say that the increase did not occur since the tray efficiencies are known only to within about 30% of their measured values.

Liquid flow was varied to study its effect on tray efficiency. While holding the gas flow constant at 8.57 mole/min (0.427 m^3/m^2-s) and while maintaining the inlet gas concentration near 3000 ppm SO_2, tray efficiencies were determined at liquid flows that were increased from 1.15 mole/min to 4.01 mole/min. The weir height was kept at 2.54 cm. Figure 6-1 shows that E_{mv} is fairly constant with liquid flow over the range that was studied. The average efficiency is 0.60 ± 0.14. Because holdup increases with liquid flow, a rise in the tray efficiency was expected. By following the same reasoning as was presented above for the case of raising the weir height, a 5% increase in E_{mv} is predicted for the measured 18% increase in holdup over the full range of solvent flows in the figure. As before, the uncertainty in the tray efficiency measurements would probably hide a 5% increase in the efficiency value.

Tray efficiencies were determined for physical absorption of SO_2 at various inlet gas concentrations. The liquid and gas flows were constant at 3.55 mole/min (6.97 cm^3/s) and 8.57 mole/min (0.427 m^3/m^2-s) respectively. The weir height was 2.54 cm. The average efficiency for these data, which are shown in Figure 6-2, is 0.59 ± 0.11. A slight trend of increasing E_{mv} with y_{in} can be seen, but this was probably due to systematic error caused by SO_2-analyzer miscalibration during those runs.

B. Tray Efficiencies for Hydrogen Sulfide

Tray efficiencies for physical absorption of H_2S by DGM were determined at 30°C and 40°C and at a total pressure of 122 kPa. The weir height was 2.54 cm, and the liquid and gas flow rates were 3.55 mole/min and 8.57 mole/min respec-

tively. The 40°C data is plotted in Figure 6-2 for comparison to the SO_2 tray efficiencies that were measured at the same conditions. The H_2S tray efficiencies average 0.16 ± 0.09 and are quite a bit lower than the SO_2 efficiencies. The lower tray efficiency for H_2S is expected because of the much lower solubility of H_2S in DGM. Sulfur dioxide is more than ten times as soluble in DGM as is H_2S. The gas solubility comes into play in equation 3-3 as λ, the ratio of the slope of the equilibrium line to the slope of the operating line. The slope of the equilibrium line, m, increases with decreasing gas solubility. For gas absorption under liquid-phase control (which is the case for this system) $\lambda / N_L >> 1/N_v$. When this is the case, $N_{ov} \simeq N_L/\lambda$. Therefore, if m increases due to lower gas solubility, λ must increase in proportion and N_{ov} must decrease, which results in a lower value calculated for E_{ov}.

The H_2S physical-absorption experiments were repeated at 30°C. These tray-efficiency data are plotted with the data taken at 40°C in Figure 6-3. The average tray efficiency at 30°C is 0.18 ± 0.08. The slightly higher efficiency is expected because of the increased H_2S solubility in DGM at the lower temperature, although the increase in tray efficiency is less that the uncertainty of the efficiency measurements. The line that is shown in the figure is a first-order fit through both sets of data.

6.2 Tray-Efficiency-Model Predictions

To compare the tray-efficiency predictions of the model of Chan and Fair (1984) to the efficiencies that were measured in this study, it is necessary to calculate the ratio E_{mv}/E_{ov} by equation 3-8 and thereby transform a point efficiency prediction into a tray efficiency prediction. This requires a value for the Peclet number for the sieve tray that was used in the apparatus. Because the eddy diffusivity correlation that was recommended by Chan and Fair (equation 3-22) gave a

negative value for D_e at the operating conditions of the small sieve tray in the apparatus, the correlation recommended by the AIChE tray-efficiency study, as given in King (1980), was used instead. The AIChE correlation, converted to SI units and multiplied by 1.25 for sieve trays, is

$$D_e = 1.25 \, [\, 0.00378 + 0.0171 \, U_a + 3.68 \, r_w \, q_L + 0.00180 \, h_w \,]^2 \qquad (6\text{-}3)$$

The parameter r_w is the ratio of the weir width to the average width of the liquid-flow path. The tray specifications of Table 4.1 give the length of the liquid flow path, Z_L, and equation 3-12 provides the average liquid contact time, t_L. At the average operating conditions of the tray, the Peclet number, *Pe*, calculated from equation 3-10 is approximately 0.01. This low *Pe* indicates that the liquid on the tray is very well mixed, as should be expected for a small diameter tray with a low liquid flow. For such a low *Pe*, equation 3-8 indicates a less-than-one percent improvement in E_{mv} over E_{ov}; therefore, the predicted point efficiencies will be used for tray efficiencies. Table 6.1 compares the measured tray efficiencies for H_2S and SO_2 at various operating conditions to the predictions of the model. The average absolute error of the tray-efficiency predictions is 9%. This very good agreement with the measured efficiencies provides encouragement for using the Chan and Fair model to provide high-pressure tray efficiencies.

Mass-transfer coefficients can be extracted from the physical absorption data. Since E_{ov} is equal to E_{mv} for the sieve tray in this apparatus, N_{ov} for H_2S and for SO_2 absorption can be calculated from equation 3-2 by using the average of the measured Murphree vapor tray efficiencies for each system at 40°C. The mass-transfer coefficient for H_2S in a phase must be related to the mass-transfer coefficient for SO_2 in the same phase. Penetration theory predicts (equations 6-1 and 6-2) that the ratio of the mass-transfer coefficient for H_2S to that for SO_2 in

a phase is equal to the ratio of the square roots of the molecular diffusivities of H_2S to SO_2 in that same phase. After substituting equations 3-4 and 3-5 into equation 3-3, the resulting equation can be written for H_2S and for SO_2 and solved for the mass-transfer coefficients. The results of these calculations give $k_L a_i$ equal to 0.337 s^{-1} for H_2S and 0.307 s^{-1} for SO_2. These values are 24% higher than the values that are predicted by the Chan and Fair correlations. For the gas-phase mass-transfer coefficients, $k_v a_i$, the results are 28.2 s^{-1} and 25.0 s^{-1} for H_2S and SO_2 respectively. These values are 65% lower than the gas-phase mass-transfer coefficients that are predicted by the correlations. The results for $k_v a_i$ are not very accurate since the mass-transfer resistance lies predominantly in the liquid phase. When this is the case, the value of $k_v a_i$ has very little effect on the tray efficiency, and so accurate results cannot be expected when calculating $k_v a_i$ from tray-efficiency data.

6.3 Absorption with Chemical Reaction

A. Calculations

Hydrogen sulfide absorption rates were also measured for the case when H_2S is absorbed and undergoes chemical reaction with SO_2 dissolved in the solvent. All the reactive-absorption experiments were with excess SO_2 (from about 2 to 7 times the stoichiometric equivalent). The volatility of SO_2 was not important in these experiments because of the circulating gas stream in the apparatus. At steady-state, the partial pressure of SO_2 in the gas stream was in equilibrium with the solution on the tray and no net desorption of SO_2 would occur. A homogeneous catalyst, 3-pyridyl carbinol (3-PC), was dissolved in the solvent, DGM, to increase the reaction rate. The catalyzed, irreversible, liquid-phase reaction between H_2S and SO_2 was found to be first-order in both reactants by Neumann (1986) and Crean (1987). Both Neumann and Crean found that the following rate expression

fit their kinetic data.

$$2\ H_2S + SO_2 \text{ -----> } 3/8\ S_8 + 2\ H_2O \tag{6-4}$$

$$r_{H2S} = k_2\ [\ H_2S\ ]\ [\ SO_2\ ] \tag{6-5}$$

The second-order rate constant, k_2, is a function of temperature and catalyst concentration. Neumann found that the catalyst activity was associated predominately with the nitrogen in the pyridine ring and, to a lesser extent, with the hydroxyl groups on the catalyst and solvent molecules. Both studies showed a linear dependence of k_2 on 3-PC concentration.

In the present study the rate expression of equation 6-5 will be used in conjunction with the reactive-absorption rate data to calculate second-order rate constants at various catalyst concentrations, temperatures, and H_2S feed rates. To accomplish this task, it is necessary to model the sieve tray as a continuously-stirred-tank reactor (CSTR). This is a good assumption because, as shown above, the low Peclet number for the tray indicates that the tray is well-mixed and will have a uniform liquid composition throughout equal to the exit composition. For this type of reactor, the rate of reaction is set by the concentrations in the bulk solution in the reactor, or in this case, on the tray. The liquid hold-up on the sieve tray will be used as the reactor volume. If the solvent feed to the tray contains no dissolved H_2S, as was the case for all the reactive-absorption experiments, the rate of H_2S absorption must equal the rate at which dissolved H_2S leaves the tray in the exiting solvent plus the rate at which H_2S is consumed by reaction on the tray. The resulting design equation for the for the CSTR-tray is

$$\bar{R} a_i H_L \text{ (moles } H_2S\text{/sec)} = Q_L\ [H_2S]_{out} + k_2\ H_L\ [H_2S]_{out}\ [SO_2]_{out} \tag{6-6}$$

where Q_L is the volumetric flow of solvent to the tray.

Use of this equation requires knowledge of the concentrations of dissolved reactants on the tray. Because concentrations could not be measured *in situ*, the concentration of H_2S on the tray was calculated from the tray efficiency for H_2S. It has been shown that the reaction is too slow to cause enhancement of the liquid-phase mass-transfer coefficient. When this is the case, the tray efficiency for physical absorption of H_2S should also apply to the case when slow liquid-phase reaction of the absorbed gas is occurring. The concentration of H_2S which is dissolved in the solvent on the tray can then be backed out from the equation for tray efficiency by using the measured physical-absorption E_{mv}. Equations 3-7a and 3-7b are combined and solved for x_{out} to give

$$x_{out} = \{ y_{out} - y_{in}(1- E_{mv})\}/(m E_{mv}) \qquad (6\text{-}7)$$

If the amount of SO_2 in the solvent feed to the tray is known, the concentration of SO_2 leaving the tray can be determined by mass balance. Since the rate of H_2S absorption, tray hold-up, and solvent flow to the tray are measured quantities, equation 6-6 can be solved for the reaction-rate constant.

If the reaction were, in fact, fast enough to cause appreciable enhancement of the liquid-phase mass-transfer coefficient, the actual tray efficiency would be higher than the physical-absorption tray efficiency. This would lead to rate constants that are too high when calculated by using the lower assumed tray efficiency since a greater portion of the absorption rate would be attributed to reaction rather than the improved tray efficiency.

The effect, if any, of dissolved constituents, other than H_2S, on the solubility of H_2S in DGM needs to be considered since gas solubility is important in the calculation of H_2S concentration on the tray. Whether dissolved SO_2 would reduce the solubility of H_2S would be hard to check since these two gases react slowly with each other even in the absence of catalyst. It is known that both H_2S and

SO_2 interact with the ether linkages of the solvent molecules and that these interactions strongly affect the gas solubility. Competition for these ether-linkage sites could affect the gas solubilities, but this is not expected when both gases are as dilute as is the case here. However, it does appear that the catalyst lowers the equilibrium backpressure, y^*, of H_2S over DGM. This effect was discovered by finding negative physical-absorption tray efficiencies for H_2S in DGM with 0.03M 3-PC present. After the last reactive-absorption experiment was completed, three H_2S physical-absorption experiments were attempted. Each experiment gave a negative tray efficiency as the result of a negative denominator in the equation for Murphree vapor tray efficiency (equation 3-7a). The negative denominator resulted because the steady-state inlet gas-phase concentration of H_2S, y_{in}, was less than the equilibrium concentration, y^*, that was predicted by Henry's Law for the solvent with an H_2S concentration equal to the measured x_{out}. The tray inlet and outlet gas-phase concentrations of H_2S were much less that the values measured previously at the same H_2S feed rate when the catalyst was not present. The most plausible explanation for the low measured values for y_{in} and y_{out} is that the catalyst was forming a complex with dissolved H_2S, thus reducing the concentration of physically dissolved H_2S in solution. The equilibrium backpressure of H_2S results only from physically dissolved (*i.e.*, uncomplexed) H_2S. The proper value of x_{out} for use in equation 3-7b is the physically dissolved H_2S concentration not the total H_2S concentration (physically dissolved and complexed) as measured by titration or calculated by mass balance.

A separate experiment was done to check whether SO_2 and 3-PC form a strong complex. In this experiment 3-PC was injected into the equilibrium flask (described in section 5.2) containing SO_2 dissolved in DGM and the reduction in SO_2 backpressure was noted. A very slight depression of only one percent in the

SO_2 equilibrium backpressure was found for a catalyst concentration of 0.03 M. This suggests that SO_2 and the catalyst do not form a complex strong enough to require its consideration in the reaction rate expression.

Although the concentration of physically dissolved H_2S in solution could not be measured directly, it can be calculated by assuming that the physical absorption tray efficiency remains unchanged from the average value of 0.16 that was measured at 40°C before any catalyst was added to the solvent. With this assumption, the concentration of physically dissolved H_2S, x_{out}, can be calculated from equation 6-7. If x_{out} is known, the equilibrium constant, K_c, for the following equilibrium reaction can be calculated. The complex is represented by C.

$$H_2S + 3PC \overset{K_c}{\longleftrightarrow} C \qquad (6\text{-}8)$$

$$K_c = [C] / ([H_2S] [3PC]) \qquad (6\text{-}9)$$

Component balances give

$$[H_2S]_o = [H_2S] + [C] \qquad (6\text{-}10)$$

and

$$[3PC]_o = [3PC] + [C] \qquad (6\text{-}11)$$

The subscript 'o' indicates the total concentrations. Equations 6-9 through 6-11 are solved algebraically for K_c

$$K_c = \frac{(1 - [H_2S]/[H_2S]_o)}{([3PC]_o[H_2S]/[H_2S]_o + [H_2S]^2/[H_2S]_o - [H_2S])} \qquad (6\text{-}12)$$

The initial concentrations of H_2S and 3-PC are known, and the concentration of physically dissolved H_2S, $[H_2S]$, is the calculated x_{out} converted to moles/liter.

The equilibrium constant was calculated for the three physical-absorption experiments which had given negative tray efficiencies. The total catalyst concentration in each was 0.030M 3-PC, and the total H_2S concentration ranged from 6.1

x 10^{-4} M to 1.9 x 10^{-3} M, a three-fold increase. The average value for K_c was 21.5 liter/mole with a standard deviation of 1.2 (6% of the average). For this value of K_c and for the total concentrations of H_2S and catalyst given above, approximately 40% of the H_2S is complexed with 3-PC whereas only about 2% of the 3-PC is complexed since 3-PC is in great excess.

For calculating the rate constant, the correct H_2S concentration to use in equation 6-6 is that of physically dissolved H_2S. This concentration is calculated from equation 6-7 by using the assumed E_{mv}. The total concentration of H_2S that has not reacted yet with SO_2, $[\ H_2S\ ]_o$, is found by using equation 6-12. Then the total H_2S concentration is used with mass balances to calculate the rate of reaction and the concentration of unreacted SO_2 on the tray, $[\ SO_2\ ]_{out}$. Equation 6-6 is then solved for k_2.

B. Reactive-Absorption Results

1. Verification of Reaction-Rate Constant

Reactive-absorption rate data were collected at various temperatures, catalyst concentrations, and H_2S feed rates. The concentration of dissolved SO_2 in the solvent feed to the tray was approximately 0.001 m.f. for all the reactive-absorption experiments. The liquid and gas flows for all the runs were constant at 3.55 mole/min (6.97 cm^3/s) and 8.57 mole/min (0.427 m^3/m^2-s) respectively, and the weir height was always 2.54 cm. At each catalyst concentration and temperature combination, two absorption runs were done for an H_2S feed rate of approximately 13.0 standard cubic centimeters per minute and two runs were performed with the H_2S feed rate set to achieve an tray-inlet gas concentration of approximately 1900 ppm. For each run the second-order rate constant was calculated by the procedure described above. The first set of reactive-absorption experiments, at a catalyst concentration of 0.015 M 3-PC and a tray temperature of 40°C, returned an aver-

age second-order rate constant of 11.2 liter/(mole-s). This value compares fairly well to the rate constant of 32 liter/(mole-s) that was measured at the same catalyst concentration by Neumann (1986), who used an adiabatic batch reactor. Extrapolating Crean's data to 0.015 M 3-PC gives a second-order rate constant of 20 liter/(mole-s). Crean's measurements were taken using a stop-flow apparatus connected to a UV-spectrophotometer. Both Neumann and Crean reported rate constants based on consumption of SO_2, whereas the rate constants reported in the present study are based on the rate of H_2S consumed by reaction. The rate constants reported above are all on an H_2S basis for comparison. This fair agreement among data collected by very different techniques suggests that the method of calculating reaction-rate constants from the reactive-absorption data is valid.

2. Effect of 3-PC Concentration on Reaction-Rate Constant

Figure 6-4 shows the effect of catalyst concentration on the rate constant at 40°C. The second-order rate constants range from about 10 liter/(mole-s) at 0.015 M 3-PC to about 80 liter/(mole-s) at 0.030M 3-PC. The extent of reaction on the tray ranges from about 50% at the lowest measured rates in the figure to about 80% at the highest rates. The large error bars are the result of the uncertainty in the assumed tray efficiency.

The relationship between rate constant and catalyst concentration is fairly linear as was found by Crean and Neumann; however, the negative intercept does not agree with the intercept through the origin which Crean's data gave. Crean also found a linear dependence of k_2 on catalyst concentration, whereas this study found a higher order dependency.

$$k_2 = k_3 [3\text{-PC}]_0 \qquad (6\text{-}13)$$

where the third-order rate constant, k_3, does not vary with catalyst concentration.

One possible mechanism that would fit this rate expression, although not confirmed, is that H_2S and 3-PC react rapidly and are in equilibrium with the complex they form as in equation 6-8. The H_2S-catalyst complex then reacts with SO_2 in the rate-limiting step to form a second complex which reacts very rapidly with a physically dissolved H_2S molecule to form sulfur and water. Crean's data are, at least, consistent with this mechanism. However, in this study, the third-order rate constant appears to be a function of catalyst concentration squared, thus making the second-order rate constant a function of catalyst concentration cubed. Crean's data were taken at excess H_2S concentrations and low SO_2 and 3-PC concentrations, and this study used excess 3-PC and SO_2 concentrations and low H_2S concentrations. It may be that the mechanism changes, depending on the relative concentrations of the reactants and catalyst, and that this is why the two sets of data show different behaviors. Some of the unpublished kinetic data that Neumann has collected on this reaction suggest this may be true; however, the cubic dependence of the second-order rate constant on the catalyst concentration would require an unlikely mechanism for this dependence to be valid. It is evident that an extensive, in depth study of the reaction will be necessary to discover the true mechanism of this very complicated reaction. Even though a proven reaction mechanism has not been found, the rate expression of equation 6-5 fits the data fairly well and is simple enough to use easily in numerical calculations.

3. Effect of Reaction on H_2S Absorption

Figure 6-5 shows the relationship between H_2S absorption rate and reaction-rate constant at an assumed tray efficiency of 0.16. The data shown were taken at a tray-inlet gas-phase concentration of H_2S of 1900 ppm. The concentration of 3-PC was varied to adjust the rate of reaction and, thereby, the rate of absorption. The measured absorption rates were then used to calculate values of k_2. Even

though the reaction is too slow to cause any enhancement in the liquid-phase mass-transfer coefficient, the reaction does provide significant improvement in the absorption rate of H_2S. It accomplishes this by lowering the bulk liquid-phase concentration of H_2S, which results in a greater overall mass-transfer driving force between the gas and the bulk liquid. This same effect could be achieved in physical absorption by increasing the liquid flow rate to the level that is necessary to achieve the same low concentration of H_2S in the bulk liquid. For example, to achieve the same rate of absorption without reaction that was measured for reactive absorption with a rate constant near 10 liter/(mole-s), the liquid flow would have to be increased by a factor of 2.4. The curve in the figure is the operating solution to a single sieve tray modeled as a CSTR and given the same feed conditions, liquid hold-up, and tray efficiency as the sieve tray in the apparatus. The complex between H_2S and 3-PC was also considered in the model. The two dashed curves represent the uncertainty in the assumed tray efficiency and provide upper and lower bounds for k_2 at a given absorption rate.

The effect of temperature on the second-order rate constant was investigated. Rate constants were measured for reactive absorption of H_2S at 30°, 40°, and 50^oC with 0.015 M 3-PC in the solvent. Because physical-absorption tray efficiencies for H_2S were not measured at 50^oC, an assumed value of 0.15 was used for calculating the reaction rate constants at this temperature. The efficiency of 0.15 was arrived at by using the predictions of the tray efficiency model to extrapolate the measured efficiencies at 30^oC and 40^oC to 50^oC.

The rate constants should follow the Arrhenius expression for temperature dependence

$$k_2 = k_2^o \exp\{ -E_a/RT \} \qquad (6\text{-}14)$$

Figure 6-6 shows a semilog plot of the rate constant vs. the reciprocal of the product of the gas constant and the absolute temperature. The activation energy,

E_a, is found from the slope of the plot and is equal to 22 kcal/mole.

6.4 Summary

The tray-efficiency model of Chan and Fair adequately predicts, to within about 10%, the measured physical-absorption tray efficiencies for H_2S and SO_2 at low pressure (122 kPa). These correlations will be used to predict tray efficiencies at the high pressures that will be used in designing the primary absorber of the UCBSRP.

A second-order rate expression (first-order in both the reactants) and a CSTR-model for the sieve tray were used to calculate second-order rate constants from the reactive-absorption data for H_2S absorption on a sieve tray. The method gave rate constants that were close to values that were determined with an adiabatic batch reactor by Neumann (1986). The rate constant increases steeply with catalyst concentration, and a rate constant of 100 liter/(mole-s) should be easily achievable at a low catalyst concentration (near 0.03 M). The reaction is too slow to cause enhancement of the liquid-phase mass-transfer coefficient; nevertheless, a substantial improvement in H_2S absorption rate occurs because the reaction lowers the bulk concentration of dissolved H_2S. This is the same effect as seen in physical absorption when the liquid flow rate is increased. Although the rate data that were collected in this study do not fit the proposed rate expression as well as the data of Neumann and Crean, the expression should be adequate for modeling and design of the primary absorber.

Extensive work is necessary to discover the true reaction mechanism and rate expression. Equilibrium studies are needed to adequately determine the effect of the catalyst concentration on H_2S solubility in the solvent. Further work on SO_2 solubility in DGM is required to determine the accuracy of the solubility data of Demyanovich.

List of Tables for Chapter 6

6.1 Comparison of Experimentally-Determined Tray Efficiencies to Predicted Efficiencies

List of Figures for Chapter 6

6-1 Effect of Liquid Flow on SO_2-DGM Tray Efficiency

6-2 Comparison of SO_2 and H_2S Tray Efficiency in DGM

6-3 Effect of Temperature and Inlet Gas Concentration on H_2S Tray Efficiency

6-4 Effect of Catalyst Concentration on Reaction-Rate Constant

6-5 Effect of H_2S Absorption Rate and Assumed E_{mv} on Reaction-Rate Constant

6-6 Arrhenius Plot

Table 6.1: Comparison of Experimentally-Determined Tray Efficiencies to Predicted Efficiencies

(V=8.60 mole/min, P=122 kPa)

Temp. ^oC	Liq. Flow mole/min	weir ht. cm	measured E_{mv}	predicted E_{mv}	error
SO_2					
40	1.62	1.91	0.50	0.48	- 4.0%
40	1.62	2.54	0.50	0.54	8.0%
40	3.55	2.54	0.59	0.54	- 8.5%
H_2S					
30	3.55	2.54	0.18	0.20	11.1%
40	3.55	2.54	0.16	0.18	12.5%
50	3.55	2.54	not determined	0.17	----

Figure 6–1: Effect of Liquid Flow on SO_2–DGM Tray Efficiency

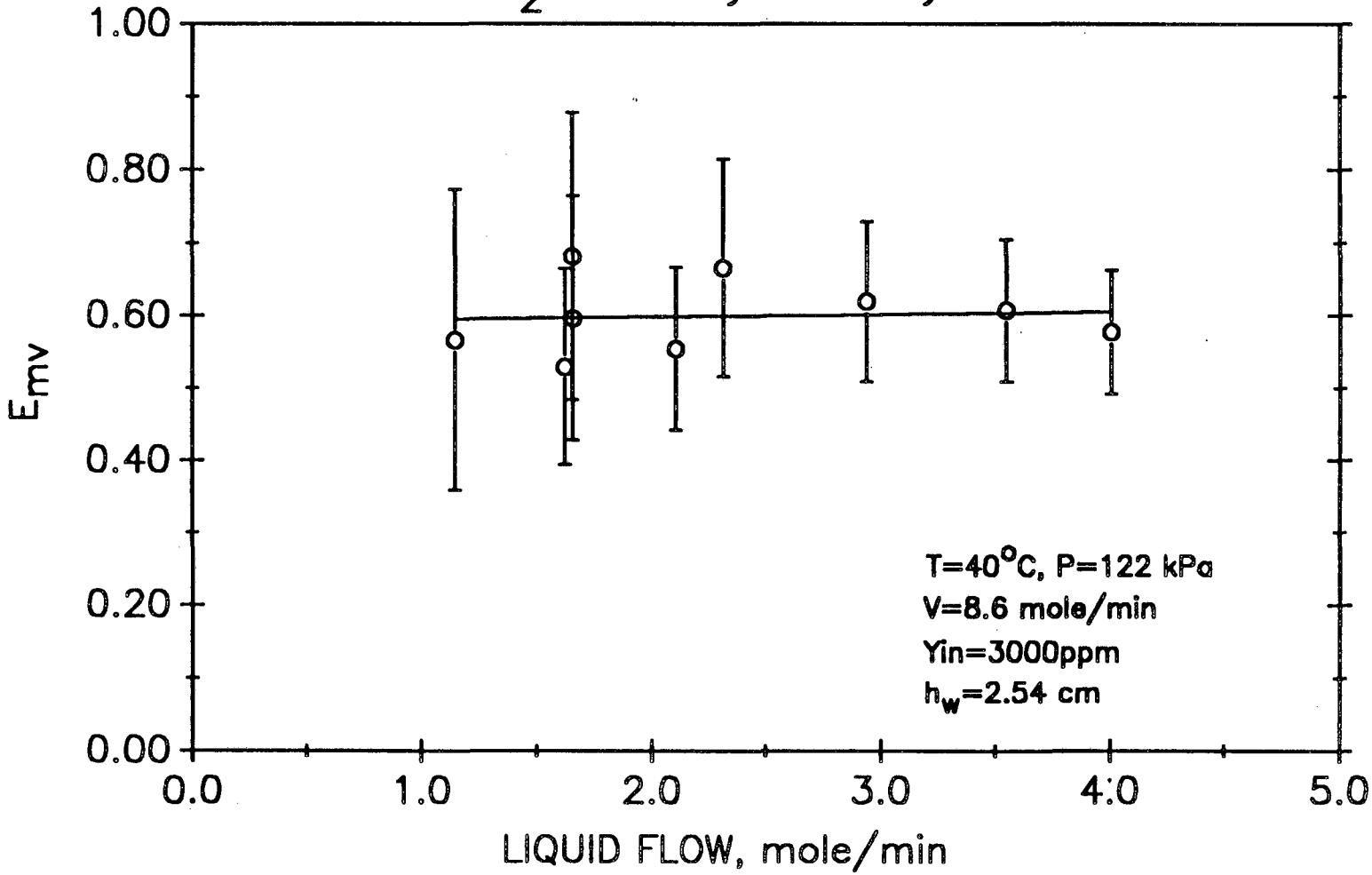

Figure 6–2: Comparison of SO_2 and H_2S Tray Efficiency in DGM

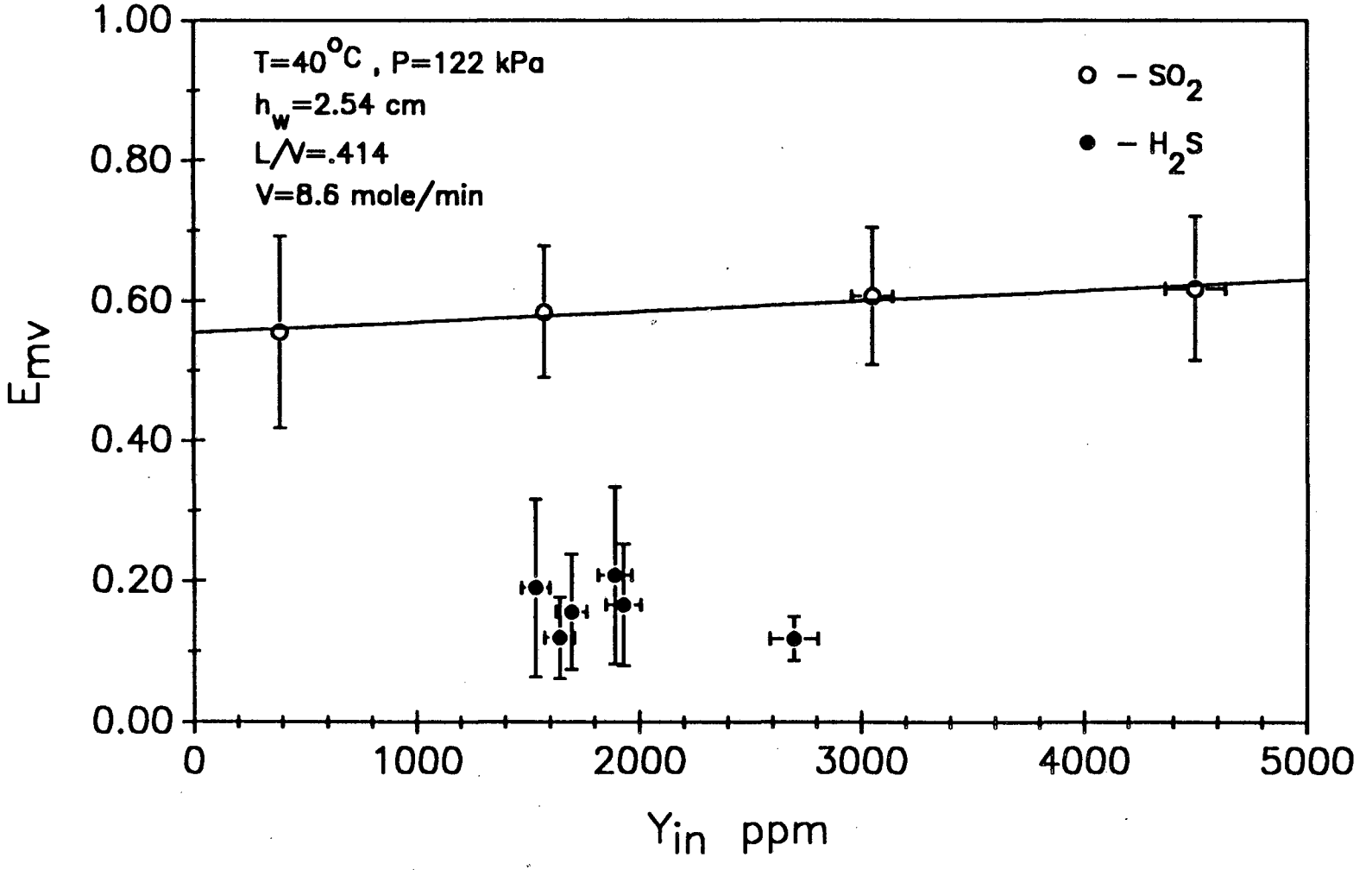

Figure 6–3: Effect of Temperature and Inlet Gas Concentration on H_2S Tray Efficiency

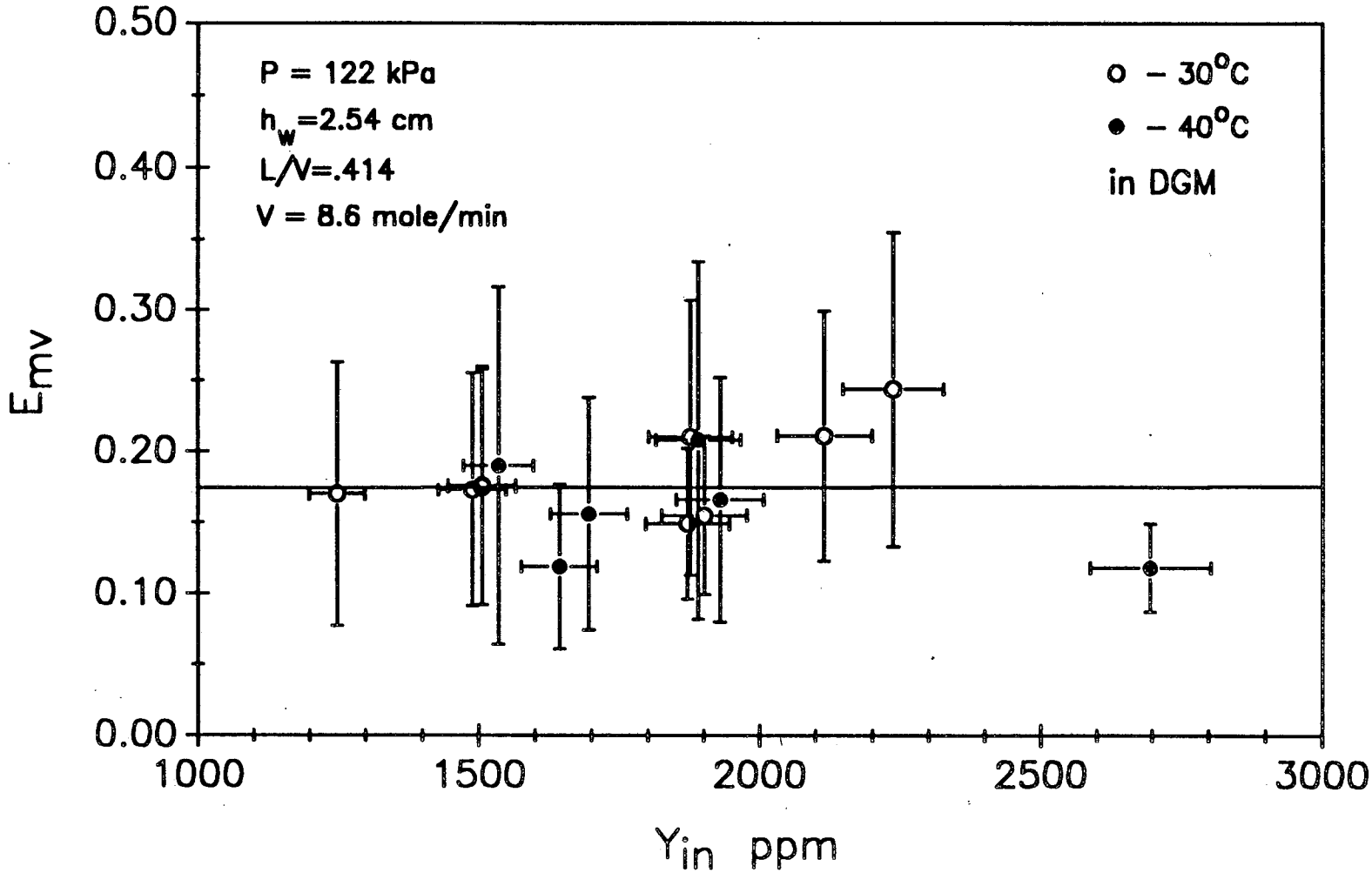

Figure 6–4: Effect of Catalyst Concentration on Reaction–Rate Constant

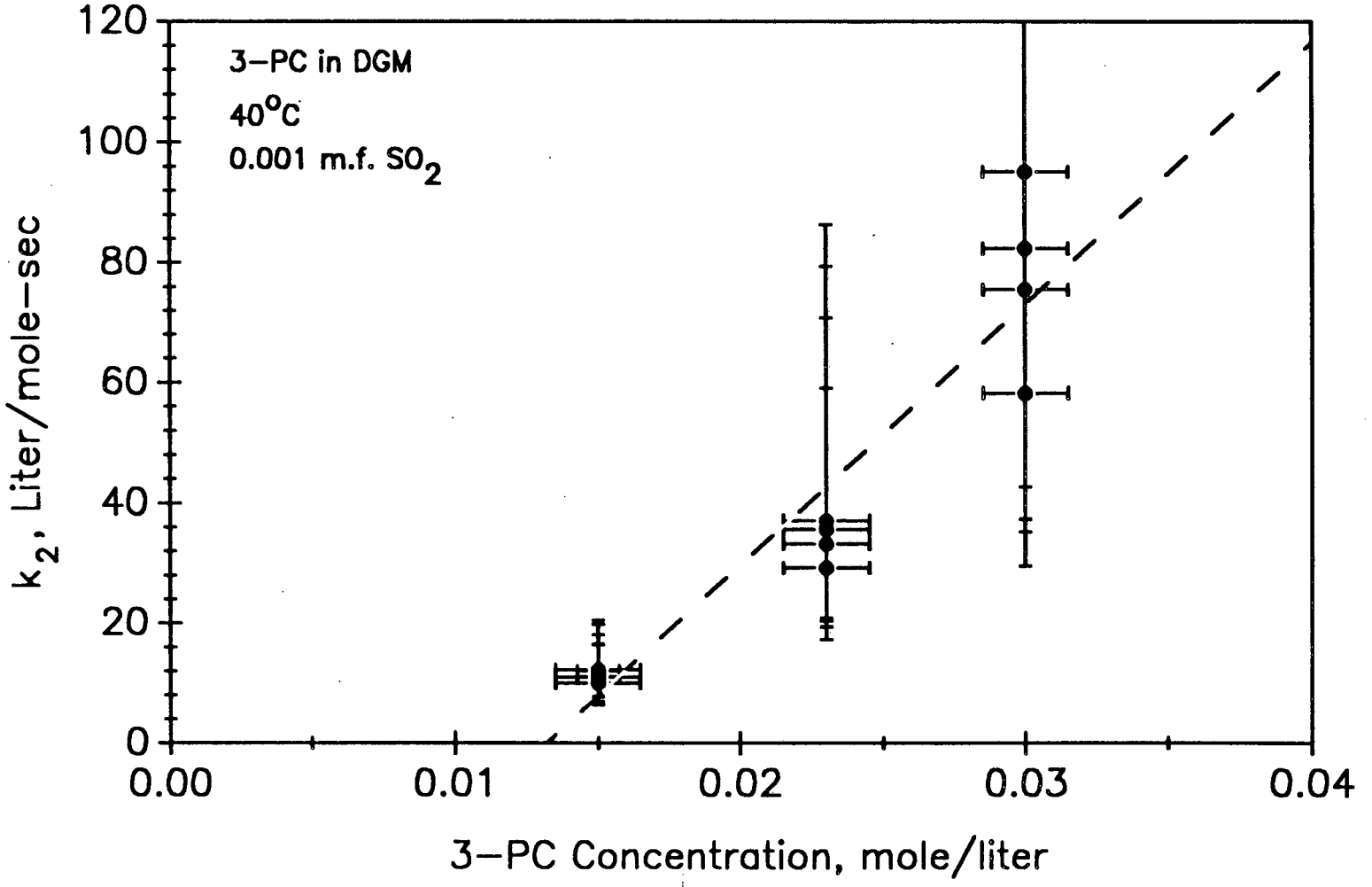

Figure 6–5: Effect of H_2S Absorption Rate and Assumed E_{mv} on Reaction Rate Constant

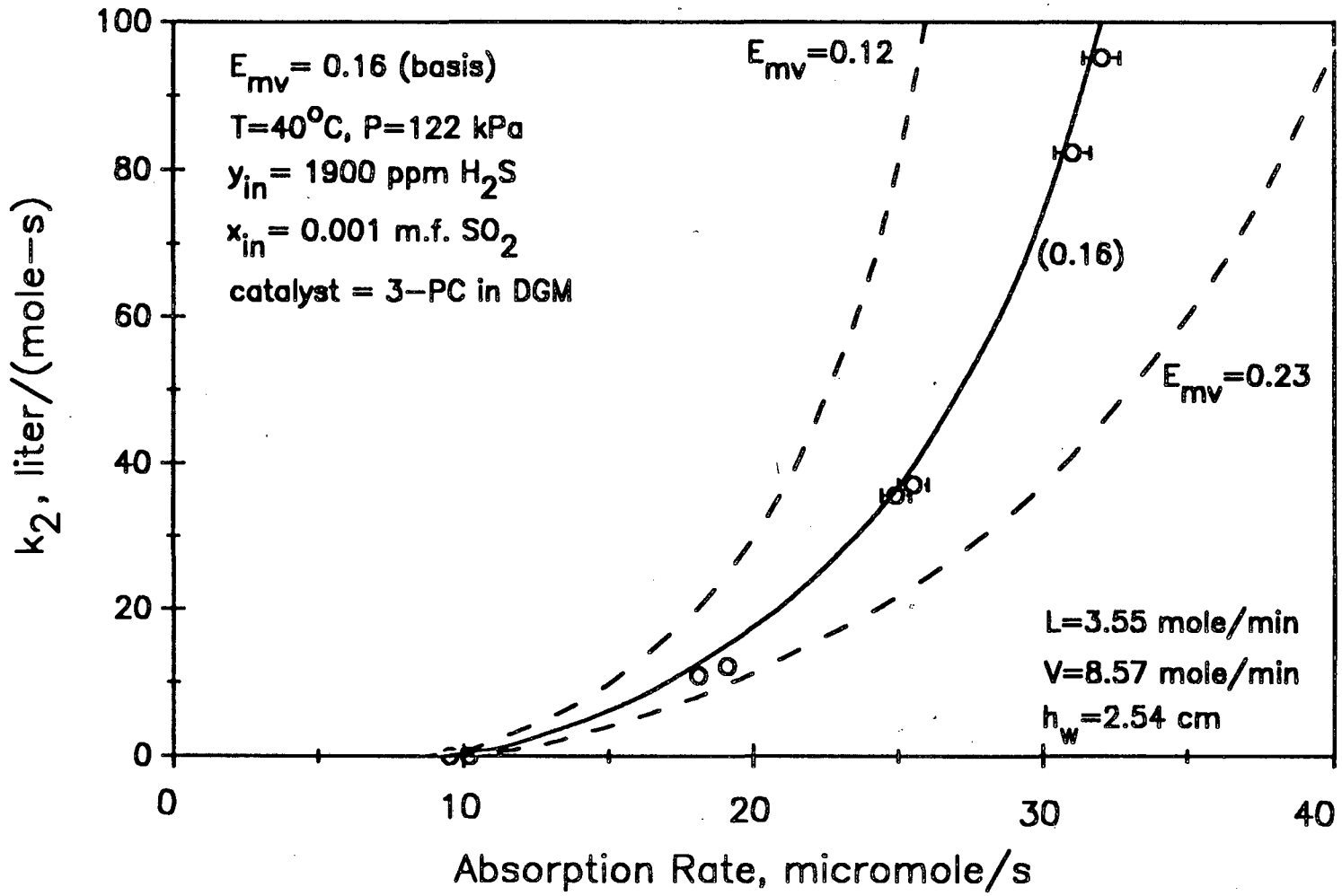

Figure 6–6: Arrhenius Plot

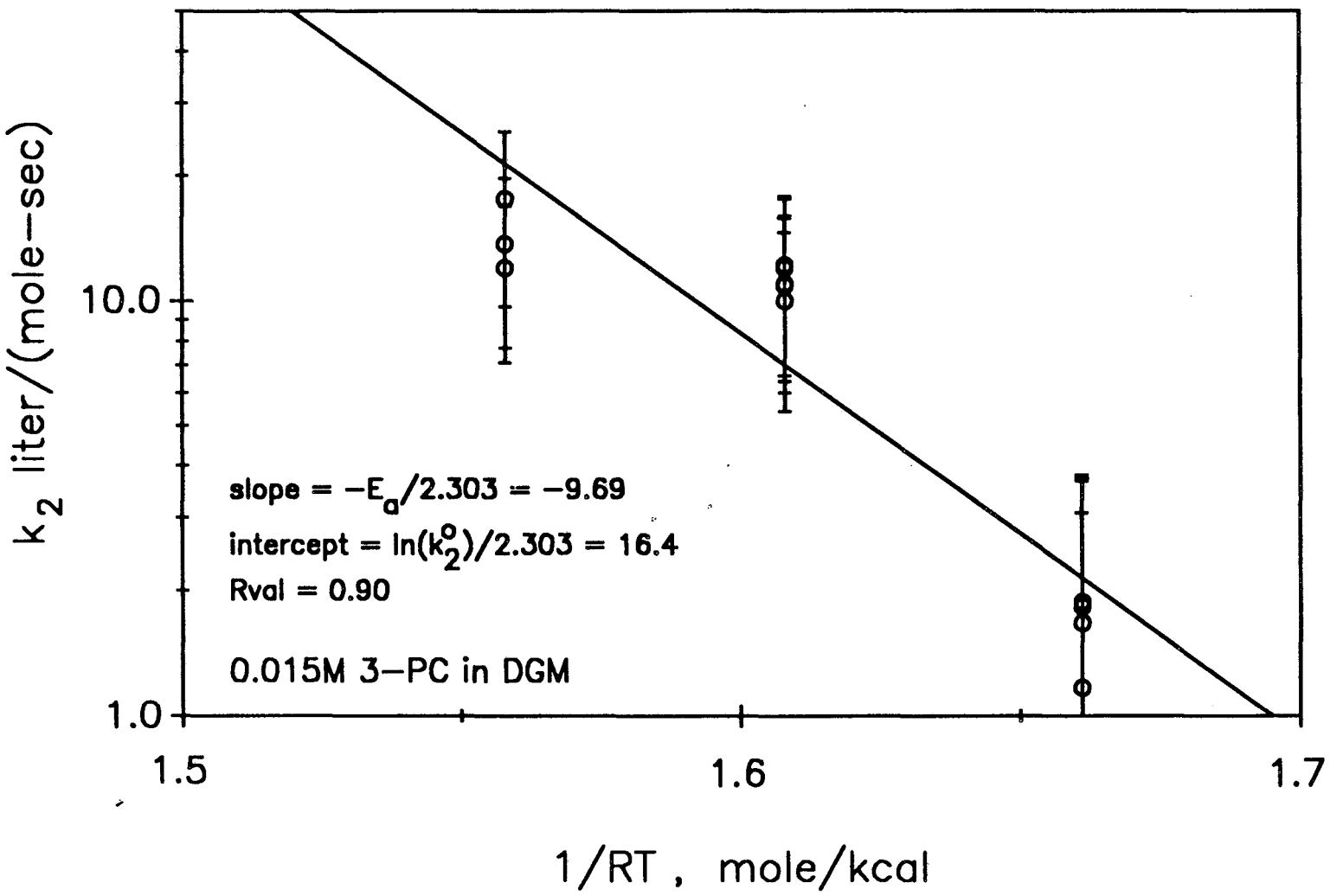

7. ABSORBER DESIGN

7.1 Introduction

The size and solvent flows of the primary absorber of the UCBSRP (Figure 7-1) are of importance in determining the economic feasibility of the UCBSRP. To aid in the analysis of the proposed process, the number of trays and the solvent flows in the primary absorber which are necessary to achieve a one-part-per-million-or-less H_2S specification in the treated gas has been determined. The composition, flow, temperature, and pressure of the sour gas used for the design basis is given in Table 7.1. Neumann (1986) used this same gas as the design basis for his process simulation of the UCBSRP in treating the coal-derived gas fuel for a 120 megawatt gas-turbine power plant. The process solvent was diethylene glycol methyl ether (DGM), and the homogeneous catalyst was 3-pyridyl carbinol (3-PC).

The primary absorber contains three trayed sections - - lower, middle, and upper. Within the lower section (trays 9 through 28) almost all the H_2S is physically absorbed from the sour gas by the process solvent. On the upper trays of this section a portion of the absorbed H_2S reacts chemically with dissolved SO_2 to produce sulfur and water. Approximately ninety percent of the total solvent flow in the column is fed to the top tray of the lower section, having been recycled from the SO_2-rich reactor/crystallizer (see Chapter 1). This solvent feed contains dissolved SO_2 for the reaction with H_2S in the column but contains no H_2S since that will have been reacted away. The concentration of SO_2 in this stream is set so that the sulfur produced by reaction does not exceed the solubility limit at the temperature in the column. The remaining ten percent of the total solvent flow is fed to the top tray of the middle, SO_2-absorption, section of the primary absorber (trays 6 through 8) and serves to scrub desorbed SO_2 from the gas stream. The solvent feed to this section contains neither H_2S nor SO_2. The upper, water-wash,

section (trays 1 through 5) uses water to recover solvent vapor from the exiting gas stream.

A tray column was chosen rather than a packed column because, near the top of the lower section, it is advantageous to have the large liquid volume that trays provide, to promote reactive absorption of H_2S. The water-wash section should also employ trays because the very low flow of water would not adequately wet the packing in a packed section. The middle section, which requires only a few theoretical stages, would use trays for the convenience of uniformity of design.

7.2 Design Method

The column design was determined by running a computer simulation of the proposed design to determine whether the proposed number of trays and solvent flows were adequate for the desired degree of H_2S removal. The number of stages in each column section and the liquid feeds to those sections were then adjusted until the outlet specifications for the treated gas were met. The simulation was written in FORTRAN and solved on a personal computer. The solution consisted of a main program which was iterated on until the mass, heat, and equilibrium relationships for each component on each stage were satisfied, a reaction subroutine which was used to converge the reactant and product flows before each main program iteration, thermodynamic subroutines which were used to determine the equilibrium constants and vapor and liquid enthalpies, and a subroutine which was used to calculate the composition of the solvent recycle for the main solvent feed.

In the main program, mass and heat balances and equilibrium relationships were written at each stage for each component. Because the stages were not equilibrium stages, the equilibrium relationships were written in terms of Murphree vapor tray efficiencies. The reaction was accounted for in the mass balance equations on each stage as constant sidedraws for reactants or feeds for products. The

thermodynamic properties were determined by subroutines developed by Neumann (1986). The balance equations and the equilibrium relationships were solved by the Newton simultaneous-convergence method (King, 1980) to provide new guesses for the component liquid and vapor flows and stage temperatures for the next iteration. Before each iteration of the main program, the reaction terms were solved outside the main program by a subroutine which converged the component flows of the reactants and products (H_2S, SO_2, H_2O, and S only); all other components were treated as inerts. In this subroutine each tray was treated as a continuously-stirred-tank reactor (CSTR). The heat balances on each stage were neglected in this subroutine, but the temperature profile from the main program was used to determine the vapor/liquid equilibrium constants, which are functions of temperature. The converged flows of the reactants and products were then sent to the main program to provide better guesses for these flows and for the reaction terms for the next iteration. This sequence was repeated until the component flows and stage temperatures in the main program converged within the desired tolerances. This technique was developed by Neumann (1986) for his process simulation of the UCBSRP because of convergence problems. Once the heat, mass, and equilibrium equations of the main program were solved, the solvent-recycle subroutine was called to determine the composition and flow of the main solvent feed that is recycled back to the primary absorber from the SO_2-rich reactor/crystallizer. This reactor/crystallizer was operated at a set concentration of dissolved SO_2. The computer code and a more detailed description of the solution are given in Appendix B.

Pressure, component tray efficiencies, and reaction-rate constant were assumed to be the same on every tray. The column diameter was determined by the column design method in Peters and Timmerhaus (1980) for a superficial vapor velocity set to 80% of the maximum allowable velocity in a column with 0.61-m

(24-inch) tray spacing. The active (bubbling) area of the tray was considered to be 90 percent of the total column area. The weir height was set at 10 cm. The volume of clear liquid on the tray (hold-up) was calculated by the product of the active area and the height of clear liquid on the tray (equation 3-13). This volume was used as the CSTR volume for the reaction calculations. The volume of solvent in the downcomers was neglected. The design specifications for the trays are given in Table 7.2.

Once the tray specifications were determined, the tray efficiencies were calculated, as discussed in Chapter 3, by the method of Chan and Fair (1984). A conservative estimate of eighty percent of the predicted efficiencies at the average temperature of the lower column section was used. The Murphree vapor tray efficiencies used in the absorber design are given in Table 7.3.

7.3 Results

The outlet specifications for the treated gas were set at a maximum of 1 ppm H_2S, 1 ppm SO_2, and 0.1 ppm solvent vapor. The low specification for solvent vapor was required because of the high cost of solvent losses in the treated gas. At the gas flow used for the design basis, 1 ppm solvent in the treated gas represents a $40,000 yearly loss.

The solvent flow was initially set to achieve an absorption factor (L/mV) for H_2S of approximately 1.5 on the bottom tray of the absorber. As the absorption factor increases, the number of trays needed to achieve a given extent of absorption decreases. For absorption factors less than one, the solvent becomes saturated with the gas, and no number of trays will allow complete removal of that gas. An absorption factor equal to one would require an infinite number of trays to achieve complete physical absorption of the gas.

The solvent flow to the SO_2-absorption section of the absorber was set at 10

percent of the total of both solvent feeds. The very low flow of water to the top section of the absorber requires five trays to meet the outlet specification for solvent in the treated gas. A higher flow of water to the top section would reduce the number of trays in this section but at the added expense of stripping this water from the solvent in the solvent stripper (see Figure 1-2). All the liquid feed temperatures were 30°C. Based on the results of the reactive-absorption experiments, the reaction-rate constant was assumed to be 100 liters/mole-s. The concentration of dissolved SO_2 in the main feed from the SO_2-rich reactor/crystallizer was set at 0.00035 mole fraction. At the solvent flow to the column, this amount of SO_2 is equivalent to less than ten percent of the H_2S in the sour-gas feed.

For the conditions stated above, the absorber solution is given in Table 7.4 (case 1). Five actual trays are required in the top section of the absorber, 3 in the middle section, and 12 in the bottom section. The absorption factor (L/mV) for H_2S was 1.5 on the bottom tray, while the average absorption factor in the lower section was 1.8. The absorption factor increased up the column because the tray temperatures decreased with increased height up the column and m, the slope of the equilibrium line, decreases as temperature decreases. The temperature difference between the top tray of the column and the bottom was not extreme since the heat capacity of the solvent (65 cal/mole-K) is over seven times greater than that of the gas stream (7.6 cal/mole-K). Very little latent heat is transferred between the two phases in this design.

A second case (Table 7.4, case 2) was run to determine the number of trays that would be required to meet the specifications for the treated gas in the absence of reaction but using the same solvent flows as in case 1. For the second case, the number of trays in top two sections remained unchanged while the number of trays in the bottom section had to be increased by 8 trays for a total of 20 trays in the lower section to achieve the same degree of H_2S removal. If no SO_2 were present

in the feed to the lower section , the SO_2-absorption section could be eliminated, so the net increase in total number of trays would be only five. Although the decrease in number of trays for the primary absorber that results from the UCBSRP flow configuration (case 1) is not large, a second (and more important) benefit of case 1 is that the reaction in the reactor/crystallizer makes it unnecessary to strip H_2S to a very low level from the solvent recycle, which represents ninety percent of the total solvent flow to the absorber.

A third case (Table 7.4, case 3) was investigated in which the same number of total trays was used as in case 2, but the reaction-rate constant of case 1 was used. The same flows to the water-wash and SO_2-absorption sections and the same concentration of SO_2 in the main solvent feed to the lower section as in the previous two cases were used. The lowest solvent flow to the main absorber section that could meet the treated gas specification was determined for this configuration. A 38% reduction in solvent recycle flow was achieved for a 35% reduction in total solvent flow. A tremendous advantage is gained by reduced solvent pumping costs. The lower flow of solvent that leaves the bottom of the absorber is much richer in H_2S, therefore a smaller reactor/crystallizer may be used.

For case 3 the tray efficiencies were adjusted downward slightly because of the change in liquid flow and composition. As discussed in Chapter 3, these parameters affect tray efficiency. The average absorption factor for H_2S in the lower column section was 1.1, compared to 1.8 for both cases 1 and 2. A sample absorber-design output showing the internal flows and temperatures for case 3 is given in Table 7.5, and Figure 7-1 reflects the feed locations of this design.

The selectivity for H_2S of the absorber configuration is quite good. The removal of H_2S was 99.99%, whereas the highest removal of any of the other constituents in the sour gas was 3.2% for CO_2. The next highest removal was 0.2% for CH_4. The selectivity arises from the saturation of the recycle solvent with respect

to the gases other than H_2S and SO_2 and from the relatively low solubility of these other gases in the solvent (DGM).

List of Tables for Chapter 7

7.1 Sour Gas Characteristics

7.2 Tray Specifications

7.3 Component Tray Efficiencies

7.4 Absorber Design Results

7.5 Primary-Absorber Design Results for Case 3

List of Figures for Chapter 7

7-1 Primary Absorber of UCBSRP

Table 7.1: Sour Gas Characteristics

Composition: (mole fraction)

N_2	= 0.4130	H_2O	= 0.00290
H_2	= 0.2729	H_2S	= 0.00614
CO_2	= 0.1902	CH_4	= 0.00145
CO	= 0.1133		

Flow = 2.488 kmole/s

T = 368°K

P = 2500 kPa

Table 7.2: Tray Specifications

Diameter, m	3.50	Weir Length, m	2.08
Active Area, m^2	8.66	Flow Length, m	2.82
Hole Fraction	0.08	Weir Height, cm	10.0
Tray Spacing, m	0.61	Hold-up, m^3	1.22

Table 7.3: Component Tray Efficiencies

Temp. = 304°K Press. = 2500 kPa

	E_{mv}		E_{mv}
DGM	.72	N_2	.01
H_2O	.79	CH_4	.04
H_2S	.69	H_2	.01
SO_2	.76	CO	.02
CO_2	.33		

Table 7.4: Absorber Design Results

(for treating gas of Table 7.1)

Solvent Flow (kmole/s) 303°K	case 1	case 2	case 3
water-wash	0.02	0.02	0.02
SO_2-absorption	0.20	0.20	0.20
main section	1.83	1.83	1.13
Rate Constant (liter/mol-s)	100	0	100
No. Trays			
water-wash	5	5	5
SO_2-absorption	3	3	3
main section	12	20	20
Total	20	28	28
Treated Gas			
H_2S	.5 ppm	.8 ppm	.8 ppm
SO_2	.6 ppm	.6 ppm	.6 ppm
DGM	.05 ppm	.05 ppm	.07 ppm

Table 7.5: Primary-Absorber Design Results for Case 3

PRESSURE = 2500.00 kPa, RXN RATE CONST. = .100E+03 L/(GMOLE*SEC), TRAY VOL. = 970.0 LITERS

	SOLV	H2O	H2S	SO2	S(DIS)	CO2	N2	CH4	H2	CO
EMV	.70	.78	.66	.75	.00	.29	.01	.03	.01	.01
m(18)	.327E-04	.390E-02	.439E+00	.288E-01	.000E+00	.310E+01	.188E+03	.396E+02	.178E+03	.894E+02

***** LIQUID FEEDS *****

STAGE #	TEMP KELVIN	TOTAL FLOW GMOLE/SEC	LIQ. MOLE FRACT. SOLV	H2O	H2S	SO2	S(DIS)	CO2	N2	CH4	H2	CO
1	303.00	.200E+02	.000E+00	.100E+01	.000E+00	.000E+00	.000E+00	.000E+00	.000E+00	.000E+00	.000E+00	.000E+00
6	303.00	.200E+03	.913E+00	.860E-01	.000E+00	.000E+00	.300E-03	.000E+00	.000E+00	.000E+00	.000E+00	.000E+00
9	303.00	.113E+04	.756E+00	.190E+00	.000E+00	.350E-03	.300E-03	.503E-01	.125E-02	.278E-04	.952E-03	.809E-03

***** LIQUID STAGE FLOWS *****

STAGE #	TEMP KELVIN	TOTAL FLOW GMOLE/SEC	LIQ. MOLE FRACT. SOLV	H2O	H2S	SO2	S(DIS)	CO2	N2	CH4	H2	CO
1	303.78	.201E+02	.190E-04	.997E+00	.334E-07	.324E-06	.695E-09	.264E-02	.124E-03	.906E-06	.101E-03	.496E-04
2	303.78	.200E+02	.818E-04	.997E+00	.334E-07	.326E-06	.140E-08	.264E-02	.124E-03	.907E-06	.101E-03	.496E-04
3	303.79	.200E+02	.290E-03	.997E+00	.336E-07	.328E-06	.212E-08	.266E-02	.124E-03	.911E-06	.101E-03	.497E-04
4	303.84	.195E+02	.999E-03	.996E+00	.342E-07	.334E-06	.292E-08	.269E-02	.124E-03	.923E-06	.101E-03	.498E-04
5	304.08	.175E+02	.371E-02	.993E+00	.366E-07	.359E-06	.424E-08	.283E-02	.121E-03	.963E-06	.990E-04	.491E-04
6	305.27	.232E+03	.786E+00	.148E+00	.158E-05	.101E-04	.258E-03	.574E-01	.346E-02	.419E-04	.241E-02	.190E-02
7	304.75	.233E+03	.784E+00	.148E+00	.200E-05	.313E-04	.258E-03	.623E-01	.237E-02	.384E-04	.166E-02	.139E-02
8	304.23	.233E+03	.783E+00	.149E+00	.219E-05	.773E-04	.258E-03	.632E-01	.230E-02	.382E-04	.160E-02	.133E-02
9	303.73	.138E+04	.755E+00	.178E+00	.156E-05	.299E-03	.292E-03	.599E-01	.313E-02	.400E-04	.217E-02	.163E-02
10	303.85	.138E+04	.754E+00	.177E+00	.356E-05	.295E-03	.293E-03	.623E-01	.256E-02	.386E-04	.178E-02	.148E-02
11	303.91	.138E+04	.754E+00	.177E+00	.765E-05	.289E-03	.295E-03	.633E-01	.235E-02	.378E-04	.163E-02	.138E-02
12	303.95	.138E+04	.753E+00	.177E+00	.163E-04	.276E-03	.299E-03	.636E-01	.227E-02	.373E-04	.157E-02	.132E-02
13	303.99	.138E+04	.753E+00	.177E+00	.352E-04	.251E-03	.307E-03	.637E-01	.224E-02	.371E-04	.155E-02	.130E-02
14	304.05	.138E+04	.753E+00	.177E+00	.769E-04	.208E-03	.322E-03	.637E-01	.223E-02	.371E-04	.155E-02	.129E-02
15	304.14	.138E+04	.753E+00	.177E+00	.170E-03	.144E-03	.345E-03	.637E-01	.223E-02	.370E-04	.155E-02	.129E-02
16	304.23	.138E+04	.753E+00	.178E+00	.367E-03	.741E-04	.370E-03	.636E-01	.224E-02	.370E-04	.156E-02	.129E-02
17	304.32	.138E+04	.753E+00	.178E+00	.715E-03	.264E-04	.388E-03	.635E-01	.225E-02	.371E-04	.157E-02	.130E-02
18	304.39	.138E+04	.752E+00	.178E+00	.121E-02	.651E-05	.395E-03	.634E-01	.226E-02	.371E-04	.157E-02	.130E-02
19	304.46	.138E+04	.752E+00	.177E+00	.183E-02	.117E-05	.397E-03	.633E-01	.227E-02	.371E-04	.158E-02	.131E-02
20	304.55	.138E+04	.751E+00	.177E+00	.255E-02	.158E-06	.397E-03	.633E-01	.228E-02	.371E-04	.159E-02	.131E-02
21	304.64	.139E+04	.751E+00	.177E+00	.339E-02	.167E-07	.396E-03	.631E-01	.230E-02	.372E-04	.160E-02	.132E-02
22	304.75	.139E+04	.750E+00	.177E+00	.435E-02	.141E-08	.396E-03	.630E-01	.231E-02	.372E-04	.161E-02	.133E-02
23	304.89	.139E+04	.749E+00	.177E+00	.546E-02	.971E-10	.396E-03	.629E-01	.232E-02	.372E-04	.162E-02	.133E-02
24	305.10	.139E+04	.748E+00	.177E+00	.672E-02	.550E-11	.395E-03	.627E-01	.233E-02	.372E-04	.163E-02	.134E-02
25	305.48	.139E+04	.747E+00	.177E+00	.813E-02	.262E-12	.394E-03	.623E-01	.234E-02	.371E-04	.164E-02	.135E-02
26	306.48	.139E+04	.746E+00	.177E+00	.962E-02	.117E-13	.394E-03	.616E-01	.232E-02	.368E-04	.163E-02	.134E-02
27	309.70	.139E+04	.746E+00	.178E+00	.109E-01	.118E-14	.394E-03	.593E-01	.216E-02	.352E-04	.154E-02	.126E-02
28	321.46	.138E+04	.752E+00	.182E+00	.105E-01	.467E-15	.397E-03	.519E-01	.128E-02	.287E-04	.982E-03	.835E-03

Table 7.5: Continued

***** VAPOR STAGE FLOWS *****

STAGE #	TEMP KELVIN	TOTAL FLOW GMOLE/SEC	VAP. MOLE FRACT. SOLV	H2O	H2S	SO2	S(DIS)	CO2	N2	CH4	H2	CO
1	303.78	.245E+04	.671E-07	.170E-02	.781E-06	.614E-06	.448E-30	.187E+00	.419E+00	.147E-02	.277E+00	.115E+00
2	303.78	.245E+04	.222E-06	.170E-02	.781E-06	.617E-06	.000E+00	.187E+00	.419E+00	.147E-02	.277E+00	.115E+00
3	303.79	.245E+04	.735E-06	.169E-02	.781E-06	.617E-06	.000E+00	.187E+00	.419E+00	.147E-02	.277E+00	.115E+00
4	303.84	.245E+04	.243E-05	.165E-02	.782E-06	.617E-06	.000E+00	.187E+00	.419E+00	.147E-02	.277E+00	.115E+00
5	304.08	.245E+04	.802E-05	.148E-02	.782E-06	.617E-06	.000E+00	.187E+00	.419E+00	.147E-02	.277E+00	.115E+00
6	305.27	.245E+04	.264E-04	.612E-03	.782E-06	.618E-06	.000E+00	.187E+00	.419E+00	.147E-02	.277E+00	.115E+00
7	304.75	.247E+04	.257E-04	.599E-03	.970E-06	.159E-05	.000E+00	.191E+00	.417E+00	.146E-02	.275E+00	.114E+00
8	304.23	.247E+04	.249E-04	.603E-03	.118E-05	.368E-05	.000E+00	.192E+00	.417E+00	.146E-02	.275E+00	.114E+00
9	303.73	.247E+04	.239E-04	.671E-03	.167E-05	.827E-05	.000E+00	.192E+00	.417E+00	.146E-02	.275E+00	.114E+00
10	303.85	.248E+04	.240E-04	.674E-03	.362E-05	.818E-05	.000E+00	.195E+00	.415E+00	.146E-02	.274E+00	.114E+00
11	303.91	.248E+04	.241E-04	.675E-03	.764E-05	.795E-05	.000E+00	.196E+00	.414E+00	.146E-02	.274E+00	.114E+00
12	303.95	.249E+04	.241E-04	.676E-03	.160E-04	.748E-05	.000E+00	.197E+00	.414E+00	.146E-02	.274E+00	.114E+00
13	303.99	.249E+04	.242E-04	.678E-03	.333E-04	.663E-05	.000E+00	.197E+00	.414E+00	.146E-02	.273E+00	.114E+00
14	304.05	.249E+04	.243E-04	.681E-03	.683E-04	.529E-05	.000E+00	.197E+00	.414E+00	.146E-02	.273E+00	.114E+00
15	304.14	.249E+04	.244E-04	.684E-03	.136E-03	.350E-05	.000E+00	.197E+00	.414E+00	.146E-02	.273E+00	.114E+00
16	304.23	.249E+04	.245E-04	.688E-03	.255E-03	.174E-05	.000E+00	.197E+00	.414E+00	.146E-02	.273E+00	.114E+00
17	304.32	.249E+04	.246E-04	.691E-03	.440E-03	.603E-06	.000E+00	.197E+00	.414E+00	.146E-02	.273E+00	.114E+00
18	304.39	.249E+04	.246E-04	.693E-03	.685E-03	.147E-06	.000E+00	.197E+00	.414E+00	.145E-02	.273E+00	.114E+00
19	304.46	.249E+04	.247E-04	.695E-03	.983E-03	.261E-07	.000E+00	.197E+00	.414E+00	.145E-02	.273E+00	.114E+00
20	304.55	.249E+04	.248E-04	.698E-03	.133E-02	.353E-08	.000E+00	.196E+00	.413E+00	.145E-02	.273E+00	.114E+00
21	304.64	.249E+04	.249E-04	.701E-03	.173E-02	.373E-09	.000E+00	.196E+00	.413E+00	.145E-02	.273E+00	.113E+00
22	304.75	.249E+04	.251E-04	.705E-03	.220E-02	.316E-10	.000E+00	.196E+00	.413E+00	.145E-02	.273E+00	.113E+00
23	304.89	.249E+04	.253E-04	.711E-03	.274E-02	.218E-11	.000E+00	.196E+00	.413E+00	.145E-02	.273E+00	.113E+00
24	305.10	.249E+04	.258E-04	.723E-03	.335E-02	.124E-12	.000E+00	.196E+00	.413E+00	.145E-02	.273E+00	.113E+00
25	305.48	.250E+04	.269E-04	.754E-03	.406E-02	.603E-14	.000E+00	.196E+00	.412E+00	.145E-02	.272E+00	.113E+00
26	306.48	.250E+04	.292E-04	.845E-03	.484E-02	.289E-15	.000E+00	.195E+00	.412E+00	.145E-02	.272E+00	.113E+00
27	309.70	.250E+04	.342E-04	.112E-02	.568E-02	.385E-16	.000E+00	.195E+00	.412E+00	.145E-02	.272E+00	.113E+00
28	321.46	.250E+04	.397E-04	.190E-02	.637E-02	.221E-16	.000E+00	.194E+00	.412E+00	.145E-02	.272E+00	.113E+00
INLET	368.00	.249E+04	.000E+00	.290E-02	.614E-02	.000E+00	.000E+00	.190E+00	.413E+00	.145E-02	.273E+00	.113E+00

YOUT(H2S) = .8 ppm; YOUT(SO2) = .6 ppm; YOUT(SOLV) = .07 ppm.

EXTENT OF H2S RXN = 5.1 PERCENT; EXTENT OF SO2 RXN = 99.6 PERCENT

DGM ABSORPTION FACTOR, L/mV, AT STAGE 1 = .258E+03; SO2 ABS. FACT. AT STAGE 6 = .325E+01

H2S ABSORPTION FACTOR AT STAGE 9 = .129E+01; AT BOTTOM = .894E+00

DISSOLVED SULFUR DID'NT EXCEED LIMIT OF .491E-03 m.f. ON STAGE 27

Figure 7-1: Primary Absorber of UCBSRP

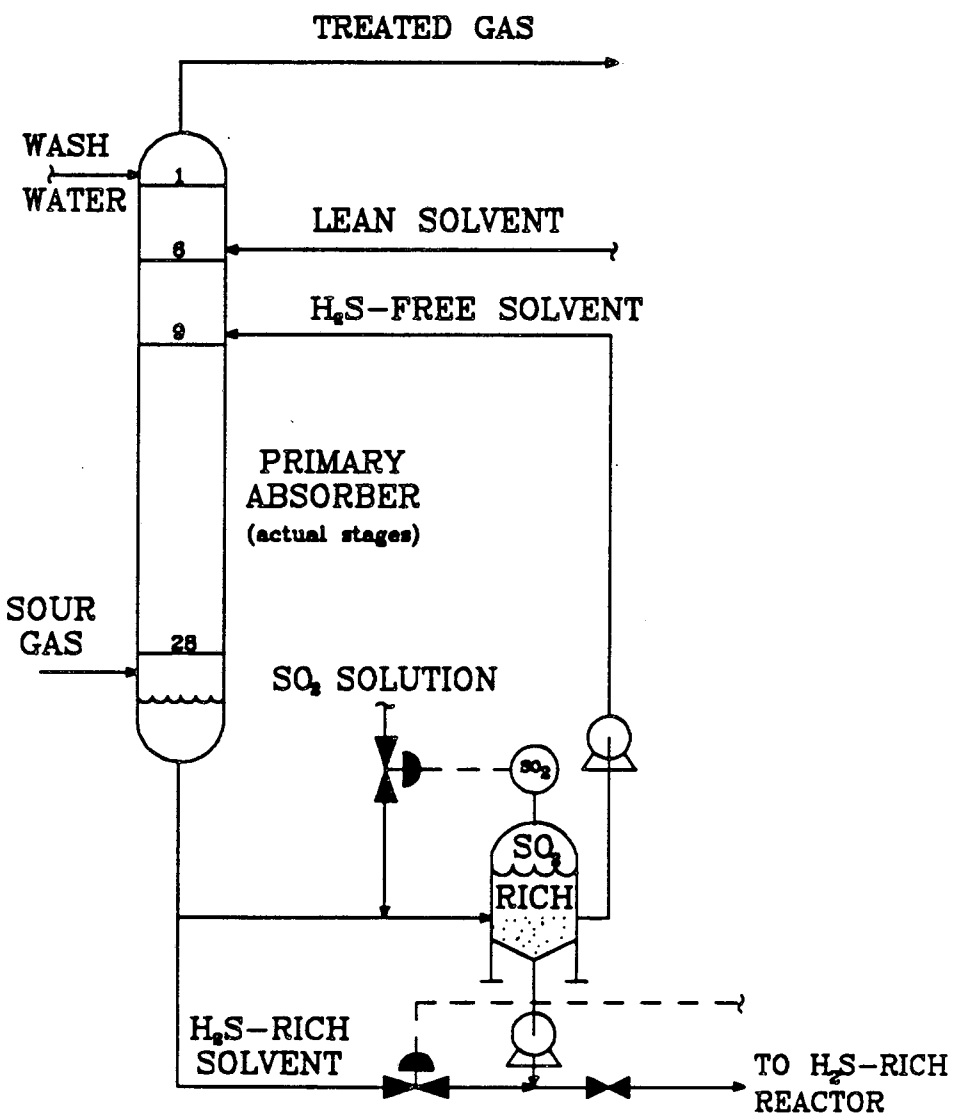

REFERENCES

Astarita, G., *Mass Transfer with Chemical Reaction*, Elsevier Pub. Co., New York, 1967.

Astarita, G., D. W. Savage, and A. Bisio, *Gas Treating with Chemical Solvents*, John Wiley and Sons, New York, 1983.

Brian, P. L. T., J. F. Hurley and E. H. Hasseltine, "Penetration Theory for Gas Absorption Accompanied by a Second Order Chemical Reaction", *A.I.Ch.E. J.*, **1961**, *7*, No. 2, p. 226.

Chan, H. and J. R. Fair, "Prediction of Point Efficiencies on Sieve Trays 1. Binary Systems", *Ind. Eng. Chem. Proc. Des. Dev.*, **1984**, *23*, p. 814.

Colson, T. E., M.S. Thesis, Department of Chemical Engineering, University of California, Berkeley, CA, 1989.

Crean, D. J., M.S. Thesis, Department of Chemical Engineering, University of California, Berkeley, CA, 1987.

Dankwerts, P. V., "Gas-Liquid Reactions", McGraw-Hill, Inc., New York, NY, 1970.

Demyanovich, R. J., Ph.D. Dissertation, Department of Chemical Engineering, University of California, Berkeley, CA, 1984.

Glasscock, D. A. and G. T. Rochelle, "Numerical Simulation of Theories for Gas Absorption with Chemical Reaction", *A.I.Ch.E J.*, **1989**, *35*, No. 8, p. 1271.

Henley, E. J. and J. D. Seader, *Equilibrium-Stage Separation Operations in Chemical Engineering*, Wiley, New York, 1981.

Higbie, R., "The Rate of Absorption of a Pure Gas into a Still Liquid During Short Periods of Exposure", *Trans. A.I.Ch.E.*, **1935**, *35*, p. 365.

Hikita, H., S. Asai, and H. Ishikawa, "Gas Absorption Accompanied By an Irreversible Second-Order Reaction with a Volatile Reactant', *Bulletin Univ. Osaka Prefecture*, **1979**, *A28*, p. 57.

King, C. J., *Separation Processes*, 2nd Ed., McGraw-Hill, New York, 1980.

Kohl, A. and F. Riesenfeld, *Gas Purification*, 4th Ed., Gulf Publ. Co., Houston, TX, 1985.

Lapidus, L., *Digital Computation for Chemical Engineers*, McGraw-Hill, New York, 1962.

Lynn, S., D. W. Neumann, S. F. Sciamanna, and F. H. Vorhis, "A Comparison of the UCB Sulfur Recovery Process with Conventional Sulfur Recovery Technology for Treating Recycle Gas from a Crude Oil Residuum Hydrotreater", *Environ. Prog.*, **1987**., *6*, No. 4, p. 257.

Neumann, D. W., Ph.D. Dissertation, Department of Chemical Engineering, University of California, Berkeley, CA, 1986.

Pangarkar, V. G., "Gas absorption with reaction in a solution containing a volatile dissolved reactant", *Chem. Eng. Sci.*, **1974**, *29*, p. 877.

Peters, M. S. and K. D. Timmerhaus, *Plant Design and Economics for Chemical Engineers*, 3rd Ed., McGraw-Hill, New York, 1980.

Pohorecki, R. and W. Moniuk, "Evaluation of Plate Efficiency for Absorption with First-Order Chemical Reaction", *Inzynieria Chemiczna I Procesowa*, **1983a**, *4*, No. 1, p. 85.

Pohorecki, R. and W. Moniuk, "Evaluation of Plate Efficiency for Absorption with Chemical Reaction", *Inzynieria Chemiczna I Procesowa*, **1983b**, *4*, No. 2, p. 353.

Pohorecki, R. and W. Moniuk, "Efficiency of Sieve Trays for Absorption with Chemical Reaction", *Inzynieria Chemiczna I Procesowa*, **1983c**, *4*, No. 3, p. 545.

Reid, R. C., J. M. Prausnitz and T. K. Sherwood, *The Properties of Gases and Liquids*, 3rd Ed., McGraw-Hill, New York, 1977.

Sciamanna, S. F., Ph.D. Dissertation, Department of Chemical Engineering, University of California, Berkeley, CA, 1986.

Shaikh, A. A. and A. Varma, "Gas absorption with chemical reaction: the case involving a volatile liquid reactant", *Chem. Eng. Sci.*, **1984**, *39*, p. 1639.

Sharma, M. M. and R. K. Gupta, "Mass Transfer Characteristics of Plate Columns without Downcomers", *Trans. Instn. Chem. Engrs.* **1967**, *45*, p. T169.

Sherwood, T. K., R. L. Pigford, and C. R. Wilke, *Mass Transfer*, McGraw-Hill, New York, 1975.

Stevens, C. A., Ph.D. Dissertation, Department of Chemical Engineering, University of California, Berkeley, CA, 1989.

van Krevelen, D. W. and P. J. Hoftijzer, "Kinetics of Gas-Liquid Reactions, Part I, General Theory", *Rec. Trav. Chim.*, **1948**, *67*, p. 563.

Whitman, W. G., *Chem. and Met. Eng.*, **1923**, *29*, p. 147.

Appendix

The three appendices to this report (see Table of Contents) are available upon request from:

Professor Scott Lynn
Department of Chemical Engineering
University of California
Berkeley, CA 94720-9989

LAWRENCE BERKELEY LABORATORY
TECHNICAL INFORMATION DEPARTMENT
1 CYCLOTRON ROAD
BERKELEY, CALIFORNIA 94720